Rain Rate and Rain Drop Size Distribution Models for Line-Of-Sight Millimetric Systems in South Africa

SUBMITTED BY

Owolawi Pius Adewale

IN PARTIAL FULFILLMENT OF THE REQUIREMENT FOR THE DEGREE OF MASTER OF SCIENCE IN ELECTRICAL ENGINEERING IN TELECOMMUNICATIONS AND INFORMATION TECHNOLOGY.

UNIVERSITY OF
KWAZULU-NATAL

SCHOOL OF ENGINEERING

Centre of Excellence in Radio Access and Rural Technologies

DATE OF SUBMISSION

February 2006

SUPERVISED BY

Prof. T.J. AFULLO

DECLARATION

I, Owolawi Pius Adewale, student Number 204001127, hereby declare that the dissertation entitled **Rain Rate and Rain Drop Size Distribution Models for Line-Of-Sight Millimetric Systems in South Africa** is a result of my own investigation and research, and presents my own work unless specifically referenced in the text. This work has not been submitted in part or in full for any other degree or to any other University.

Name: _____

Signed: _____

Date: _____

ABSTRACT

Radio frequencies at millimeter wavelengths suffer greatly from rain attenuation. It is therefore essential to study rainfall characteristics for efficient and reliable design of radio networks at frequencies above 10GHz. These characteristics of rain are geographically based, which need to be studied for estimation of rain induced attenuation. The ITU-R, through recommendations P.837 and P.838, have presented global approaches to rain-rate variation and rain-induced attenuation in line-of-sight radio links. Therefore, in this dissertation characteristics of rainfall rate and its applications for South Africa are evaluated.

The cumulative distributions of rain intensity for 12 locations in seven regions in South Africa are presented in this dissertation based on five-year rainfall data. The rain rate with an integration time of 60 minutes is converted into an integration time of 1 minute in accordance with ITU-R recommendations. The resulting cumulative rain intensities and relations between them are compared with the global figures presented in ITU-R Recommendation P.837, as well as with the work in other African countries, notably by Moupfuma and Martin. Based on this work, additional rain-climatic zones are proposed alongside the five identified by ITU-R for South Africa.

Finally, the study compares the semi-empirical raindrop-size distribution models such as Laws and Parsons, Marshall and Palmer, Joss, Thams and Waldvogel, and Gamma distribution with the estimated South Africa models.

ACKNOWLEDGEMENTS

Firstly and most importantly I would like to thank God who makes all things possible. I would like to give sincere thanks and affection to my parents, brothers and sisters for their support, understanding and encouragement during the period of my studies.

I will like to deeply thank my supervisor Prof. T.J Afullo, during the several months in which this research lasted, provided me with useful and helpful assistance. Without his care and consideration, this research would likely not have matured.

My humble gratitude to all the academic staffs in the department and especially the administrator Mrs. Rene Truter, for their moral support and advises throughout the research period.

I would like to thank all the contributors, for their dedication and interest. To Mr. and Mrs. Odedina for their good company and moral supports. Prof. and Mrs. Ogulu for their guidance and encouragement. Mr. Bello for all his patience throughout an editing and cross-reviewing process which constitutes a rather difficult balancing act.

Finally, I would like to thank all those people who have not been mentioned but have contributed to the success of this dissertation.

TABLE OF CONTENTS

CHAPTER FOUR

RAINFALL RATE DISTRIBUTION MODELS FOR SOUTH AFRICA

CHAPTER FIVE

RAINDROP-SIZE DISTRIBUTION

CHAPTER SIX

CONCLUSION

LISTS OF FIGURES

LIST OF TABLES

ABBREVIATIONS

SHF	Super High Frequency
EHF	Extended High Frequency
GHz	Giga Hertz
ITU-R	International Telecommunication Union-Radio Sector
ETS	European Telecommunication Service
LOS	Line of Sight
SA	South Africa
dB	Decibel
AWM	Average Worst Month
AY	Average Year
SAWS	South Africa Weather Service
pdf	Probability Density Function
RF	Radio Frequency
DSD	Drop size Distribution
MTI	Moving Target Indication
EIRP	Isotropically Radiated Power
FM	Frequency Modulation
Km	Kilometer
CCIR	International Radio Consultative Committee

CHAPTER ONE

INTRODUCTION

In this chapter, the background of the research is introduced along with dissertation overview. The background explains the importance of millimeter-wave band and the principal offender which is rain.

1.1 BACKGROUND

The study of precipitation effects on line-of-sight SHF/EHF radio links has increased in recent years as a result of the need for broadband data/voice and video networks. The millimeter wave spectrum 30-300 GHz is of great interest to service providers and systems designers today because of the wide bandwidths available for communications in this frequency range. Such wide bandwidths are valuable in supporting applications such as high speed data transmission and video distribution [1].

Signal transmission at frequencies above 10 GHz is influenced by various meteorological conditions, which impose severe limitations on the line-of-sight coverage distance of radio systems operating in the millimetric region of the spectrum [2]. Absorption and scattering of signal energy by rain, snow, fog, water vapour, oxygen and other gases in the atmosphere all affect the propagation of radio waves at frequencies above 10 GHz, and these effects must be taken into consideration when designing millimeter-wave systems.

To ensure that millimetric communication systems are able to achieve the same degree of availability and performance as systems operating in the lower frequency bands of the spectrum, accurate propagation models are required to estimate the effect of atmospheric attenuation on the performance of the system over specified periods of time. It is therefore very important for system planning tools, particularly propagation prediction models, are make widely available to system designers, so that the probability and severity of signal fading occurring due to signal attenuation and absorption by hydrometeors and other atmospheric effects can be estimated.

Considerable effort has therefore been devoted in recent years to studying the propagation of millimeter waves, so that accurate attenuation prediction models can be produced to aid the design of millimetric systems. A lot of research was concentrated on quantifying more precisely the effects of rain, since rain is the most dominant attenuation factor at frequencies above 10 GHz [3].

The aim of this research is to gather sufficient propagation data so that attenuation effects can be predicted probabilistically. These probabilities can then be incorporated into system planning tools, to facilitate the development of future millimeter-wave communications systems.
A lot of work in this area has been carried out within some temperate regions like U.S.A., Japan, Europe, and Australia [4, 5].

A number of ITU-R reports and recommendations have been published containing millimeter-wave propagation data and prediction models, and these are referred to in the ETS equipment specifications for millimetric systems [6, 7].

Rain attenuation is the major factor limiting the reliability of both terrestrial and Earth-to-satellite links, operating at frequencies above 10 GHz. Short integration time rainfall rate is the most essential input parameter needed in the prediction model for rain attenuation. Statistical distribution of rain attenuation is essential for the dependable planning of microwave and millimeter wave links.

Therefore, rain-related statistics are very much important for system designer. Rain rate, drop size distribution, rain height, path length, etc. are some of rain parameters which are required for the estimation of attenuation. The height of the rain cell (rain height) is an important parameter in the calculation of Earth-to-satellite link attenuation. It is generally considered that the rain structure reaches a maximum height equal to the 0^0C isothermal. Above this, precipitation is assumed to have the form of ice, snow or melting snow [8].

Planning for millimeter wave spectrum use must take into account the propagation characteristics of radio signals at this frequency range. While signals at lower frequency bands can propagate for many kilometers and penetrate more easily through buildings, millimeter wave signals can travel only a few kilometers or less and do not penetrate solid materials very well. However, these characteristics of millimeter wave propagation are not necessarily disadvantageous. Millimeter

waves can permit more densely packed communications links, thus providing very efficient spectrum utilization, and they can increase security of communication transmissions.

However, radio signals at millimeter wavelengths suffer greatly from rain attenuation [9]; indeed, the major offender to propagation at millimeter wave is precipitation, rainfall being the principal one. It has been a common practice to express rainfall loss as a function of precipitation rate. Such a rate depends on the liquid water content and the fall velocity of the drops [10]. Rain attenuation can be obtained directly through measurement or predicted from knowledge of rain rate and drop-size distribution. It is thus possible to estimate the attenuation by means of indirect measurements performed with rain gauges, radiometers and radars.

Considering the horizontal and vertical non-uniformity of the rain structure, the radar is, undoubtedly, the leading tool for observing the spatial variation of rain intensity, thus allowing the estimation of the attenuation along the propagation path [11]. However, due to its high initial investment, high operation and maintenance costs and the difficult calibration for a direct measurement of attenuation, this method has not been widely applied. Radiometers have also been used to stimulate the measurement of slant path attenuations; nevertheless, the most common attenuation prediction methods are those based on point rainfall rate distribution.

Daily rainfall accumulations are universally recorded and hourly data are also fairly widely available by national weather bureaus [12]. This is because global national weather services are established to satisfy more traditional requirements such as those of agriculture, hydrology and forest management. But the precipitation data requirements of the radio communications community are generally more demanding than the hourly data available. The allowable outage on a microwave system resulting from combined multipath fading and rain attenuation is typically less than 60 minutes per year; therefore, fairly precise rainfall rate statistics are essential [12]. It has been determined that the use of one-minute rain rates gives the best agreement with the ITU-R stipulations for the design of microwave radio links [13]. Therefore, there is a need to convert the available one-hour rain rates measured by most national weather bureaus to one-minute data. At this one-minute conversion, it is essential to study rainfall characteristics, rain rate distribution model and raindrop size distribution model for efficient and reliable design of radio network at frequencies above 10GHz in South Africa.

1.2 Dissertation Overview

The background of this research is introduced in chapter 2. The physics and classification of rain are briefly explained. The climatic and physical features of South Africa are discussed. The characteristics of rainfall in South Africa are investigated and related to tropics and equatorial regions. Millimeter wave band and its advantage are also explained. The propagation loss and the principal causes of impairment at this band are discussed.

Chapter 3 deals with characteristics of rain rate in South Africa. The cumulative distributions of rain intensity for twelve locations in South Africa are presented based on a five year rainfall data. The rain rate having an integration time of 1-hour is converted to an integration time of one minute for the required application. The resulting cumulative rain intensities and relations between them are compared with the relevant ITU-R Recommendation P.837 [14]. Based on this work, an additional three rain zones are determined alongside the five ITU-R rain zones in South Africa. Variability of rainfall rate distribution and worst month are subsequently investigated for the twelve locations and compared with ITU-R P.581-2 [15].

In chapter 4, we look at rain rate distribution models for South Africa. The semi-empirical approach of Moupfouma and Martin is used and the results are compared with ITU-R model (Moupfouma global model). The effects of integration time on the proposed models are investigated.

The primary meteorological parameter that determines rain attenuation; that is the drop-size distribution is discussed in chapter 5. Based on the available rain rate data, Law and Parson's median equivalent diameter relation is used to estimate an equivalent diameter for the respective rain rate. The methods of measuring rain drop size and different raindrop size distribution models are discussed. The relation between diameter, rainfall rate and specific attenuation is also explained.

In chapter 6 of this research, conclusion and recommendations are given. Ideal for future work is briefly explored.

CHAPTER TWO

THE IMPACT OF RAIN ON MILLIMETERIC WAVES

In this chapter, we provide an overview of physics of rain in general. We also look into the climatic and physical features of South Africa. The precipitation effects at the millimetric band are discussed. These effects actually give us principal reason to investigate the rainfall effects on the line of sight (LOS).

2.1 PHYSICS OF RAIN

Precipitation occurs when cloud particles, which grow in complex processes like condensation and aggregation, reach such a size that their falling velocity is larger than the upward wind speed in the air. Precipitation is called rain when its particles are liquid water at ground level. Apart from complex formation in clouds, rain is basically a population of falling drops interaction with each other (collision, breakup) and with their environment (electromagnetic wave) [16].

In a first approximation, the minimum size of raindrops falling on the ground depends on vertical wind speeds in clouds. In clouds with updraugths of less than 50 cm/s, drops of 0.2 mm diameter (terminal velocity of 70 cm/s) and more will fall out. In air of 90 % humidity such a drop can fall 150 m before total evaporation and thus reach the ground. A drop of 1mm diameter can fall 40 km. Rain which mainly consists of drops of 0.1 mm diameter, is call drizzle, and is produced by low layer clouds. The maximum diameter of raindrops is about 7 mm, because larger drops will break apart during the fall [16].

Only drops of diameter of less than 0.3 mm are nearly perfect spheres at terminal (falling) velocity. Therefore for larger drops one can not unambiguously describe the shape by one length. This problem is solved by the definition of an equivalent diameter: the diameter of a sphere with same volume as the deformed drop. Falling drops of (equivalent) diameters of 0.3 to 1 mm resemble oblate spheroids. Drops larger than 1mm resemble oblate spheroid with flat based [16].

The terminal velocity is the maximum vertical velocity which a drop reaches. It is, in other words, the velocity when the gravitational force equals the drag force. Gunn and Kinzer have presented a table with terminal velocity data as a function of drop diameter as measured in the laboratory [17]. In the past, power-law expression (2.1) has been used:

$$V = aD^b \tag{2.1}$$

where V is the terminal velocity of rain drop in stagnant air and D is the drop diameter. The letter a and b are constants .The expression is applies to a very small range of diameter and thus, a more realistic representation of V is given by the following formula for a standard air pressure of $P_0 = 1013\ hPa$ [18]

$$V(D, P_0) = \begin{cases} 0; D \le 0.03\ mm \\ 4.323\,(D - 0.03\ mm);\ 0.03\ mm < D \le 0.6\ mm; \\ 9.65 - 10.3\ \exp(-0.6D);\ D > 0.6\ mm \end{cases} \tag{2.2}$$

The first expression valid for diameter less than or equal to 0.03 mm and second expression is for diameter ranges between 0.03mm to 0.6 mm. The expression is widely used in the calculation of attenuation because majority of rain drop sizes fall within 0.03 mm to 0.6 mm. This second expression had found to have a linear fit with Gunn and Kinzer results [17] .The third expression, valid for diameter greater than 0.6 mm [19] and has been widely used for larger rain drop size [20].

2.2. *Classification of rain*

Broadly speaking, rainfall can be classified into two categories, namely: Stratiform and Convective rainfall.

Stratiform precipitation results from the formation of small ice particles joined together to form bigger nuclei. The growing nuclei become unstable and as they pass through the so-called melting layer, extending from about 500 m to 1 km below the zero degree Celsius isothermal, turn into rain drops that fall down to the surface. Stratiform precipitation consists of drizzle and widespread rainfall while the convective rainfall consists of shower and thunderstorm rainfall

[21]. Drizzle distribution is associated with drops of diameter of the order of 1.0 mm and the maximum rainfall intensity is about 5 mm/h. Widespread rain is made up of raindrops with diameter range between 1.0 mm and 3.5 mm. The rainfall time duration is usually long (greater than 1.0 hour) and has a maximum rainfall intensity of 50 mm/h. Shower rainfall consists of extremely few raindrops about 2.0 mm diameter. It is of small time duration and its maximum rainfall intensity is about 150 mm/h. Thunderstorm rain distribution, on the other hand has a distribution of relatively high congestion of large drops typically greater than 3.0 mm, with a maximum rain fall intensity of 210 mm/h. These classifications are often used in the calculation of propagation parameters when their variations are examined with respect to the change of size distribution [20].

Convective precipitation is associated with clouds that are formed in general below the zero degrees Celsius isothermal and are stirred up by the strong movement of air masses caused by differences in troposphere pressure. In the process water drops are created and grow in size, until gravity precipitate them. Tropical rainfall is predominantly convective and characterized by high precipitation rates, it occurs in general, over limited extensions and for short duration of time.

Regardless of the precipitation type, rainfall is characterized by space and time variable structure constituted by cells of various dimensions that move horizontally with speed depending on the tropospheric winds and the height of the clouds [21].

Wilson A. Bentley [20] classified rain by using pellet size categorization in respect to their diameters. The table below gives the summary:

Table 2-1: Classification of rain [20]

Pellet Size category	**Diameter Range**
Very small	<0.85 mm
Small	0.85 to 1.4 mm
Medium	1.7 to 3.2 mm
Large	3.6 to 5.1 mm
Very large	>5.1 mm

It can be seen from table 2-1 that for very small size classification the diameter is less than 0.85 mm and for very large size classification, the diameter is greater than 5.1 mm.

2.3. *The Climatic of South Africa.*

South Africa occupies the southernmost portion of the African continent, stretching from the Limpopo River in the north to Cape Agulhas in the South. This is a latitudinal span of $13^0 (22^0 S \text{ to } 35^0 S)$. Longitudinally, the country reaches from 17^0E at the upper end mouth of the Orange River (in the West) to 33^0 at Ponta do Ouro in the East.

Figure 2-1: Map of South Africa. (Source [22])

Figure 2-1 [22] shows the map of South Africa. To the north, South Africa shares common boundaries with Namibia, the republic of Botswana, and Zimbabwe. Mozambique and the Kingdom of Swaziland lie to the north-east. The country is bounded by the Indian and Atlantic Ocean to the South-east and south-west respectively.

The location of South Africa has had a great influence on many aspects of its geography and development. Firstly, the fact that the country is by and large subtropical in location accounts for many features of its climate. Only a fraction of its area (the extreme northern Transvaal) falls within the tropics. Secondly, the low latitude means a small variation between summer and winter daylight periods.

The influence of environment on radio system determines the signal availability and its quality. Thus, the vegetation, topography and climatic condition of South Africa need to be studied especially for millimetric band. The subtropical location, on either side of 30 ^0S accounts for the warm temperate conditions so typical of South Africa. At the same time this position also means that it falls squarely within the subtropical belt of high pressures.

The wide expanses of ocean on three sides have a certain moderating influence on the climate. More immediately apparent, however, are the effects of the warm Agulhas and cold Benguela currents along the east and west coasts respectively. Thus while Durban (east coast) and Port Nolloth (west coast) lie more or less in the same latitude, there is difference of no less than 6 ^0C in their mean annual temperatures.

East coast air masses are warmer; they tend to be less stable and more likely to give rise to abundant rain. Thus Durban records 1000 mm of rain annually, and moist warm Indian Ocean air masses are in fact the chief source of rain for most of the country. Over the west coast, however, air masses are chilled at their base by the cold Benguela waters. Together with the strong subsidence and adiabatic heating of air in the upper layers of the offshore anticyclone, this produces a very steep and virtually permanent upper air inversion over the west coast, usually at a height of about 600 m. These conditions discourage rain-forming processes-hence Port Nolloth's meager annual total of 63 mm [23].

2.4. Characteristics of Rainfall in South Africa.

South Africa has an average annual precipitation of 502 mm, as against a world mean of 857 mm. Twenty-one percent of the country receives less than 200 mm annually, 48 percent between 200 and 600 mm, while only 31 percent records a total above 600 mm.

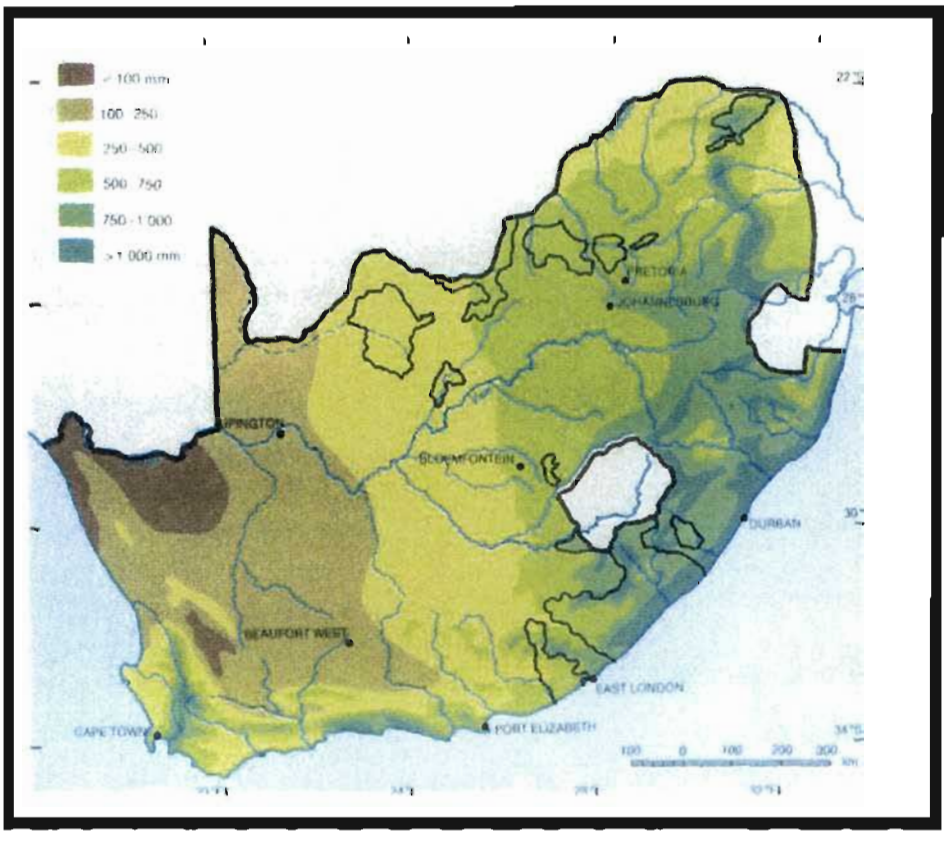

Figure 2.2: Generalised mean annual precipitation. (Source [23])

Figure 2-2 shows that the distribution of annual precipitation has two main features. Firstly, there is a fairly regular decrease over the plateau from east to west. Thus the 400 mm rainfall line divides the country into wet eastern and a dry western half. The moist Indian Ocean air masses, which are the chief source of rain over most of the country, gradually lose their moisture as they move towards the western interior. The second main feature of the rainfall distribution pattern is the strong orographic influence. The highest rainfall occurs on the windward slopes of the Cape ranges, the Drakensberg, and the eastern Transvaal escarpment.

Figure 2.3 shows the basic division between winter and summer rainfall regions (In either case more than 60 percent of the annual total is received in the half-year concerned). The winter rainfall region is a relatively small area along the Cape west and south-west coasts and has a rainfall regime of the Mediterranean type with a conspicuous winter maximum. The summer rainfall region covers most of the rest of the country. On the basis of the period of maximum rainfall it can be divided into three sub- regions.

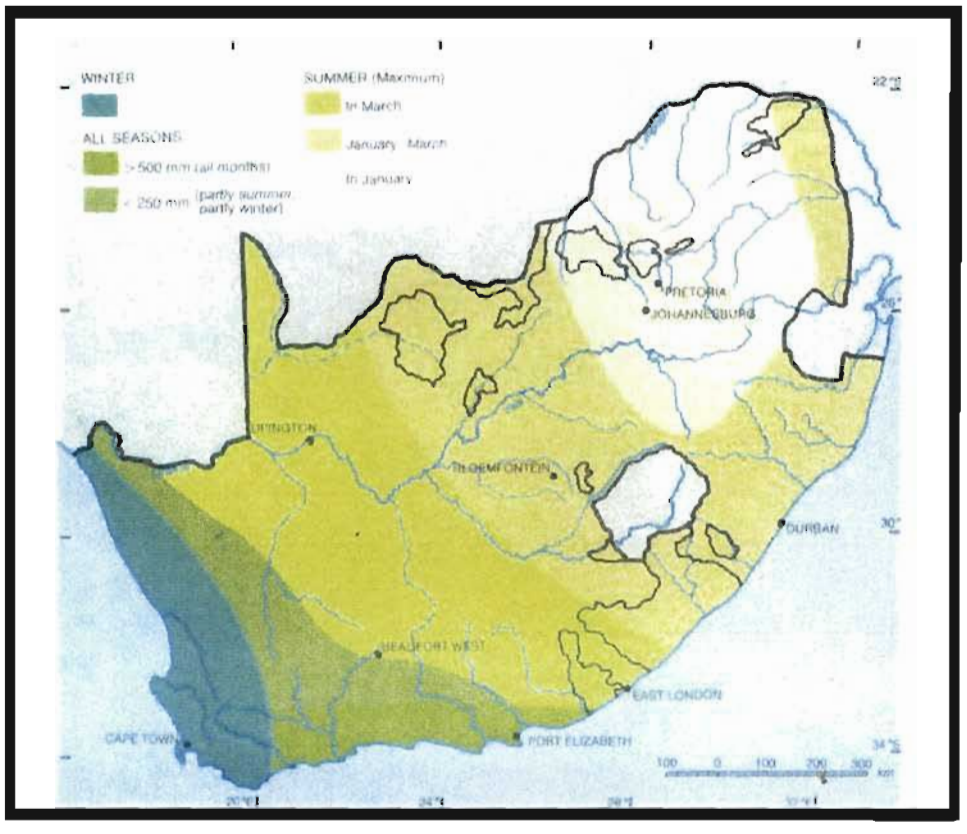

Figure 2-3: Seasonal rainfall regions. (Source [23])

Between the winter and summer rainfall regions lies a transitional area where rain come in all season .i.e. neither in winter nor in summer is more than 60 percent of the annual total recorded. There is in fact a clear double maximum, in autumn and spring respectively. This transitional area can be divided into two sub regions: a southern coastal strip with an annual total of 375 mm, and a drier inland corridor behind the coastal ranges with an annual total of 50 to 250 mm.

In the winter rainfall area, rain is often long lasting and not very intense, except along the mountains, where the orographic effect may induce heavy showers.

In the summer rainfall region, light orographc rains are common along the windward slopes of the eastern escarpment. Over most of the summer rainfall region, however, violent convection storms, accompanied by thunder, lighting, sudden squalls and often hail, is the source of most of the rainfall.

The rainfall is unreliable and unpredictable throughout the country [23]. Large fluctuations around the mean annual figure are the rule rather than the exception. Years with a below-average

figure are more common than years with an above-average total. The map shows further that the likelihood of large deviations from the normal is least in the wetter areas, i.e. the north-eastern parts of the plateau, the east and south coast and the south-western Cape. As it gets drier towards the west, the unreliability increases rapidly.

2.5. Precipitation Effects in the Millimeteric Band

The term millimeter waves generally refer to that portion of the electromagnetic spectrum between 30 and 300 GHz, corresponding to wavelengths of 10 to 1 mm [24]. Thus, as shown in figure 2-4, the millimeter wave spectrum lies between the microwaves and infrared portions. The Institutes of Electrical and Electronics Engineers (the IEEE) identifies the millimeter wave region as lying between 30 and 300 GHz [25].

Millimeter wave characteristics differ from those of microwaves and infrared as well, and it is these differences that make millimeter wave systems ideal candidates for certain application.

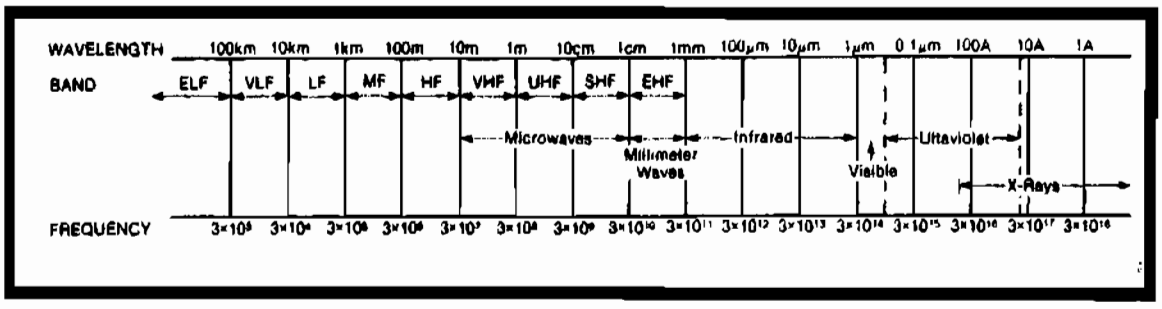

Figure 2-4: The electromagnetic spectrum. (Source [24])

2.6. Advantages and Disadvantages of Millimeter waves

The three principal characteristics of millimeter waves, short wavelengths, large bandwidth and interaction with atmospheric constituents, translate into both advantages and disadvantages depending on the application in mind.

Advantages in millimeter waves are [25, 26].

1. Smaller wavelength, which enables reduction of component size, resulting in compact systems which are desirable for missiles, satellite, and aircraft. This also allows the

achievement of narrow bandwidths, which in turn provide high immunity to jamming due to the narrow bandwidth; high antenna gain with accompanying advantages of lower peak and average power requirements. As an example of narrow bandwidths available, a 12-cm diameter aperture antenna provides a 1.8^{o} bandwidth at 94 GHz compared to 18^{o} at 10 GHz.

2. Wide bandwidths , from figure 2-5 it can be seen that the principal windows in the millimeter wave band exist at 8.6-, 3.2-, 2.1- and 1.4-mm wavelengths corresponding to frequencies of 35, 94, 140, and 220 GHz. The bandwidth available at each of these windows is extremely large, roughly 16, 23, 26, and 70 GHz, respectively. Thus all the lower frequencies, including

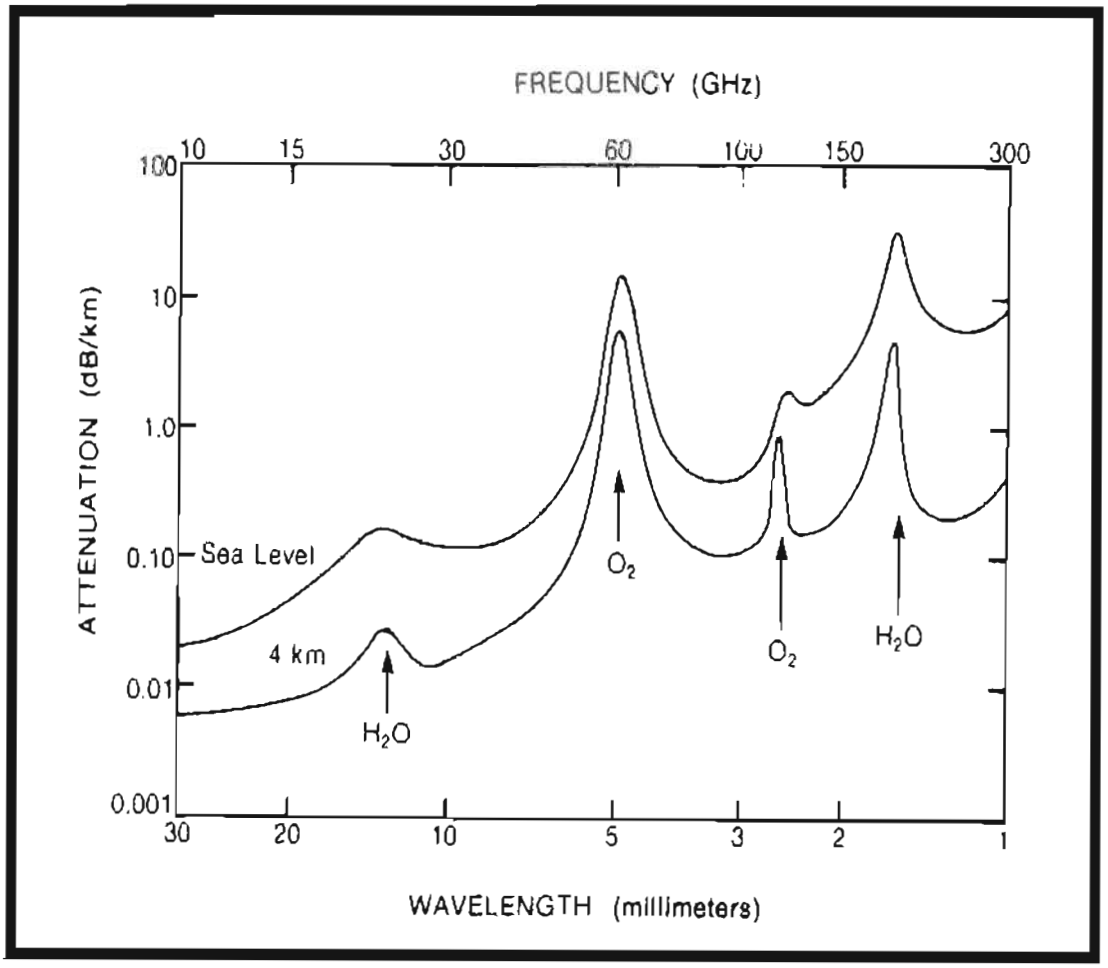

Figure 2-5: Average atmospheric absorption of millimeter waves for horizontal propagation. (Source [24])

the microwave band can be accommodated in any of these windows. Similarly, the absorption maximal or "absorption bands" at 5-, 2.5-, 1.6 mm wavelengths corresponding to 60, 119, and 183 GHz also have large bandwidths. The principal benefits of these large bandwidths include:

- High information rate capability for obtaining fine structure detail of target signature with narrow pulses or wide-band FM in radar systems and high information transmission per unit time in communication systems.
- Wide-band spread-spectrum capability for reduced multipath and clutter.
- High immunity to jamming and interference, due to large number of frequencies that can be used .this also allow multiple radar operation without interference.

Very high range resolution for precision tracking and target identification in radars and greater sensitivity in radiometers.

- Large Doppler frequency shifts from low radial velocity targets resulting in increased detection and recognition capability of slowly moving or vibrating objects.

3. Environmental interaction characteristics such as:

➢ Atmospheric attenuation and losses that are relatively low in the transmission windows compared to infrared and optical frequencies.

➢ Lower attenuation in aerosols and conditions of dust, smoke, and battlefield contaminants compared to infrared and optical frequencies.

The following two proceeding factors give millimeter waves an edge over infrared and optical frequencies.

➢ High absorption around transmission windows (relative to microwaves), which provide secure operation by selection of suitable frequencies and difficulty in long-range jamming.

➢ Low terrain scatters resulting in reduced terrain clutter and lower multipath interference.

Disadvantages /Limitations in millimeter waves are [25, 26]:

1. Smaller wavelength, resulting in:

➢ Smaller component size, increasing the need for greater precision in manufacturing, resulting in higher cost. Costs have also been high for millimeter wave components due to low production quantities. However, with the development of microstrip and dielectric waveguides, these costs are expected to decrease.

➢ Narrow bandwidths, which can be a problem in target search. Thus millimeter wave radars are not suitable for large volume search.

➢ Smaller antennas, which collect less energy in a receiving system, thereby reducing the sensitivity.

➢ Large Doppler shifts, which can be outside the receiver bandwidth.

2. Environmental interaction, causing:

➢ Limited communication range due to atmospheric attenuation (10-20 km).for an average atmosphere containing 7.5 g/m^3, the attenuation is approximately 0.06, 0.14, 0.8, and 1 dB/km at 10, 35, 94, and 140 GHz, respectively.

➢ Reduced range capability in adverse weather. However, this range attenuation due to aerosols such as fog, snow, or rain may sometimes be overcome by using higher power levels, increasing antenna gain, optimum modulation and data processing.

➢ Increasing backscatter in rain, which can mask targets. Use of moving target indication (MTI), narrow bandwidths, narrow pulse widths, and optimum operating frequencies will minimize rain backscatter effects.

➢ Poor foliage penetration, particularly in dense green foliage.

2.7. Millimeter-Wave Propagation Loss Factors

In microwave systems, transmission loss is accounted for principally by the free-space loss [27]. However, in the millimeter-wave bands additional loss factors come into play, such as gaseous losses and rain in the transmission medium. Factors that affect millimeter wave propagation are: attenuation due to rain, attenuation by fog, attenuation by snow and attenuation by atmospheric gases.

2.7.1. Attenuation due to rain.

The theory relating to attenuation and scattering of radio waves by rain is based on the calculation of the attenuation and scattering cross sections of a single raindrop [28]. In the millimeter-wave range of the radio spectrum the shape of raindrops is important, since the cross-section of the drop is comparable to the wavelength of the radio-wave. For a particular raindrop, the drop shape will depend on its size and the rate at which it is falling.

In order to model the effects of rain attenuation and scattering on radio-waves, rainfall is usually characterised by drop-size distribution, N (D), which is defined as the number of raindrops falling per cubic meter, with drop diameters, D, within a specified range. The drop-size distribution is a function of the rain rate, R, which is usually measured in millimeters-per-hour (mm/hr). Attenuation of radio waves by rain at millimeter frequencies is therefore dependent on a number of factors relating to the water particles making up the rainfall at a certain time, including the size of the raindrops, the velocity at which the drops are falling, the time of year and the drop-size distribution.

In order to predict accurately the attenuation of millimeter-waves due to rain, it is necessary to measure the rainfall occurring in a specified geographic area over periods of time, and then to accumulate the data gathered to form statistical models of the events that have occurred. The data collected can then be used to form cumulative distributions of the degrees of signal attenuation, rainfall rate, temperature and humidity occurring within a specific geographic area monthly and annually. These distributions can then be compared to average distributions for that particular geographic area, to illustrate when and by how much the measured data exceeds the average distribution for various percentages of time.

This information can then be used by system planners, to estimate averages and extremes of system performance and predict the reliability of a particular communications system under a range of geographic and meteorological conditions.

2.7.2. Attenuation by Fog

Theoretical predictions of the attenuation of millimeter-waves by fog are derived in roughly the same way as for rain. The main difference is that fog consists of a suspended mist of water drops with very small diameters [28].Radio wave attenuation by fog is therefore less significant than that of rain. In general, therefore, if a particular communication system is designed to overcome rain attenuation, then attenuation by fog will have no additional effect on the performance of the system.

2.7.3. Attenuation by Snow

Snow and hail consist of a complex mixture of water, air and ice crystals. Hence the attenuation of radio waves due to snow is considerably harder to estimate than that of rain. The problems involved in measuring radio wave attenuation due to snow are made further complicated because the shape of snow and ice crystals is very varied. Hence it is very difficult to create accurate probability distributions of snow flake sizes and shapes.

Experimental data so far indicates that the effect of snow on the propagation of millimeter-waves depends on the consistency of the snow [28]. Studies have shown that the attenuation of radio waves above 20 GHz in dry snow is less than in rain, for the same precipitation rate. Investigations into wet snow, however, have indicated that the attenuation that occurs is in excess to that of rain.

2.7.4. Attenuation by Atmospheric Gases

At higher frequencies, above 15 GHz, the attenuation due to atmospheric gases will add to the total propagation loss of a radio relay path. The attenuation here is due to absorption in uncondensed water vapour [26]. This effect is highly frequency-dependent, which means that attenuation due to atmospheric absorption is much greater in some frequency bands than in others. A band of very high atmospheric absorption occurs near 60 GHz, for instance.

In bands such as 60 GHz, where atmospheric attenuation is high, the line of sight coverage path of radio waves is severely limited. Although this may initially appear to be a disadvantage, the limited path length achievable at 60 GHz can offer considerable operating advantages to short range radio systems. This is because multiple frequency re-use over very short distances is possible. Furthermore, because systems are only transmitting at very high frequencies with very small wavelengths compact high-gain antennas can be used.

2.8. Loss In Free Space.

Loss in free space is a function of frequency squared plus distance squared plus a constant. Let's see how this relationship is developed. Consider power P_T radiated from an isotropic transmitting antenna. This transmitting antenna is a point source radiating power uniformly in all directions. Let's imagine a sphere with radius d, which is centered on that point source.

If free-space transmission is assumed, meaning transmission with no absorption or reflection of energy by nearby objects, the radiated power density will be uniform at all points on the sphere's surface. The total radiated power P_T will pass outward through the sphere's surface. The directed power density at any point on the surface of the sphere is given by [10]:

$$\text{Power density} = \frac{P_T}{4\pi d^2} \tag{2.1}$$

If a receiving antenna with an effective area A_R is located on the surface of the sphere, the total receive power P_R is equal to the power density times the area of the antenna. This is expressed as:

$$P_R = \frac{P_T \times A_R}{4\pi d^2} \tag{2.2}$$

A transmitting antenna with an effective area of A_T, which concentrates its radiation within a small solid angle or beam, has an on-axis transmitting antenna gain, with respect to an isotropic radiator, of:

$$g_T = \frac{4\pi A_T}{\lambda^2} \tag{2.3}$$

where λ is the wavelength of the emitted signal. Let's use this antenna in place of the familiar isotropic radiator. The receive power relation in equation (2.2) now becomes:

$$P_R = \frac{P_T (4\pi A_T A_R)}{4\pi d^2 \lambda^2} \tag{2.4}$$

We rearrange equation (2.4) to describe the transmitting and receiving antennas in terms of their gains relative to an isotropic antenna. This then gives us:

$$P_R = P_T (4\pi A_T / \lambda^2)(4\pi A_R / \lambda^2)(\lambda / 4\pi d)^2 \quad (2.5a)$$

$$= P_T (g_T)(g_R)(\lambda / 4\pi d)^2 \quad (2.5b)$$

where $g_R = 4\pi A_R / \lambda^2$ is the receiving antenna gain referenced to an isotropic radiator. Restating in decibels, the ratio of P_T to P_R is:

$$10 \log (P_T / P_R) = 20 \log (4\pi d / \lambda) - 10 \log g_T - 10 \log g_R \quad dB \quad (2.6)$$

The distance- and frequency-dependent term in equations (2.5a) and (2.5b) is called the free-space path loss between isotropic radiators. Expressed in decibel form, the free-space loss is:

$$FSL_{dB} = 20 \log\left(\frac{4\pi d}{\lambda}\right) \quad (2.7)$$

or

$$FSL_{dB} = 21.98 + 20 \log(d / \lambda) \quad (2.8)$$

Converting λ to the more familiar frequency term and using kilometers (km) for distance and megahertz (MHz) for frequency, we have:

$$FSL_{dB} = 32.45 + 20 \log D_{km} + 20 \log F_{MHZ} \quad (2.9a)$$

If D is measured in meters, we have:

$$FSL_{dB} = -27.55 + 20 \log D_m + 20 \log F_{MHZ} \quad (2.9b)$$

Returning to equation (2.8), substitute λ for D. This means that if we go out one wavelength (λ) from an antenna, the loss is just under $22\,dB$. These free-space loss formulas are useful on point-to-point links assuming no nearby obstacles and clear weather. The ITU-R organization in CCIR Rec.525.1 provides the following formula to calculate field strength on point-to-point area links:

$$E = \sqrt{\frac{30p}{D}} \tag{2.10}$$

where E is the root mean square (rms) field strength, in volts per meter; p is the isotropically radiated power (EIRP) of the transmitter in the direction of the point in question, in watts; and D is the distance from the transmitter to the point in equation, in meters. Equation (2.10) is often replaced by equation (2.11), which uses practical units:

$$E_{mV/m} = 173\sqrt{\frac{P_{kw}}{D_{km}}} \quad \text{(linear polarization only)} \tag{2.11}$$

It should be noted that there is no frequency term in the above equation.

2.9. Summary of Chapter Two.

In this chapter, the following points have emerged; firstly, a millimeter wave is a portion of electromagnetic spectrum between 30 and 300 GHz. Its characteristics differ from those of microwaves and infrared and it is these differences that make millimeter wave systems ideal candidates for certain applications such as LOS radio link and Earth-to-satellite path. It offers advantages such as smaller wavelength length which encourages miniaturization of equipment and components, wide bandwidths which are valuable in supporting application such as high speed data transmission and video distribution.

However, successful design of any millimeter wave system requires a good knowledge of millimeter wave propagation characteristics in free space under various environmental conditions such as attenuation due to rain, attenuation by fog, attenuation by snow, and attenuation by atmospheric gases.

Secondly, millimeter waves experience significant attenuation due to precipitation, in particular rain, because of absorption and scattering. Attenuation by rain starts to become important at frequencies exceeding 10 GHz, and by the time the range that interest us here is reached, it has become the dominant factor determining link availability. This pushes rain very much to the fore

in system-performance analysis. Compared with liquid rain, the effects of atmospheric, ice and cloud are much less.

Various statistical models describing the effects of rain and other hydrometeors on the transmission of radiowaves have been developed in Europe. The most widely accepted rain attenuation models for the planning and design of line-of-sight radio systems are summarised in ITU-R Report 721-2, "Attenuation by hydrometeors, in particular precipitation, and other atmospheric particles"[7]

The spatiotemporal pattern of heavy rain occurrence is highly variable and unpredictable. Thus attenuation due to rain must be considered a random process, inherently probabilistic in nature and statistically dependent on carrier frequency, geographic location, climate, local terrain, season, rainfall rate , and so on. The climatic conditions in South Africa generally range from Mediterranean in the south- western corner of the country to temperate in the interior plateau, and subtropical in the northeast. A small area in the northwest has a desert climate. Rainfall generally occurs during summer (November through March), although in the southwest, around Cape Town, rainfall occurs in winter (from June through August).Climatic conditions vary noticeable between east and west, largely in response to the warm Agulhas ocean current, which sweeps southward along the Indian Ocean coastline in the east for several months of the year, and the cold Benguela current, which sweeps northward along the Atlantic Ocean coastline in west. These two currents contribute to rainfall distribution across the country.

CHAPTER THREE

CHARACTERISTICS OF RAINFALL RATE IN SOUTH AFRICA.

The cumulative distributions of rain intensity for 12 locations in South Africa are presented in this chapter based on 5-year rainfall data. The rainfall rate having an integration time of 60 minutes is converted to the ITU-R recommended integration time of 1 minute for Durban in South Africa. Consequently, values of coefficients a and b so determined are used to convert 60-minute into 1-minute rainfall rates for other regions of South Africa. The resulting cumulative rainfall rate and relations between them are compared with the relevant ITU-R Recommendation-P837. Based on this work, additional three rain zones are determined alongside the five ITU-R rain zones in South Africa [30].

The cumulative distributions for rainfall rate for individual worst months and average years are observed. The comparison of obtained distributions for average year (AY) and average worst month (AWM) with relevant recommendation ITU-R were carried out. The relation between AY and AWM were obtained for the 12 locations.

3.1 Rain Statistics Measurement In South Africa

Rainfall is a natural and time varying phenomenon. There are seasonal and year-to-year variability of the rainfall rate distribution. In a measurement campaign spearheaded by URSI, annual cumulative distribution of rain rate has been obtained at several locations in the tropical and sub-tropical regions in the world. In India, Sakar et al have produced the Reference Data Manual for rainfall rate distribution over the Indian sub-continent, making use of the heavy rainfall data of 5 minutes and 15 minutes available at 35 different geographical regions in India [31]. The rapid response rain gauges with 10-second integration time were used to measure the rain rate in Delhi, Shillong, Calcutta, Bombay and Tirupati. The resulting rain rates at 0.01% probability (denoted as $R_{0.01}$) are 130 mm/h for Shillong, 128 mm/h for Calcutta, 130 mm/h for Bombay, 120mm/h for New Delhi, and 80 mm/h for Tirupati [31].

At the same time, a rain rate measurement campaign in Africa in 1994 covered Cameroon, Nigeria and Kenya. Although the total rain accumulation was highest in Cameroon, the rain rate exceeded 0.01% of the time were comparable at Doula in Cameroon and Ile-Ife in Nigeria. The rainfall cumulative distributions in Doula in Cameroon and Nairobi in Kenya showed that the rain climate was not well described by the ITU-R predictive distributions [31]. Ajayi and Ezekpo used the Rice-Holmberg technique to predict short integration time (one-minute) rainfall rate from long- term precipitation data from 37 stations in Nigeria over a period of 30 years [31]. Adimula et al compared the cumulative rainfall rate distribution obtained at Ilorin and Ile-Ife (Nigeria), Belem (Brazil), and Brazzaville (Congo) with the ITU-R rainfall rate distribution; while measurements in Brazil showed that ITU-R recommended distribution overestimate the measured distributions for all sites [31].

As a result of the rapidly varying nature of rainfall at a given point, the cumulative rainfall rate distribution measured is dependent on the sampling time of the rain gauge. Since in radio wave prediction techniques, an integration time of one minute is used, Segal has defined a conversion factor, $\rho_\tau(P)$ for converting data obtained with a gauge having an integration time of τ minutes to equivalent one-minute statistics, as follows [12]:

$$\rho_\tau(P) = \frac{R_1(P)}{R_\tau(P)} \tag{3.1}$$

where R_1 and R_τ are the rainfall rate exceeded, with equal probability P, for the two integration times. The factor $\rho_\tau(P)$ is also given by the power law [12]:

$$\rho_\tau(P) = a.P^b \tag{3.2}$$

over the range $0.001\% \leq P \leq 0.03\%$, with a and b being constants that depend on the climatic zone. Watson et al [32] considered the conversion factors C_R and C_e for rain gauge integration times in the range of 10s to 60 min, given by:

$$C_e(R) = \frac{e_T}{e_\tau}$$
$$C_R(t) = \frac{R_T}{R_\tau} \tag{3.3}$$

where C_e refers to the ratio of the exceedances (with the same probability P) for a given rain rate R measured using gauges with integration times T and τ; $C_R(t)$ refers to the ratio of rain rates exceeded for a given percentage of time t as measured by rain gauges with integration times T and τ. Here, $C_R(t)$ depends on the percentage of time considered [13, 32]. The conversion factors C_R and C_e obtained at Ile-Ife in Nigeria for the measurement period September 1979 to December 1981 using the rainfall rate data obtained from a fast response rain gauge with an integration time of 10 seconds are based on Watson's method [32]. It has also been found that a power law relationship exists between the equiprobable rainfall rates of two integration times. The power law relationship is given by [31]:

$$R_\tau = aR_T^b \tag{3.4}$$

where R is the rain rate, τ is the integration time at which the rain rate is required, and T the integration time at which the rain rate is available. Flavin [33] also sought a direct and universal expression between 1-minute and 5-minute rainfall rates by examining the cumulative distributions for four locations in Europe, four in North America and five in Australia. From a scatter plot of resulting data points a simple power-law fit was produced giving:

$$R_1 = u.R_5^v \tag{3.5}$$

where R_1 and R_5 are the 1-minute and 5-minute rainfall rates exceeded with equal probability, u and v are the regression coefficients [12]. The results obtained between 1-minute and 5-minute and 6-minute integration times at Ile-Ife have been compared with the results obtained by Flavin, and the following relationships were established [13]:

$$R_1 = 0.991R_5^{1.098} \quad \text{(Ajayi \& Ofoche, Ile-Ife) [13]}$$

$$R_1 = 0.991R_6^{1.054} \quad \text{(Flavin, Austr, USA, Europe) [33]} \tag{3.6}$$

where R_1 is the 1-minute rain rate, R_5 is the equiprobable 5-minute rain rate value, and R_6 is the equprobable 6-minute value. The coefficient a may not be very dependent on climate, while the dependence of b on climate may require further investigation [13].

3.2 *Effect Of Integration Time On Rain-Rate Statistics*

From the 5-year rain rate data measured with an integration time of 60 minutes for 12 different locations in South Africa, the Segal and the Ajayi approaches were used to determine the conversion factor and to convert from 60-minute integration time to an effective 1-minute integration time. As noted before, a rain gauge with 1- or 2-minute time resolution resolve the small but significant cells, while gauges with longer averaging time miss the peak rain rate values [31].

The rain rate data of equalpropable at different integration time 1 minute and 60 minutes in Durban are compared by using equations (3.1) and (3.2):

$$\log\left(\frac{R_{1\min}}{R_{60\min}}\right) = \log a + b\log P \tag{3.7a}$$

Figure 3-1 shows straight line with expression give by:

$$y = mx + c \tag{3.7b}$$

where $y = \log\left(\frac{R_{1\min}}{R_{60\min}}\right)$, $m = b$, $x = \log P$, and $c = \log a$

From these, the power law relationship was determined for South Africa. The coefficients a and b were determined for Durban in South Africa. P is the percentage of time for which rain rate is exceeded. This was then used to generalize for other locations in South Africa. Therefore, the conversion factor obtained is used on the Segal power law relationship in equation (3.2). This

result has a linear scatter plot of data points, in which a simple power law fit is achieved. Therefore for Durban in South Africa, the relationship is determined from the figure as [30]:

$$R_{1\min} = 9.228 R_{60\min}^{0.8207} \tag{3.7c}$$

Table 3-1: Coefficients for $R_\tau = aR_T^b$ for τ = 1min (based on [13] and measurements)

Integration time T(min)		**Value of Coefficient**	
Station	T	a	b
Ile-Ife	2	0.872	1.055
Ile-Ife	5	0.991	1.098
Ile-Ife	10	1.797	1.016
Ile-Ife	20	4.311	0.853
Ile-Ife	60	11.565	0.798
Durban	60	9.228	0.8207

Table 3-2: values of Equiprobable rain rates for different Integration times for probabilities of 0.1% or less.

% of time rain rate was exceeded	**1 min (mm/h)**	**60 min (mm/h)**
0.1	68.98	11.6
0.08	74.78	12.8
0.06	85.89	15
0.05	88.89	15.8
0.04	92.57	16.6
0.03	108.75	20.2
0.02	129.54	24
0.01	138.83	27.2
0.005	148.8	29.6
0.002	152.92	30.6

Table 3-3: Climatic Zone Classification in South Africa (source: South Africa Weather Service)

Locations	Latitude South	Longitude East	Climatic Regions (SAWS)
Durban	29°.97'	30°.95'	Coastal Savannah
Richards Bay	28°.78'	32°.02'	Coastal Savannah
Cape town	33°.97'	18°.60'	Mediterranean
Brandvlei	30°.47'	20°.48'	Desert
East London	33°.03'	27°.83'	Savannah
Ladysmith	28°.57'	29°.77'	Inland Temperate
Newcastle	27°.77'	29°.98'	Inland Temperate
Vryheid	27°.78'	30°.80'	Inland Temperate
Pretoria	25°.73'	28°.18'	Temperate
Bloemfontein	29°.10'	26°.30	Steppe
Ulundi	28°.30'	31°.42'	Inland Savannah
Pietermaritzburg	29°.63'	30°.40'	Inland savannah

Thus, the Durban coefficients of a and b in equation (3.7) are used to convert other 60-minute rainfall rate data from other locations in South Africa to an effective 1-minute integration time [30,13]. The results obtained between 1-minute and 60-minute integration time rain rates in Durban from January 2000 to December 2004 were compared with those obtained by Ajayi and Ofoche [13]. The latter examined the effective 1-minute, 2-minute, 5-minute, 10-minute, and 20-minute cumulative distributions of rainfall rate for Ile-Ife, Nigeria from September 1979 to December 1981.

Table 3-1 shows a comparison between the Durban coefficient of a and b and coefficients obtained for Ile-Ife in [13]. In order to compare the values, linear extrapolation gives a = 11.565 for Ile-Ife for 60-minute integration time, while a logarithmic extrapolation gives b = 0.7982. These are quite close to the Durban values in (3.7). Table 3-2 shows the values of equiprobable rainfall rate for integration time of 1-minute and 60-minute for occurrence probability of 0.1% or less. The table confirms the power law relationship between equiprobable rain rates of two different integration times. Figure 3-2 shows the cumulative distribution of rain rate for 60-minute and 1-minute.

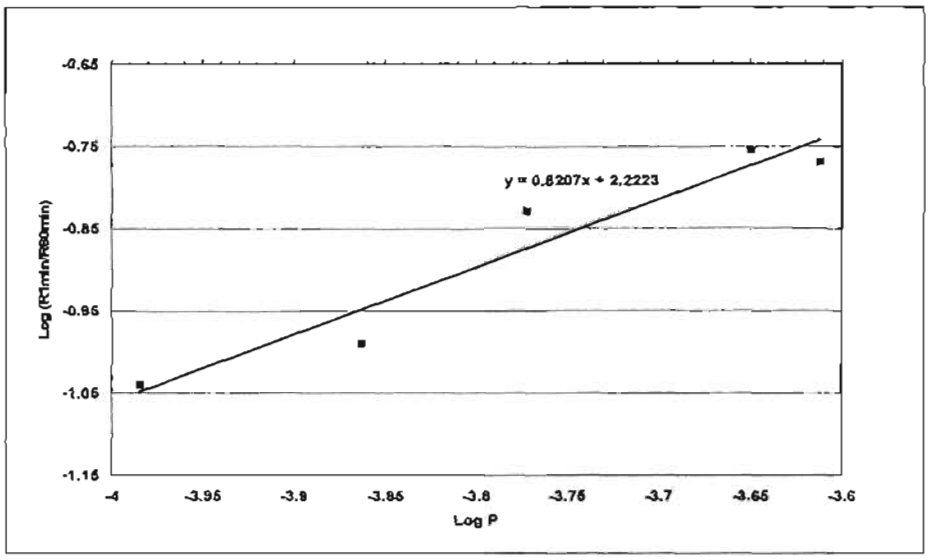

Figure 3-1: Determination of coefficient a and b for Durban, South Africa

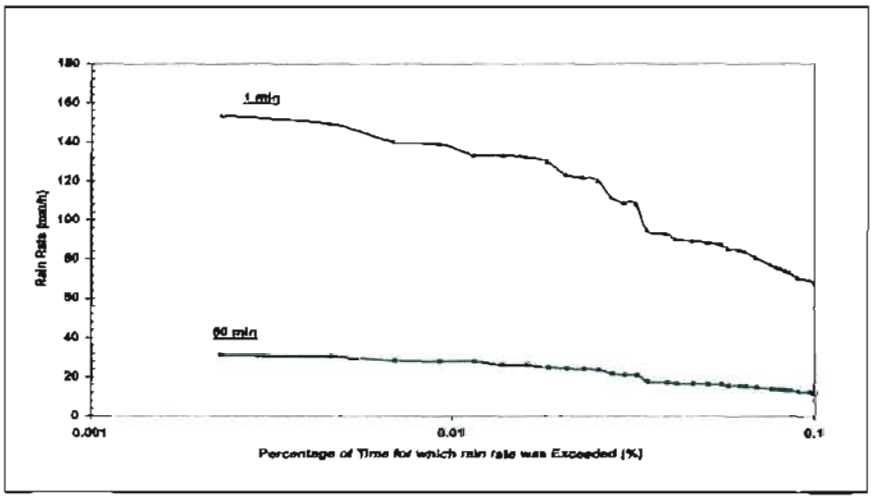

Figure 3-2: Cumulative Distribution of Rain-rate for Durban for 1-min and 60-min integration times

3.3 Comparison of Rain Rate Statistics for South Africa

We compare the rainfall rate statistics for South Africa over a period of 5 years for 12 locations. The locations are then classified according to the South Africa climatic regions. Table 3-3 shows the locations where precipitation data was obtained from South African Weather Service

(SAWS), as well as the corresponding climatic categorization. The yearly 1 min integration time rainfall rate statistics at 0.01% exceedance of the time for each location within the same climatic regions are compared in Figures 3-3, 3- 4 and 3-5. These give the variation in the annual rain intensity for a period of 5 years. It has been observed that the main factors that cause the differences in the annual rain intensities in South Africa are the influence of the South Atlantic Ocean, Indian Ocean, and the topography [34]. The combinations of these effects cause the differences in the annual rain intensities among the South Africa climatic regions. The rainfall is unreliable and unpredictable throughout the country. Large fluctuations around the regions are compared in figure 3-4; 3-5 and 3-6.These give the variation in the annual rain intensity for a period of 5 years. Large fluctuations around the mean annual figure are the rule rather than exception [34].

Tyson observed that over the period of 1910-1972, much of the summer rainfall area of South Africa experienced a quasi 20-year oscillation rainfall [34]. The rainfall spectrum shows a clear peak at about 20 years as well as peaks in 2-3 and 3-4 year bands [22]. In figure 3-3, Richards Bay consistently records the highest yearly rainfall rate in the initial three years (2000-2002),

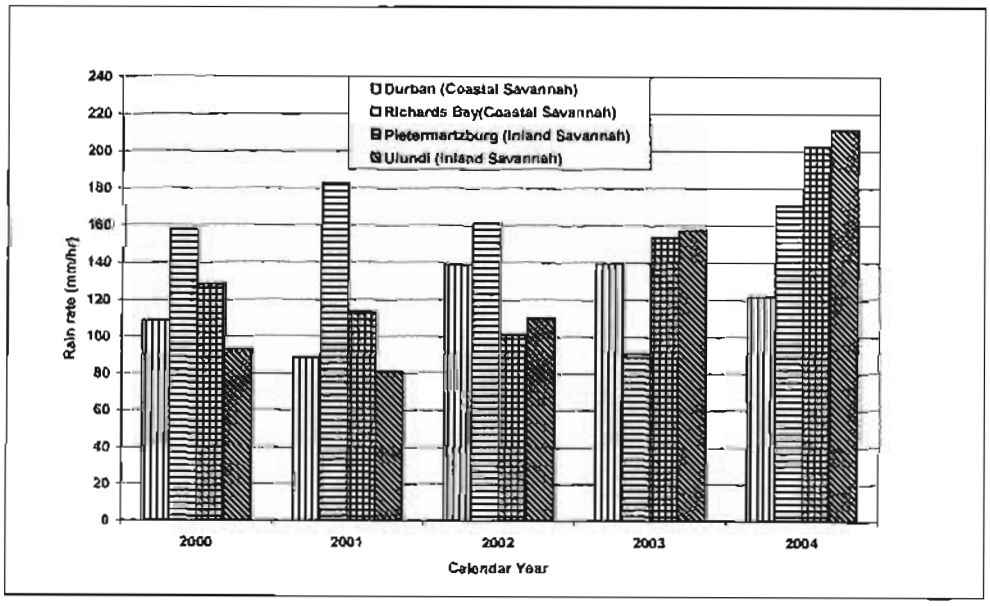

Fig 3-3: Variation in the Annual Rain Intensity (mm/h) Exceeded for 0.01% of the Time for South Africa (Coastal & Inland Savannah Regions)

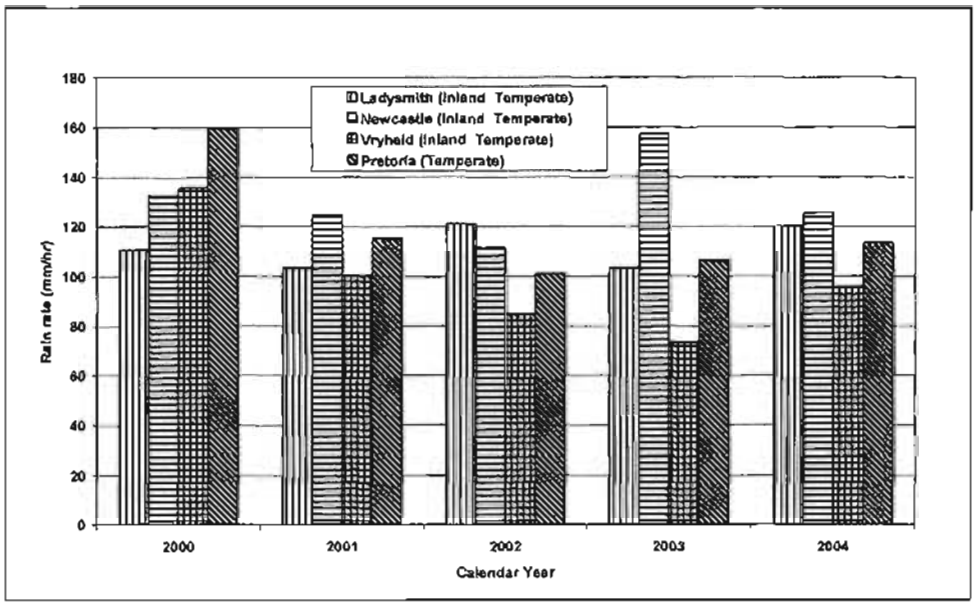

Fig 3-4: Variation in the Annual Rain Intensity (mm/h) Exceeded for 0.01% of the Time for South Africa (Temperate and Inland Temperate Regions)

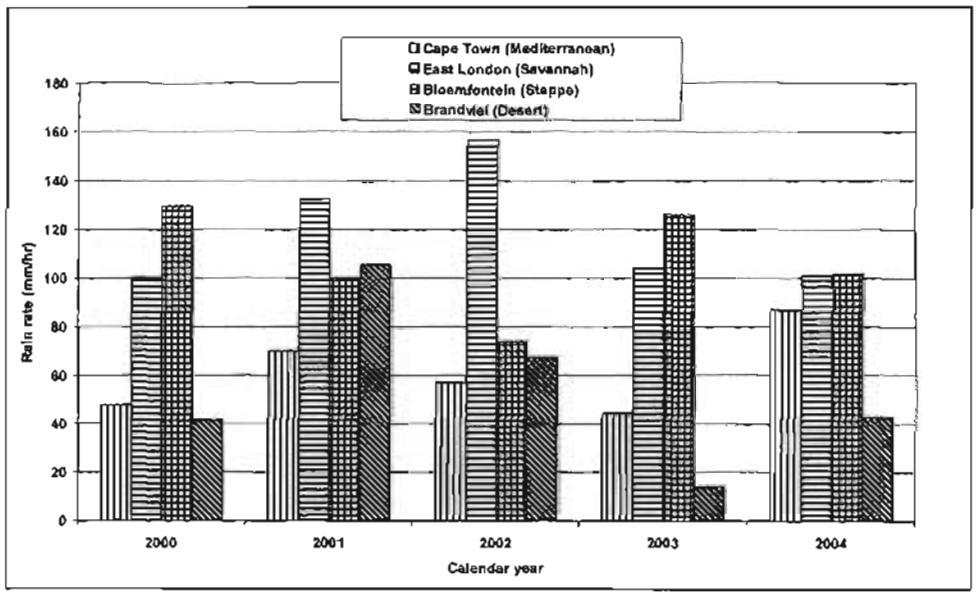

Fig 3-5: Variation in the Annual Rain Intensity (mm/h) Exceeded for 0.01% of the Time for South Africa (Mediterranean, Steppe, Savannah & Desert Regions)

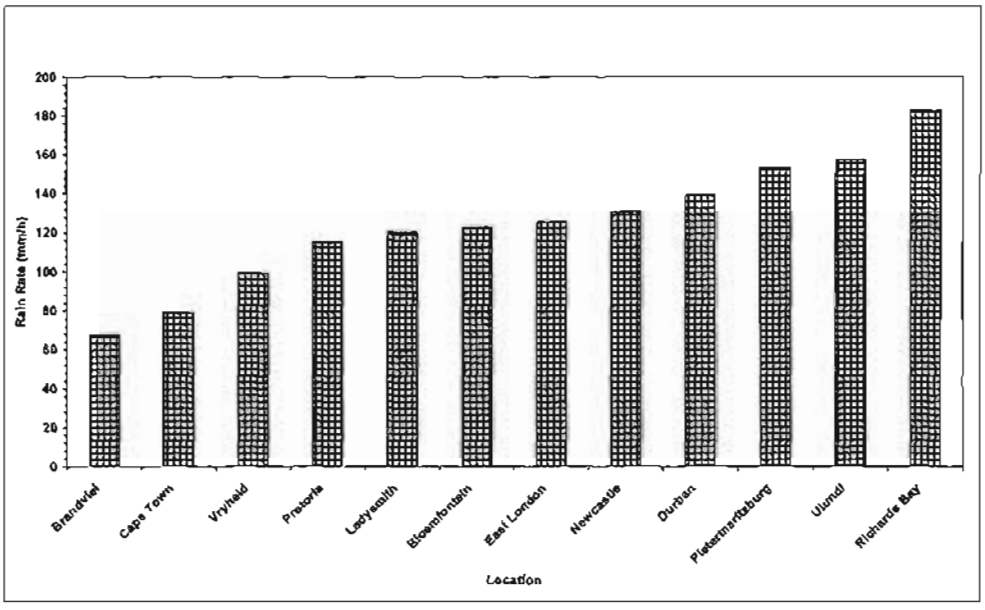

Fig 3-6: Comparison of the 5-year Rain Intensity (mm/h) for 12 locations in South Africa Exceeded for 0.01% of the Time.

with a peak of 182.66 mm/h in 2001. Over these three years, Durban recorded the second highest of 139.66 mm/h in 2002, while Pietermaritzburg has a high value of 126 mm/h in 2000 and 115 mm/h in 2001. Despite the fact that Durban and Richards Bay lie in the same climatic region, there are differences in the rain intensity from year to year.

The highest rainfall rate in the zone was recorded in the year 2004 with values 211.38 mm/h and 202.16 mm/h for Ulundi and Pietermaritzburg respectively. For three consecutive years, 2002-2004, Ulundi recorded a progressive increment in rain rate, as is also applicable to Pietermartzburg. For two consecutive years 2000-2001, a decrement in rainfall rate was recorded in both locations. A measure of differences is also noticed between the two locations in this climatic region but the differences are not as large as that of the Coastal Savannah. In Figure 3-4, we plot yearly rain rate variations for temperate and inland temperate regions. We observed that Newscastle and Pretoria recorded the two highest rates of 160mm/h (in 2000) and 157mm/h (in 2003), respectively. Veryheid is seen to record the lowest rates in this category, with a minimum rate of 76mm/h in 2003.on the other hand, the rain intensity in Ladysmith appears to be roughly uniform over four years 2001-2004, with a mean value of 103mm/h. As already stated, Pretoria

has a high rate of 160mm/h in 2000, while the rain intensities for 2001 and 2004 are quite close (115mm/h and 113mm/h, respectively), with the corresponding values for 2002 and 2003 also remaining almost the same at 101mm/h and 106mm/h, respectively.

Finally, in Figure 3-5, we compared four different climatic zones, namely: Mediterranean, Savannah, Steppe and dessert. East London in the savannah zone recorded the highest two rates over the five years, namely, 133mm/h in 2001 and 157mm/h in 2002. This is followed by Bloemfontein in the steppe zone, which records two similar highs in 2000(130mm/h) and 2003(127mm/h). Note that there is a discernible periodicity for Bloemfontein (with almost similar rates in 2000 and 2003, followed by similar ones in 2001 and 2004) and Cape Town. However, there is no obvious pattern for East London and Brandvlei (desert region).Cape Town which lies in the Mediterranean region of South Africa has its highest rain intensity of 87.04mm/h in the year 2004. Rain intensities in the other years are relatively low. Rain rate in the year 2000 and the year 2003 are almost of the same value (47.7mm/h and 44.5mm/h respectively). It can be observed that the rain intensities in Cape Town for the period of 5 years appear to have varied rain intensities as the year changes.

East London has its highest rain rate of 156.97mm/h recorded in year 2002.Year 2003 and 2004 appears to have the same rain rates value of 103.2mm/h and 100.72mm/h respectively. The lowest rain rate was recorded in the year 2000 at 99.83 mm/h. Bloemfontein which lies in the steppe region of South Africa has its maximum rain rate of 129.54 recorded in the year 2000. It can also be seen that the rain rate gradually decreased from year 2002. In year 2003, there is a rise in the rain rate value which is almost the same as that recorded for the year 2000, and for year 2004 the rain rate value decreases again to a value as close as the one recorded for the year 2001. Brandvlei which lies in the desert region of South Africa is seen to have an irregular and unpredictable type of rain intensity. On average Brandvlei is seen to have low rain intensities as compared to other climatic regions in South Africa. Brandvlei has its highest peak of rain intensity of 105.2 mm/h recorded in the year 2001 and lowest rain rate recorded in the year 2003 with 13.67mm/h.It is also observed that year 2000 and 2004 have almost identical rain rate values of 41.25 mm/h and 42.34 mm/h respectively.

The 5-year rain statistics with a 1minute integration time for the 12 locations in different climatic regions at 0.01% exceedance of the time are compared in Figure 3-6. It is seen that Richards Bay which lies in the coastal savannah has the highest rain intensity, followed by Ulundi,

Pietermaritzburg and Durban. Ulundi and Pietermaritzburg lie in the Inland area of Coastal Savannah region. The high rain peaks that occur in these areas are mostly due to Indian Ocean influence in the region. The moist Indian Ocean air masses which are the chief source of the rain over most of the countries gradually losses their moisture as they move towards the western interior. The very lowest rain fall occur on the west cost with, Brandvlei which is found in the desert area showing the lowest rain intensity .Cape Town which lies in the Mediterranean climate is seen to have low rain fall intensity, similar to that of the Brandvlei which lies in the desert region of South Africa. This is because Cape town is situated towards the western coast of South Africa and its rain fall mostly occur during winter (June through August) as against other places in South Africa which have their rain fall during summer (November through March)[23]. We can conclude that the north –eastern area of South Africa (which has the coastal Savannah and Inland Savannah climate zones) have higher rainfall rates than the north-western parts (which have Mediterranean and desert climate zones) [30].

3.4. Cumulative Distribution of Rain Intensities

Cumulative distributions (CD's) of 5yrs 1min rain intensities for each climatic region in South Africa are plotted in figure 3-7. The obtained cumulative distribution is based on rain intensities and percentages of time. The higher the rain intensity the lower the correspond percentage of time recorded and the lower the rain intensity the higher the percentage of time. The analysis is done for a single site in each of the eight climatic regions in South Africa.

The range of rain rate can be evaluated by estimating the difference between rain rates at a certain percentage of time it is exceeded. For Durban, at the higher time percentage of 0.1%, the rain rate recorded is 68.98 mm/h, while at the lower time percentage of 0.01%, the rain rate is 138.83 mm/h. The rain rate margin is therefore 69.85 mm/h. For Petermariztburg at 0.1% the observed rate is 79.55 mm/h, and at 0.01%, the rate is 152.92 mm/h; thus the margin is 73.37 mm/h. Similarly, Newcastle records 63.07 mm/h at 0.1%, and at the lower time percentage of 0.01%, the rate is 130.39 mm/h; this results in a difference of 67.32 mm/h.

In the case of Pretoria, the distribution shows that at 0.1% the rain intensities is 61.07 mm/h while at 0.01% it is 114.90 mm/h; thus resulting in a difference of 53.83mm/h. For Cape Town, we can see that at the higher time percentage of 0.1% the rain intensity is 37.95 mm/h while at the lower

time percentage of 0.01% the rain intensity is 78.60 mm/h. The rain intensity difference is 40.65 mm/h.

The difference is almost very close to that of Brandvlei. For East London, the time percentage of 0.1 % has a corresponding rain intensity of 61.07 % mm/h, and at 0.01 % the rain intensity is 125.27 mm/h. The difference in rain intensity between 0.1 % and 0.01 % is 64.20 mm/h. At the higher time percentage of 0.1 % the rain intensity is similar to Pretoria. In Bloemfontein at higher time percentage of 0.1 % the rain intensity is 56.01 mm/h, while the lower time percentage has value of 122.70 mm/h. the difference between higher and lower time percentage recorded 66.69 mm/h rain intensity. Finally, for Brandvlei, the lowest rain intensity is observed at both higher and lower time percentages. At higher percentage of 0.1% the rain intensity is 25.19 mm/h and lower time parentage of 0.01% is 67.02 mm/h. The rain intensity difference between higher and lower time percentages is 41.83 mm/h, which is almost quite close to the difference in Cape Town.

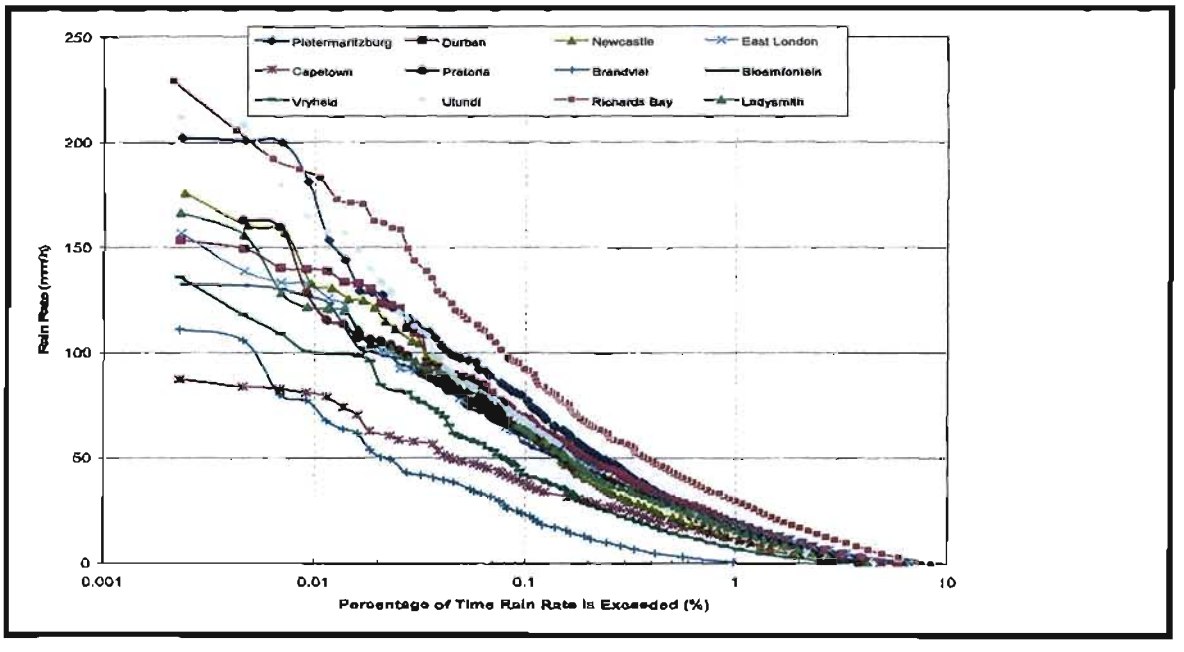

Fig 3-7: Cumulative Distribution of Rain Intensities for an Average of 5 years

3.5 *Variability of rainfall rate Distribution for South Africa*

Rain occurrences are randomly distributed in time and space. There is, therefore, month-to-month, seasonal and year-to-year variability of the rainfall rate distribution. The rainfall rate is more important in estimation of the effect of rain induced attenuation; it thus needed in this work to study the changes.

The seasonal variations of rainfall rate obtained in 12 locations are shown in figure 3-8a to 3-8l respectively for four climatologically seasons. The period between January and March (summer period) normally have highest distribution. This period is characterized by higher rainfall rate with intense rainfall than the other seasons. In the summer rainfall region, light orographic rains are common along the windward slopes of the eastern escarpment. Over most of the summer rainfall region, however, violent convection storms, accompanied by thunder, lightning, sudden squalls and often hail, are the source of most of the rainfall. The period between July and September (winter period) is characterised by often long lasting and not very intense, except along mountains, where the orographic effect may induce heavy showers. Between the winter and summer rainfall regions lies a transitional area where rain comes in all seasons.

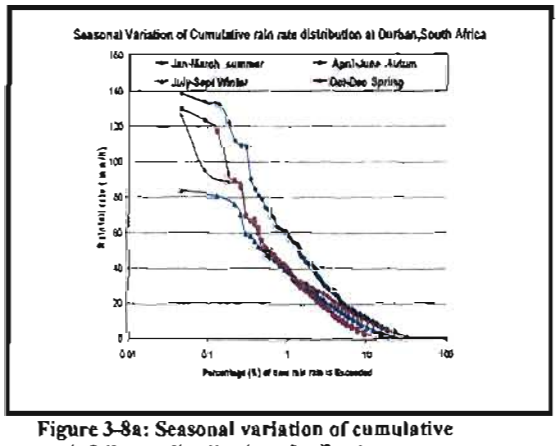

Figure 3-8a: Seasonal variation of cumulative rainfall rate distributions for Durban

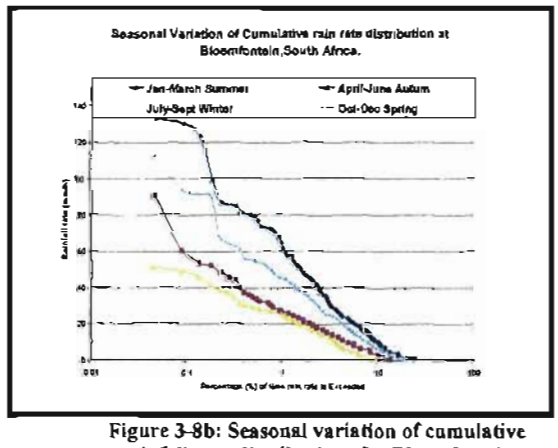

Figure 3-8b: Seasonal variation of cumulative rainfall rate distributions for Bloemfontein

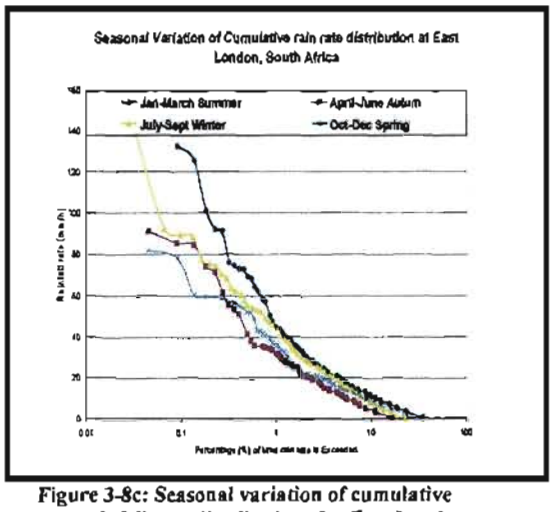

Figure 3-8c: Seasonal variation of cumulative rainfall rate distributions for East London

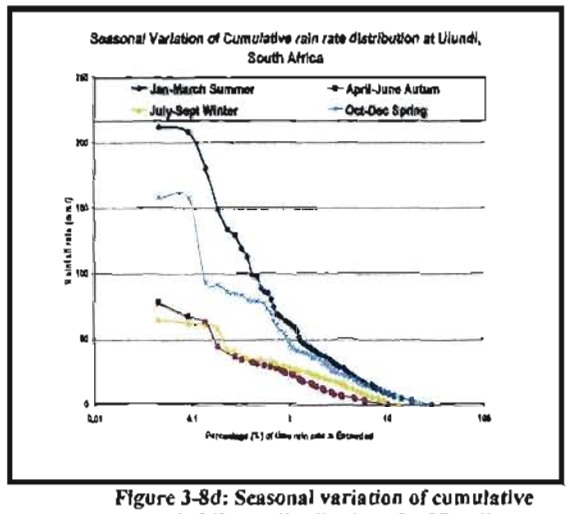

Figure 3-8d: Seasonal variation of cumulative rainfall rate distributions for Ulundi

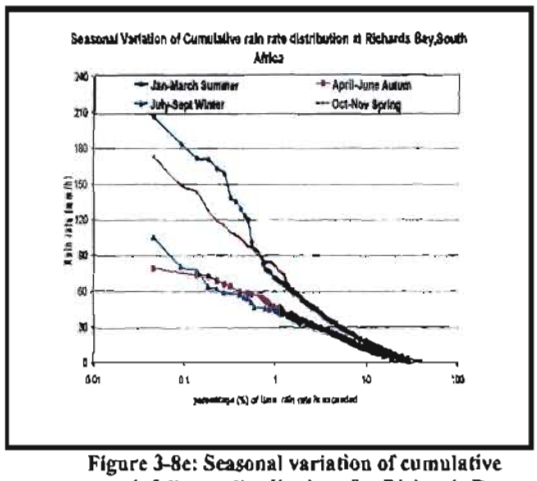

Figure 3-8e: Seasonal variation of cumulative rainfall rate distributions for Richards Bay

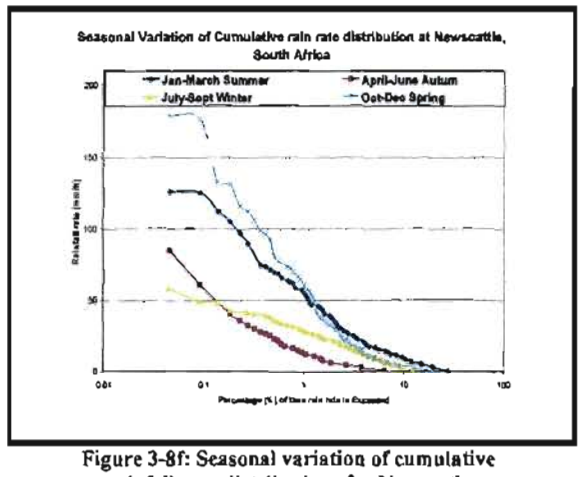

Figure 3-8f: Seasonal variation of cumulative rainfall rate distributions for Newcastle

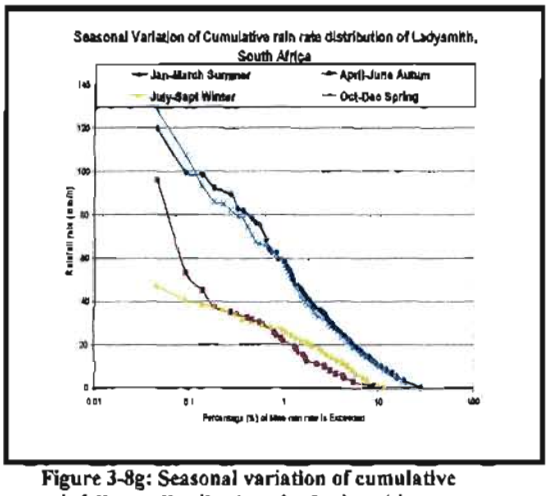

Figure 3-8g: Seasonal variation of cumulative rainfall rate distributions for Ladysmith

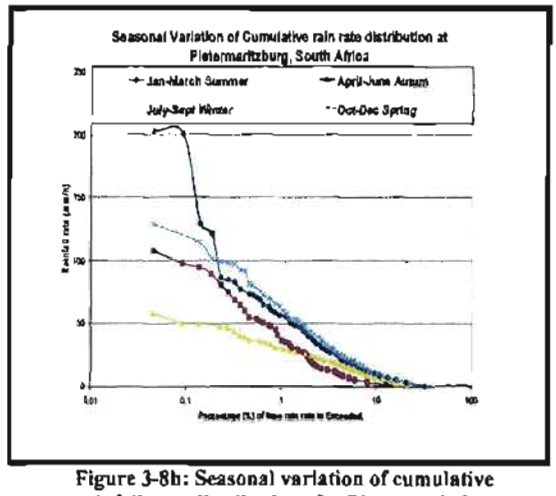

Figure 3-8h: Seasonal variation of cumulative rainfall rate distributions for Pietermaritzburg

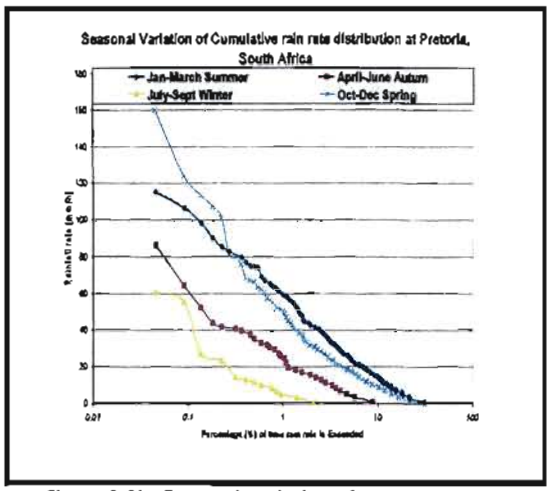

Figure 3-8h: Seasonal variation of cumulative rainfall rate distributions for Pretoria

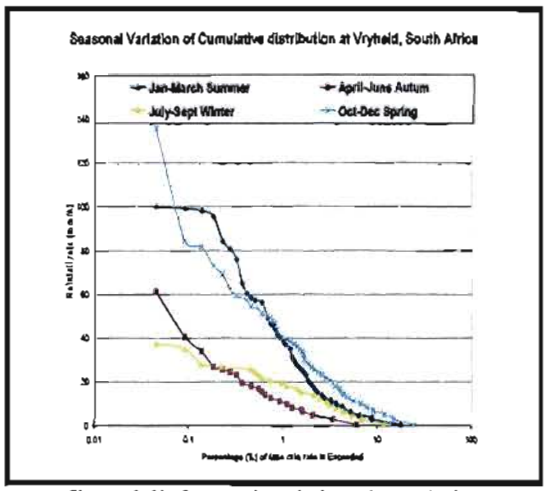

Figure 3-8j: Seasonal variation of cumulative rainfall rate distributions for Vryheid

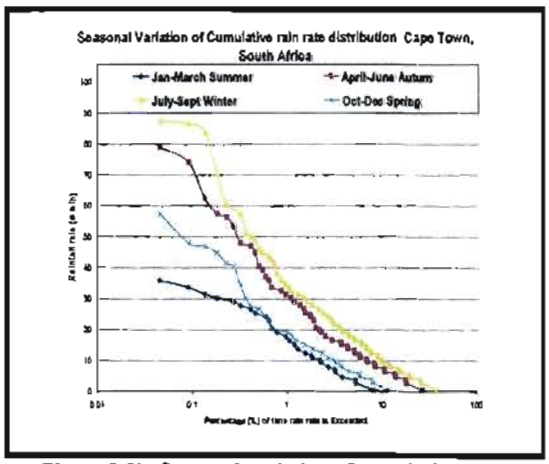

Figure 3-8k: Seasonal variation of cumulative rainfall rate distributions for Cape Town.

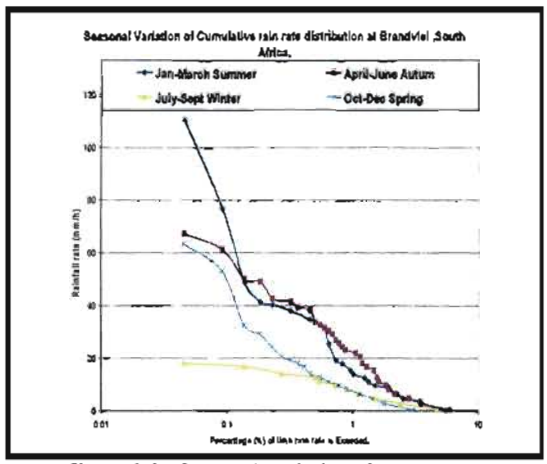

Figure 3-8l: Seasonal variation of cumulative rainfall rate distributions for Brandvlei

The seasonal variation cumulative at Bloemfontein, Ladysmith, Pietermaritzburg, Durban, Ulundi, Vryheid, and Brandvlei have their maximum rainfall rate in January and March (summer period) and minimum in July and September(winter period) while is vice versa in the case of Cape Town. Newcastle and Pretoria which have their maximum rainfall rate in October and December (spring period) and minimum rainfall rate in July and September (winter period). Lastly, East London and Richard Bay have their maximum rainfall rate in summer but minimum in spring and autumn respectively.

3.6 *Determination of South Africa Rain Climatic Zones*

The ITU-R climatic map for the world divides the whole globe into 15 climatic zones. This shows the rain intensity for the various climatic zones [31]. According to the ITU-R classification, Southern Africa has six rain zones, namely: C, D, E, J, K and N of which South Africa has five. They are: C, D, E, K and N. However, these ITU-R designations are not necessarily adequate; there is a need to redefine the ITU-R regional climatic zones based on the actual local data.

From the 5-year actual rain data for 12 different geographical locations which is converted to 1 minute integration time in South Africa, a compiled table of 1 minute rainfall rate distribution at 1.0%, 0.3%, 0.1%, 0.03% and 0.01% probability level (Percentage of time ordinate exceeded) considering for 5 years is shown in Table 3- 4.

The rain intensity exceeded (mm/h) shown in Table 3-4 for the 12 selected geographical locations in South Africa is compared with the ITU-R rain climatic zone table 3-5. The estimated errors for each location at different ITU-R climatic zones are shown in table 3-4a. The least error value for each geographical location is chosen as its rain climatic zone. The climatic rain zones are shown in table 3-6.

From the local data measured by South Africa Weather Services for 12 locations, four climatic rain zones are determined. They are: N, M, P and Q. Hence three additional rain climatic zones are added to ITU-R rain Climatic zone for South Africa.

Table 3-4a: Estimated Errors for determination of rain zones in South Africa

ıtion	A	B	C	D	E	F	G	H	J	K	L	M	N	P
ɔan	360.84	353.24	344.24	330.14	333.74	319.54	304.74	317.74	279.74	293.74	259.74	236.74	161.74	28.08
ards	487.23	479.63	470.63	456.53	460.13	445.93	431.13	444.13	406.13	420.13	386.13	363.13	288.13	142.13
e ı	195.05	187.45	178.45	164.35	167.95	153.75	138.95	151.95	113.95	127.95	93.95	70.95	44.69	150.39
ıdvlei	130.32	122.72	113.72	99.62	103.22	89.02	75.3	87.22	67.86	63.22	29.22	12.86	68.78	214.78
don	316.94	309.34	300.34	286.24	289.84	275.64	260.84	273.84	235.84	249.84	215.84	192.84	117.84	47.68
y h	313.59	305.99	296.99	282.89	286.49	272.29	257.49	270.49	232.49	246.49	212.49	189.49	114.49	43.49
le	328.07	320.47	311.47	297.37	300.97	286.77	271.97	284.97	246.97	260.97	226.97	203.97	128.97	17.77
heid	229.49	221.89	212.89	198.79	202.39	188.19	173.39	186.39	152.25	162.39	128.39	105.39	30.39	115.61
ɔria	308.76	301.16	292.16	278.06	281.66	267.46	252.66	265.66	227.66	241.66	207.66	184.66	109.66	45.66
ɛmfon	302.26	294.66	285.66	271.56	275.16	260.96	246.16	259.16	221.16	235.16	201.16	178.16	103.16	49.9
ndi	369.93	362.33	353.33	339.23	342.83	328.63	313.83	326.83	288.83	302.83	268.83	245.83	170.83	24.83
erma burg	392.08	384.48	375.48	361.38	364.98	350.78	335.98	348.98	310.98	324.98	290.98	267.98	192.98	46.98

Table 3-4b: Rain Intensity Exceeded (mm/h) for the 12 selected Geographical Locations in South Africa.

Percentage of time	Ladysmith	Durban	Richards Bay	Cape Town	Vryheid	Bloemfontein
1.0	16.29	18.93	28.79	12.17	6.07	14.95
0.3	35.7	41.25	57.03	25.2	21.49	34.58
0.1	62.07	68.98	91.65	37.95	41.25	56.01
0.03	95.32	108.75	143	57.03	77.65	89.92
0.01	120.11	138.83	182.66	78.60	98.93	122.7
Percentage of time	**Pretoria**	**East London**	**Ulundi**	**Brandvlei**	**Newcastle**	**P'martzburg**
1.0	14.95	18.93	14.95	2.46	12.17	18.93
0.3	35.71	36.83	34.58	9.22	31.14	43.43
0.1	61.07	61.07	67.02	25.19	63.07	79.55
0.03	98.03	90.74	112.27	42.33	105.2	113.15
0.01	114.90	125.27	157.01	67.02	130.39	152.92

Table 3-5: ITU-R rain climatic Zones (Rain Intensity)

Percentage of time (%)	A	B	C	D	E	F	G	H	J	K	L	M	N	P	Q
1.0	<0.1	0.5	0.7	2.1	0.6	1.7	3	2	8	1.5	2	4	5	12	24
0.3	0.8	2	2.8	4.5	2.4	4.5	7	4	13	4.2	7	11	15	34	49
0.1	2	3	5	8	6	8	12	10	20	12	15	22	35	65	72
0.03	5	6	9	13	12	15	20	11	21	23	33	40	65	105	96
0.01	8	12	15	19	22	28	30	32	35	42	60	63	95	145	115
0.003	14	21	26	29	41	54	45	55	45	70	105	95	140	200	142
0.001	22	32	42	42	70	71	65	53	55	100	150	120	180	250	170

Table 3-6: Rain Climatic Zone for 12 Geographical Locations in South Africa

Location	ITU-R P.837-1	ITU-R P.837-4	Proposed Zone
Durban	L	M	P
Richards Bay	N	M	P
Cape Town	E	E	N
Brandvlei	D	D	M
East London	K	K	Q
Ladysmith	K	L	Q
Newcastle	K	L	P
Vryheid	K	L	N
Pretoria	K	L	Q
Bloemfontein	K	L	P
Ulundi	L	L	P
Pietermaritzburg	L	L	P

3.7 Statistic Of Worst Month.

The need to design a radio communications system to meet performance and availability objectives in any month is a tall order. Propagation conditions vary considerably from month to month, and the monthly variability can change significantly from year to year. Furthermore, it is not possible to be certain about what might happen in any monthly period for the next 20 years or more, as it could be more extreme than anything so far observed. However, under the worst conditions for which propagation engineers must design which ultimately determine link availability [35]. In order to provide propagation data to help the designer who is faced with quality objectives based on any month, it necessary to get away from this totally open-ended concept. To address this, ITU propagation working groups came up with the concept of worst month, as defined in Recommendation ITU-R P.581-2.

Worst-month propagation data has to be determined from extended measurement periods to ensure that a representative monthly variability is observed, particularly for the tails of the propagation distributions. The propagation worst month concentrates on calendar months from each year (e.g. all the individual January data sets) can be averaged. The long-term averaged data

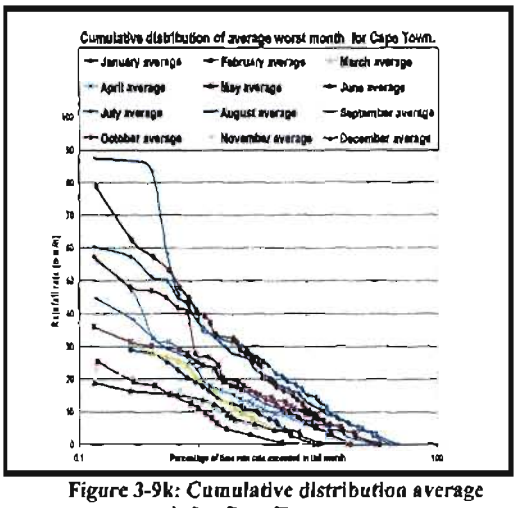

Figure 3-9k: Cumulative distribution average worst month for Cape Town.

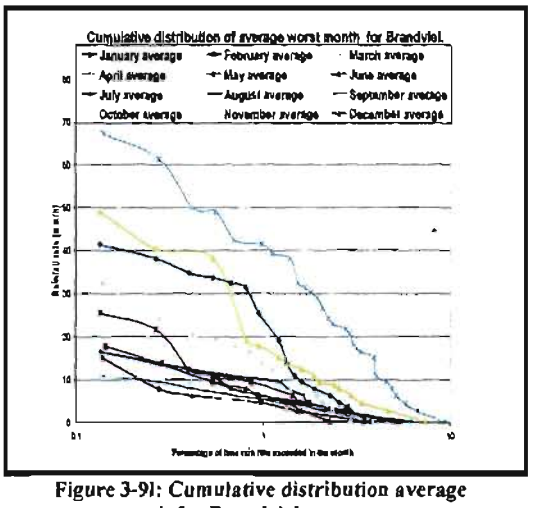

Figure 3-9l: Cumulative distribution average worst month for Brandvlei

The exception is Cape Town which has its maximum average worst month rainfall rate in August and the minimum in December. The winter rainfall region covers relatively small area along the Cape west and south-west coasts and has a rainfall regime of Mediterranean type with a conspicuous winter maximum.

3.8 Relation Between AY And AWM

Cumulative distributions of 1-minutes rainfall rate for average year (AY) and average worst month (AWM) for 12-locations are obtained by statistical processing of rainfall rate data. Figure 3-10a, 3-10b, 3-10c and 3-10d show dependence of percentage of time of AY and AWM for all the locations. The obtained dependence of percentage of time of the average year P_{AY} on percentage of time of the average worst month P_{AWM} for the same average 1-minute rainfall rate is shown by these two equations (3.8) and (3.9) which is validated by using correlation coefficient R^2.

$$P_{AY} = a P^{b}_{AWM} (\%) \tag{3.8}$$

$$P_{AWM} = \alpha P^{\beta}_{AY} (\%) \tag{3.9}$$

Where a, b, α, and β are coefficients of the equations (3.8) and (3.9).The values of the coefficients are shown in the table 3-7.

Figure 3-11a to 3-11l show comparisons of obtained distributions for AY and AWM with relevant Recommendation ITU-R. The probability of rain occurrence in Bloemfontein, Cape Town, Ladysmith, Pietermaritzburg, Ulundi, Brandvlei, East London, Newcastle, Pretoria, Vryheid, Richards Bay, and Durban for AY are 1.27%, 1.96%, 4.07%, 2.31%, 1.61%, 0.06%, 2.13%, 1.21%, 1.01%, 1.21%, 1.73%, 1.84% and for AWM it are 5.48%, 9.20%, 21.1%, 11.18%, 7.78%, 0.31%, 8.92%, 6.22%, 4.57%, 5.56%, 7.48%, 9.82% respectively.

Table 3-7: Coefficients a, b, α, and β, correlation coefficients R^2 and validity for approximation (3) and (4).

Location	a	b	α	β	R^2	**Rainfall rate range**
Durban	0.2217	0.9593	4.7465	1.0353	0.9931	$0.01 \leq R(1) \leq 152.92$
Richards Bay	0.2593	0.9631	4.0561	1.0373	0.999	$0.01 \leq R(1) \leq 205.25$
Cape Town	0.2183	1.0197	4.4329	0.979	0.9983	$0.01 \leq R(1) \leq 87.04$
Brandvlei	0.2016	1.0014	4.9488	0.9986	1	$0.01 \leq R(1) \leq 110.51$
East London	0.2542	0.9978	3.9358	1.0007	0.9985	$0.01 \leq R(1) \leq 156.19$
Ladysmith	0.2448	0.8946	4.7797	1.1125	0.9952	$0.01 \leq R(1) \leq 127$
Newcastle	0.2201	1.030	4.3085	0.9662	0.9958	$0.01 \leq R(1) \leq 175.53$
Vryheid	0.2161	0.963	4.8787	1.0357	0.9973	$0.01 \leq R(1) \leq 135.47$
Pretoria	0.2298	0.9848	4.4291	1.0128	0.9974	$0.01 \leq R(1) \leq 127.84$
Bloemfontein	0.2188	0.9789	4.7097	1.0197	0.9981	$6.07 \leq R(1) \leq 132.09$
Ulundi	0.2252	0.9969	4.0414	1.0016	0.9985	$0.9985 \leq R(1) \leq 211.38$
Pietermaritzburg	0.2635	0.9484	4.0414	1.0481	0.9985	$6.07 \leq R(1) \leq 132.09$

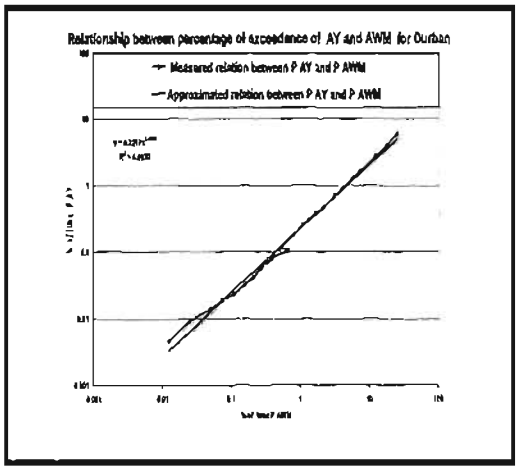

Fig 3-10a: Dependence of P_{AY} on P_{AWM} for Durban

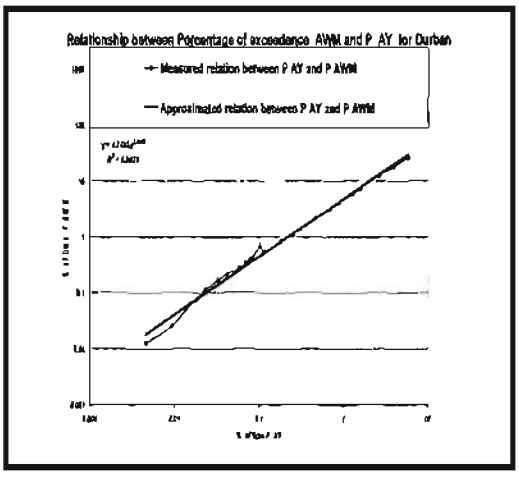

Fig 3-10b: Dependence of P_{AWM} on P_{AY} for Durban

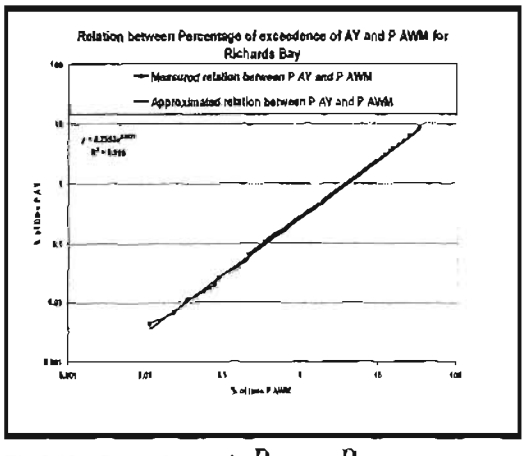

Fig 3-10c: Dependence of P_{AY} on P_{AWM} Richards Bay

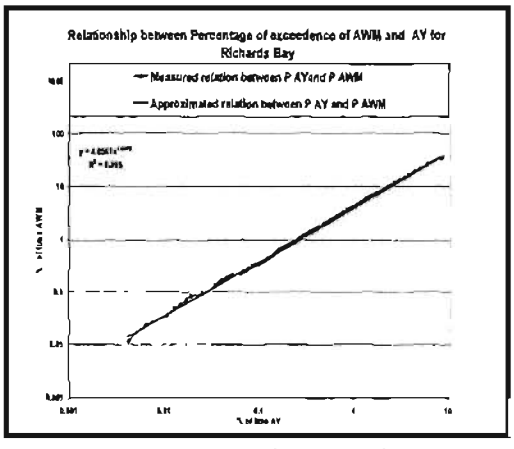

Fig 3-10d: Dependence of P_{AWM} on P_{AY} for for Richards Bay

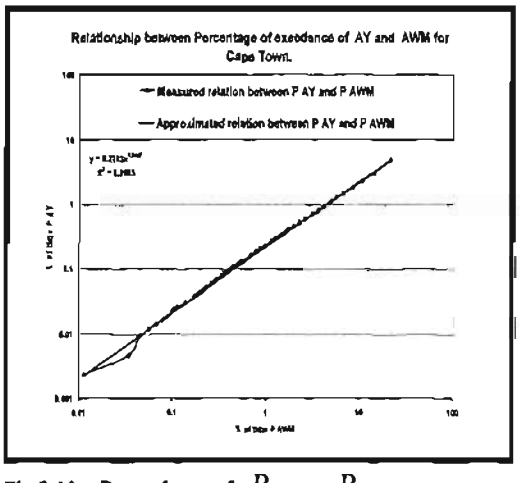

Fig 3-10e: Dependence of P_{AY} on P_{AWM} for Cape Town

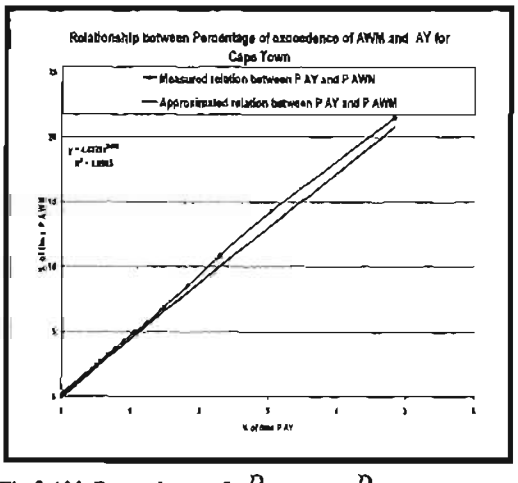

Fig 3-10f: Dependence of P_{AWM} on P_{AY} for Cape Town

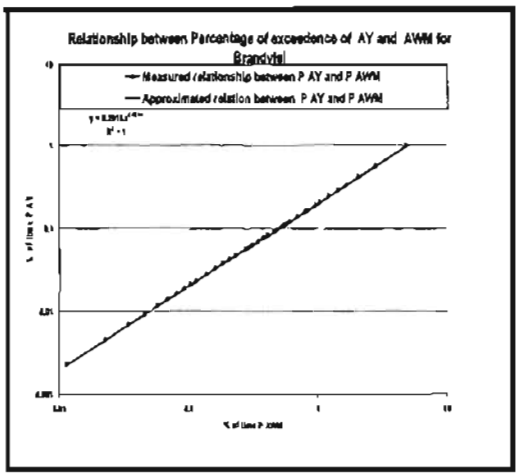

Fig 3-10g: Dependence of P_{AY} on P_{AWM} for Brandvlei

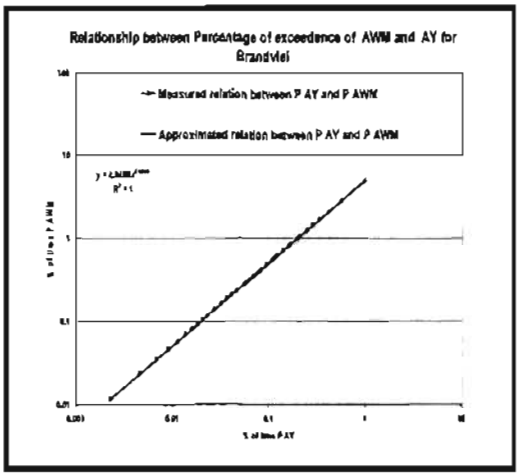

Fig 3-10h: Dependence of P_{AWM} on P_{AY} for Brandvlei

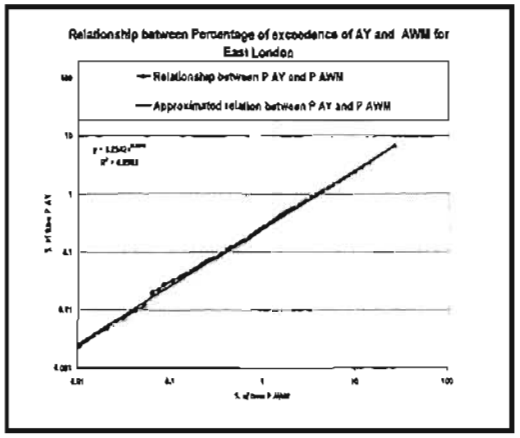

Fig 3-10i: Dependence of P_{AY} on P_{AWM} for East London

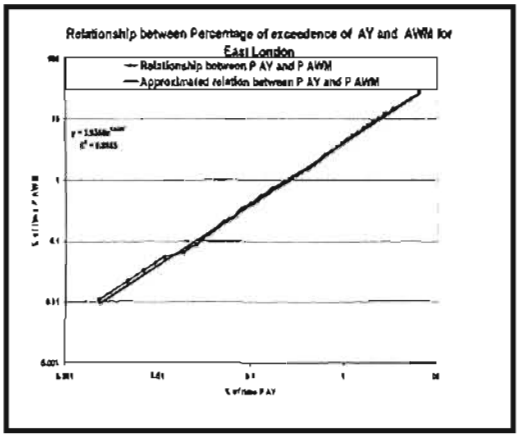

Fig 3-10j: Dependence of P_{AWM} on P_{AY} for East London

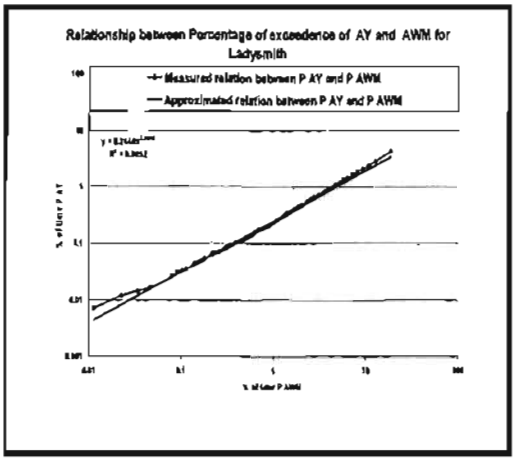

Fig 3-10k: Dependence of P_{AY} on P_{AWM} for Ladysmith

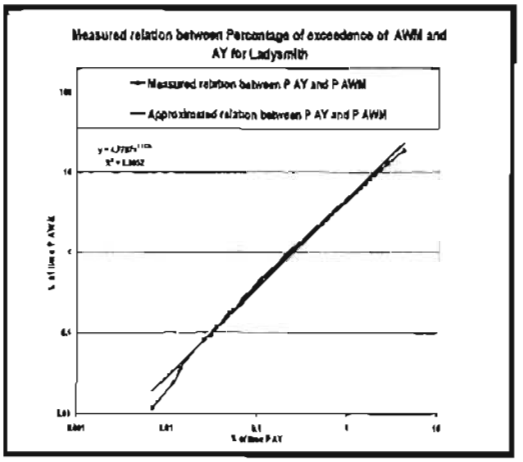

Fig 3-10l: Dependence of P_{AWM} on P_{AY} for Ladysmith

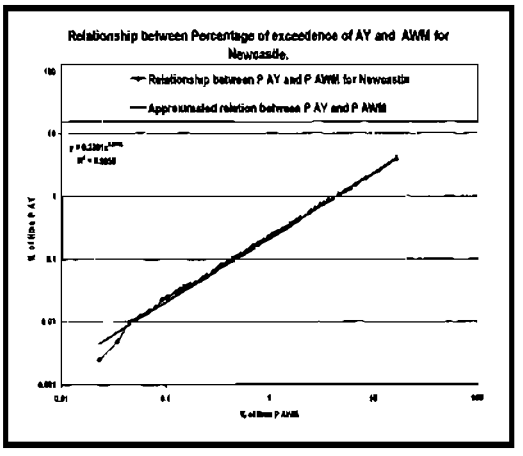

Fig 3-10m: Dependence of P_{AY} on P_{AWM} for Newcastle

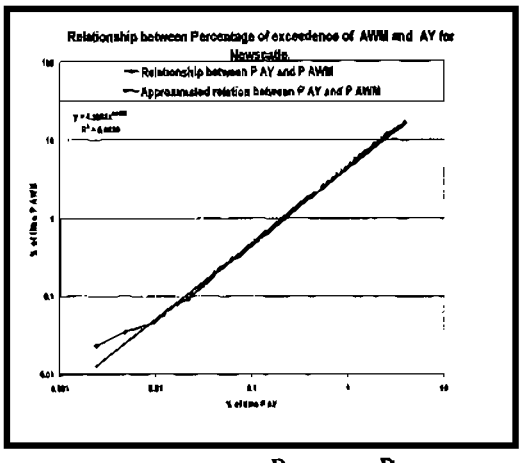

Fig 3-10n: Dependence of P_{AWM} on P_{AY} for Newcastle

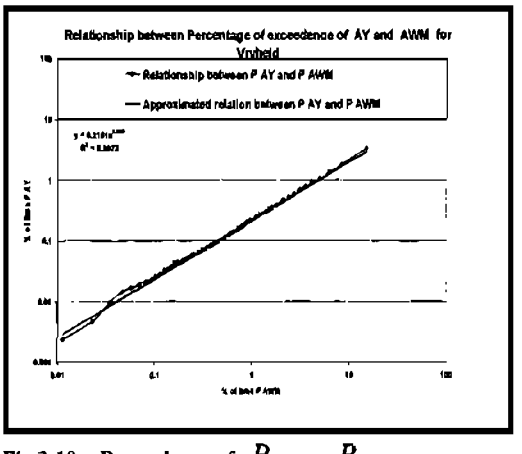

Fig 3-10o: Dependence of P_{AY} on P_{AWM} for Vryheid

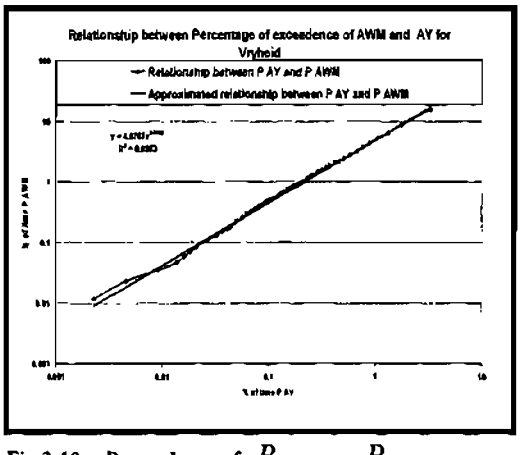

Fig 3-10p: Dependence of P_{AWM} on P_{AY} for Vryheid

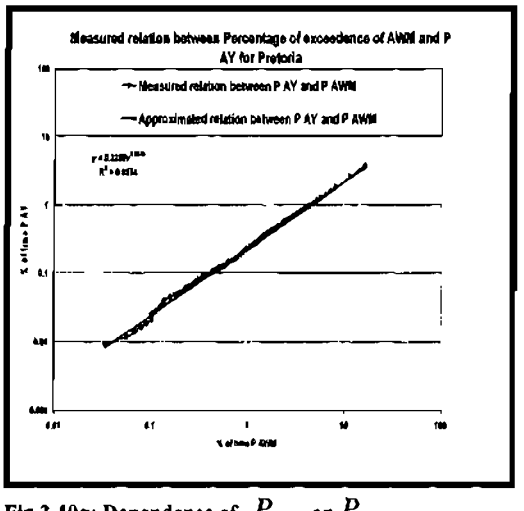

Fig 3-10q: Dependence of P_{AY} on P_{AWM} for Pretoria

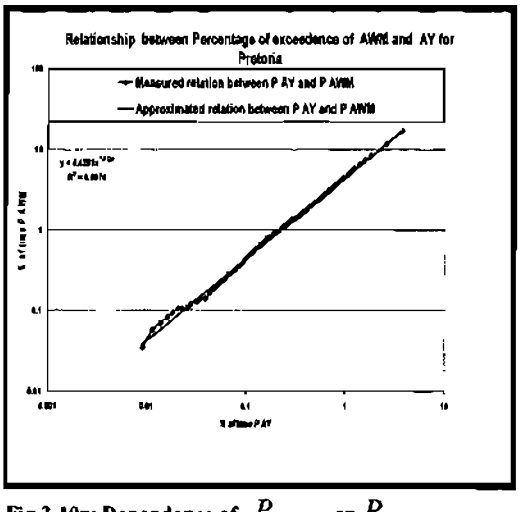

Fig 3-10r: Dependence of P_{AWM} on P_{AY} for Pretoria

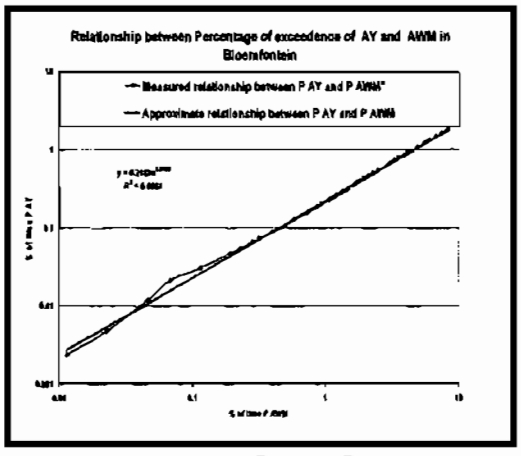

Fig 3-10s: Dependence of P_{AY} on P_{AWM} for Bloemfontein

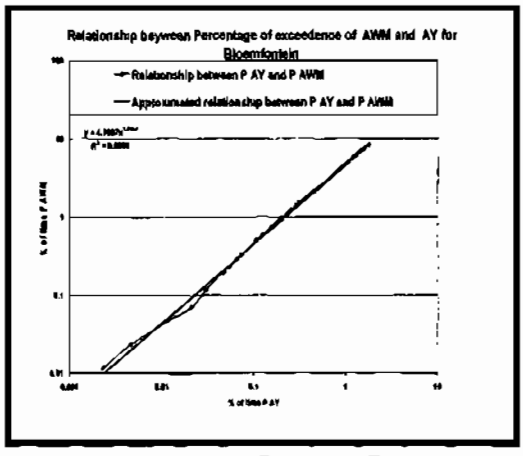

Fig 3-10t: Dependence of P_{AWM} on P_{AY} for Bloemfontein

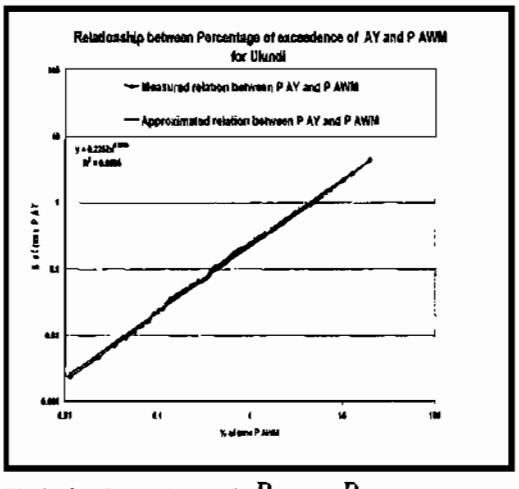

Fig 3-10u: Dependence of P_{AY} on P_{AWM} for Ulundi

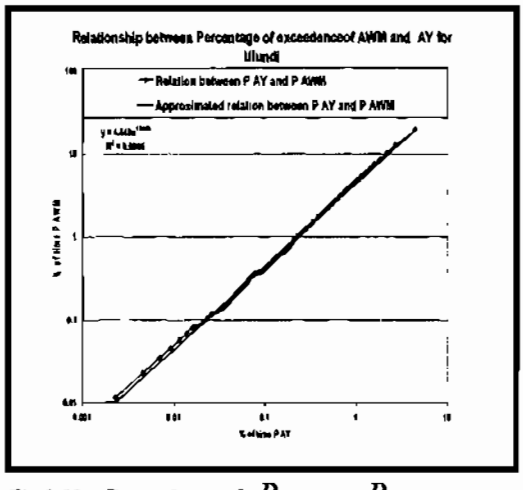

Fig 3-10v: Dependence of P_{AWM} on P_{AY} for Ulundi

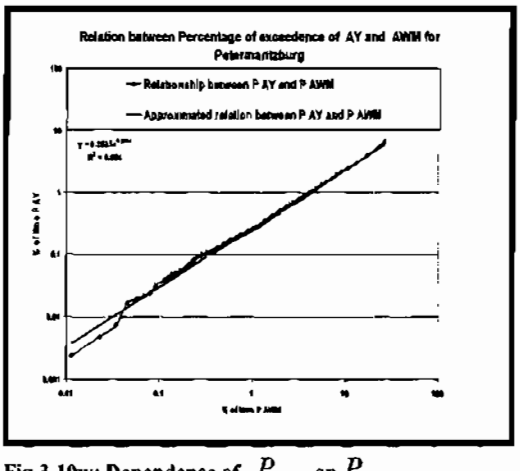

Fig 3-10w: Dependence of P_{AY} on P_{AWM} for Pietermaritzburg

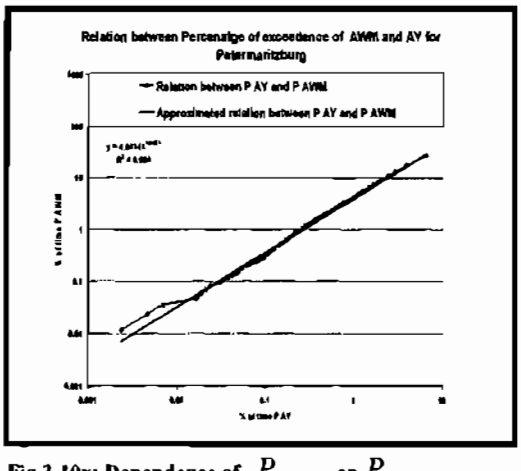

Fig 3-10x: Dependence of P_{AWM} on P_{AY} for Pietermaritzburg

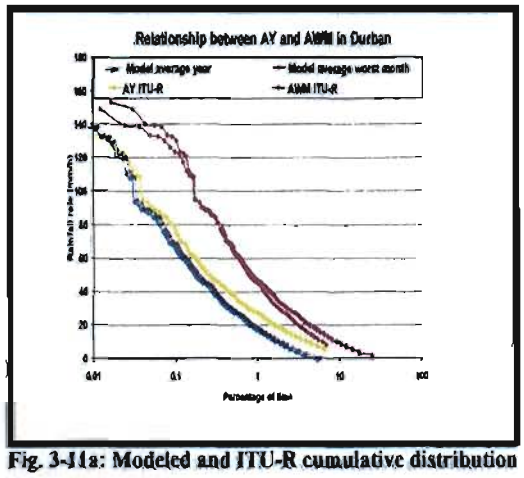

Fig. 3-11a: Modeled and ITU-R cumulative distribution of rain intensities for AY and AWM for Durban

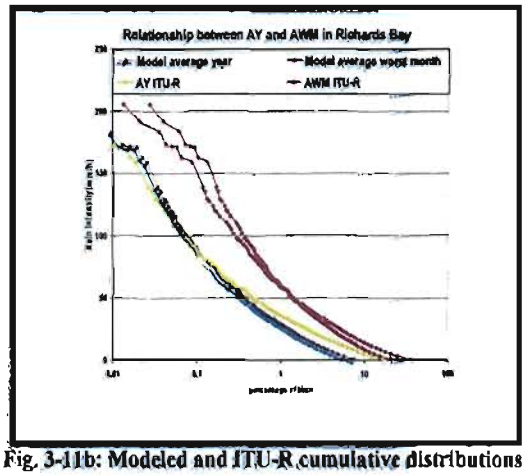

Fig. 3-11b: Modeled and ITU-R cumulative distributions of rain intensities for AY and AWM for Richards Bay

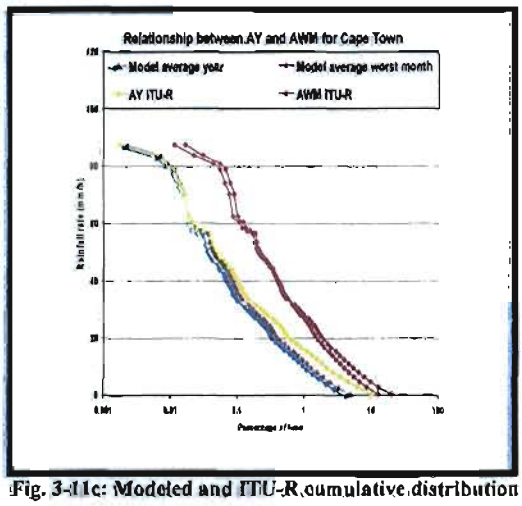

Fig. 3-11c: Modeled and ITU-R cumulative distribution of rain intensities for AY and AWM for Cape Town

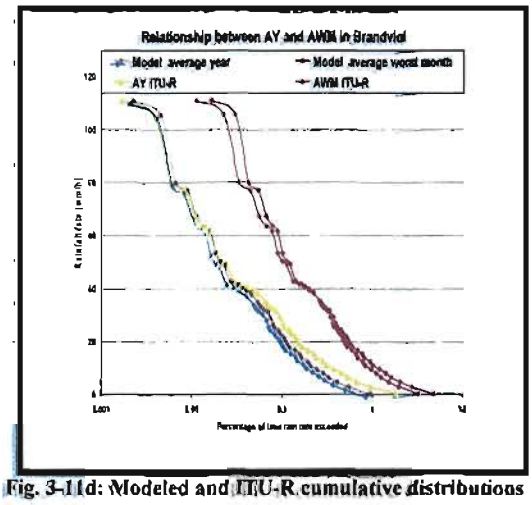

Fig. 3-11d: Modeled and ITU-R cumulative distributions of rain intensities for AY and AWM for Brandvlei

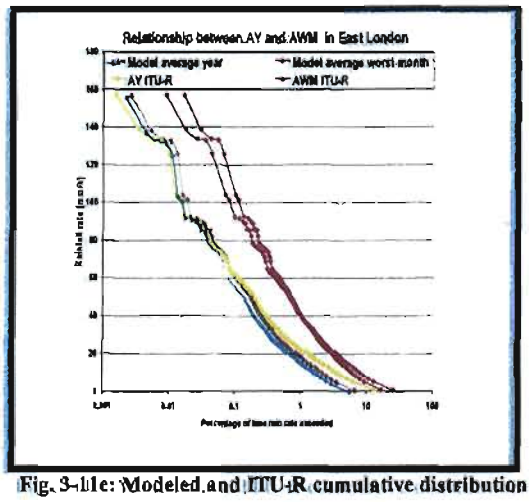

Fig. 3-11e: Modeled and ITU-R cumulative distribution of rain intensities for AY and AWM for Bloemfontein

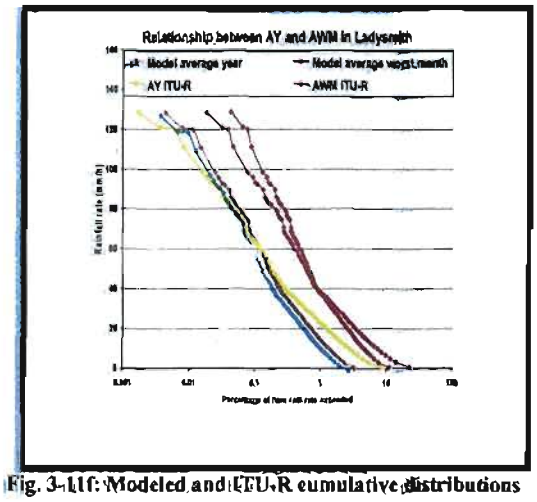

Fig. 3-11f: Modeled and ITU-R cumulative distributions of rain intensities for AY and AWM for Ladysmith

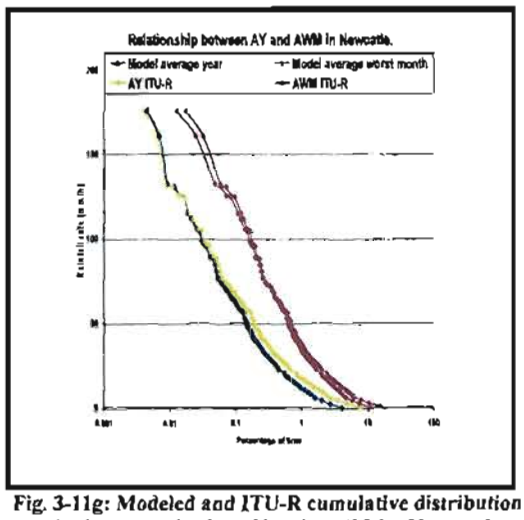

Fig. 3-11g: Modeled and ITU-R cumulative distribution of rain intensities for AY and AWM for Newcastle

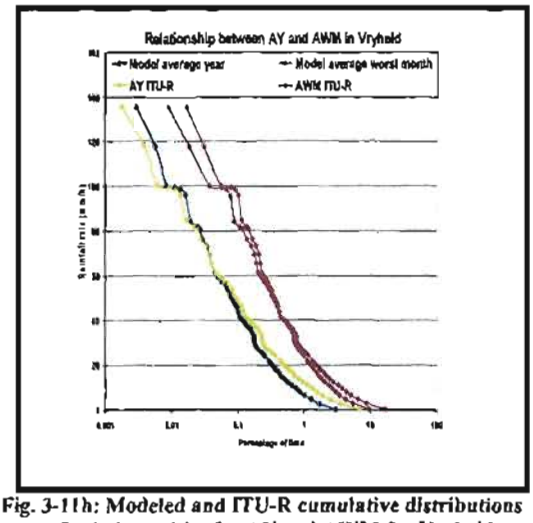

Fig. 3-11h: Modeled and ITU-R cumulative distributions of rain intensities for AY and AWM for Vryheid

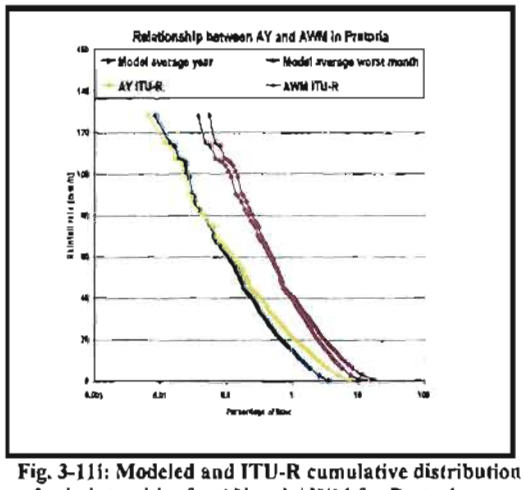

Fig. 3-11i: Modeled and ITU-R cumulative distribution of rain intensities for AY and AWM for Pretoria

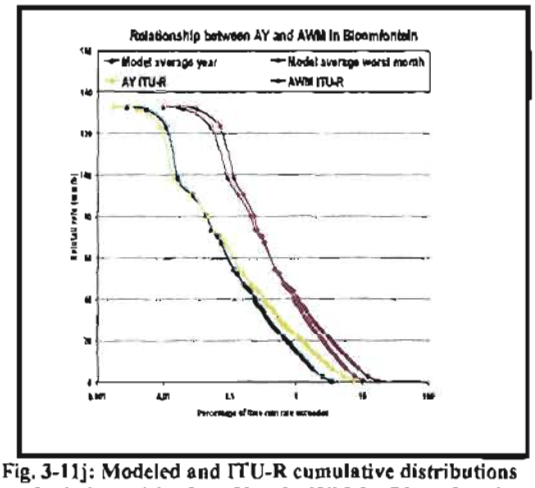

Fig. 3-11j: Modeled and ITU-R cumulative distributions of rain intensities for AY and AWM for Bloemfontein

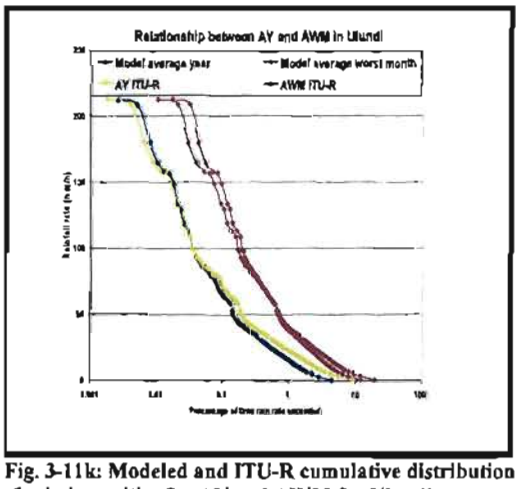

Fig. 3-11k: Modeled and ITU-R cumulative distribution of rain intensities for AY and AWM for Ulundi

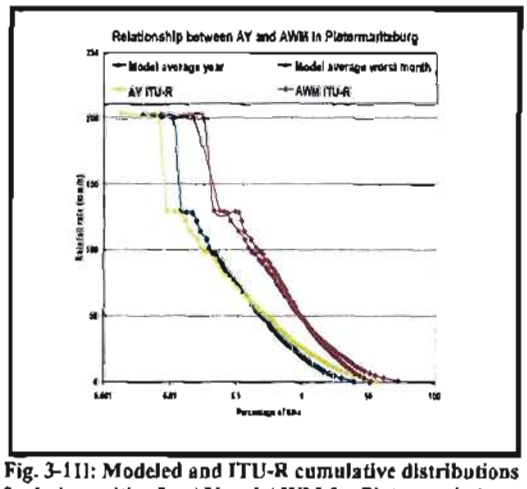

Fig. 3-11l: Modeled and ITU-R cumulative distributions of rain intensities for AY and AWM for Pietermaritzburg

3.9 Summary Of Chapter Three.

The 5-year rainfall data measured by the South Africa Weather Services for 12 different locations have been utilized to study the effect of integration time on the cumulative distribution of rain rate for South Africa. Values of equiprobable rain rate for 1 minute and 60 minutes integration times for probabilities of 0.1% or less have been employed to confirm the power law relationship between the rain rates at 1 minute and 60 minutes integration times. The coefficient a and b obtained for the conversion of 60 minutes rain rate to 1 minutes rain rate are comparable with the results of Ajayi and Ofoche for Ile-Ife in Nigeria which is tropical. Also, the obtained coefficient a and b in Durban, South Africa is extrapolated with the obtained coefficient a and b in Ile- Ife Nigeria. This shows a reasonable agreement with tropical region, which confirm large areas of South Africa to be subtropical.

The variation in the annual rain rate statistics for the 12 locations shows that most of the South Africa rainfall is unreliable and unpredictable. The comparison of the 5-year rain intensities for the 12 locations shows the variability of the rain statistics from one location to another. Richards Bay which lies in the coastal area of South Africa has the highest rain intensity of 182.66 mm/h at $R_{0.01}$ and Brandvlei which is found in the desert region has the lowest rain intensity 67.02 mm/h. The cumulative distributions of 1 minute rain intensities for a period of 5 years are obtained for each location that lies in the same climatic region. The differences are computed by using high and low time percentage probability of 0.1% and 0.01% respectively. At the high time percentage of 0.1%, the highest rain rate of 79.55 mm/h is observed at Pietermaritzburg and the correspondence 152.92 mm/h rain rate is gotten at the lower time percentage of 0.01%.

Based on the available local data converted to1 minute integration time, four climatic rain zones N, M, P and Q are determined for South Africa as against the ITU-R classification of C, D, E, K and N.

The variations in rainfall intensities are based on ocean on three sides of the country and the altitude of the interior plateau. In this study, it is observed that Western Cape gets most of its rainfall in winter, while the rest of the country is generally a summer rainfall region. The addition factors that contribute to this anomalous variation is the striking contrast between temperatures on the country's east and west coasts, due respectively to the warm Agulhas and cold Benguela

currents that sweep the coastlines. Being in the Southern hemisphere, the seasons stand in opposition to those of Europe and North America.

The rain intensity data collected over a 5-year period were statistically processed. The cumulative distributions of average 1-minute rain intensities for AY, and AWM were obtained. The obtained maximum absolute differences between the recalculated average 1-minute rain intensities of percentage of exceedence for AY and AWM are 0.0026 and 0.012 respectively. Both the calculated percentage of exceedences for AY and AWM in accordance with ITU-R recommendation are slightly underestimate and overestimate respectively in comparison with the measured ones. This might be balanced by a longer observation.

CHAPTER FOUR

RAINFALL RATE DISTRIBUTION MODELS FOR SOUTH AFRICA

Designing line-of-sight (LOS) or satellite link systems, needs yearly rainfall rate statistics for several percentages of time, in the locations of interest. This is necessary to estimate within an average year, the time percentage during which attenuation due to rain is significant, and consequently the future link performance and availability.

This chapter discusses various rainfall rate models such as Rice-Holmberg rainfall rate model, Salonen-Baptista model and Moupfouma model. Here, the Moufouma approach is used to derive the South Africa models. The reason for choosing this model is because of its simplicity and ability to derive the statistics of rainfall rate from short integration-time and long integration-time. The improvement over other models makes the approach more flexible and more accurate for development of the South Africa rainfall rate distribution model.

4.0 Rainfall Rate Climatological Models.

There are several rainfall rate climatological models for short integration-time and long integration-time statistics of precipitation. They are Rice-Holmberg, Salonen-Baptista, and Moupfouma's [36].

The rainfall rate model by Rice and Holmberg [37] enables the calculation of annual cumulative distribution of the rainfall rate for a given integration time. In order to convert the rainfall rate statistics into attenuation statistics, an integration time of 1 minute is chosen as recommended by ITU-R. The Rice-Holmberg rainfall rate model contains three basic parameters:

- the average annual rainfall, M_r in mm
- the ratio of thunderstorm rain to total rain, β
- the annual average number of days with rainfall $\geq$ 0.25 mm, D

The ratio of thunderstorm rain to total rain β is not readily available from meteorological databases. Thus, Dutton et al [38] have presented a calculation method for β from three parameters, which are available from long-term meteorological observations:

1. maximum monthly rainfall amount over a period of 30 years,
2. average number of thunderstorm days in a year,
3. average number of rainy days in a year.

This method was successfully used in the propagation studies for low fade margin systems in the Europe [38].

Salonen-Baptista model was developed because it was found that Rice-Holmberg rainfall rate model is not accurate enough for high availability systems [39]. The Salonen-Baptista model first tried to find proper functions, which describe well rainfall rate distributions, both in tropical and mid-latitude climates. It was found, that the probability, that the rainfall rate r is exceeded, can be described well with the function:

$$P(r)=P_0 . e^{-ar\frac{(1+br)}{(1+cr)}} \tag{4.1}$$

The next step was to develop empirical functions to calculate parameters a,b,c and the rain probability P_0 from the statistical meteorological data. This model is simple but not accurate for all locations, limited dataset and also depends on the latitudes.

4.1 Rain Rate Distribution Models

The log-normal model was been found to be appropriate for low and medium rainfall rates, while the gamma model gives a good representation of medium and high rain rates. The asymptotical distributions merge at about 20 to 50 mm/h, depending on the climate. This region is of great importance to radio communication.

Making use of the rain rate data collected over a period of two years in Brazzaville (Congo), Moupfouma, [40] proposed for rain rate greater than 2 mm/h the following:

$$P(R \geq r) = a\frac{e^{-ur}}{r^b}, \quad r \geq 2mm/h \tag{4.2}$$

with the parameter a, b, u which are displayed in the table 4-1, depending on the integration time of the raingauges used as well as the climatology of the location.

Table 4-1: Estimated values of a, b, and u for different regions in the world.

Name	a	b	u	Yr of data collected
Kjeller (Norway)	1.4×10^{-2}	1.53	2.2×10^{-2}	1975-1976
Paris(France)	1.32×10^{-2}	1.27	1.62×10^{-2}	1975-1977
Roma(Italy)	1.16×10^{-2}	0.771	2.464×10^{-2}	1yr
Palmetto(USA)	0.865	1.907	1.02×10^{-2}	2yr
Calcutta(Indian)	0.236	1.39	2.014×10^{-2}	1979-1980

Moupfouma [40] obtained expressions for the parameter a and b in terms of the rain rate $R_{0.01}$, (mm/h) exceeded for 0.01% of the time for any integration time:

$$a = 10^{-4} R^{b}_{0.01} \exp(U R_{0.01}) \tag{4.3}$$

$$b = 8.22 R^{-0.584}_{0.01} \tag{4.4}$$

$R_{0.01}$ and U determines the shape of the distribution and the slope of the curve, respectively. The parameter U was found to be dependent on climate and geographical features of the localities of interest. For the tropical zones, U was found to be 0.042 for coastal areas and 0.025 for the average rolling terrain.

From the statistical results of rainfall rates in China, Huang and Hu, 1991 found that the Moupfouma model was good with a modification of the parameter b as follows:

$$b = 2.494 R^{-0.218}_{0.01} \tag{4.5}$$

The Moupfouma model is a semi-empirical model which approximates a gamma distribution at high rainfall rates and a log-normal distribution at low rainfall rates. The model is, however, hampered on the one hand in a statistical point of view because it is not a probability law, and on the other hand by the parameter U which has no analytical expression.

Moupfouma and Martin [41] proposed a new prediction procedure of rainfall rate cumulative distribution, which probability law is leading to a more accurate prediction of rainfall rate cumulative distribution for all climates. Provided the rainfall rate $R_{0.01}$ (mm/h) exceeded during 0.01% of time is known, Moupfouma showed that the prediction procedure of rainfall rate cumulative distribution can be expressed as:

$$P(R \geq r) = \left(\frac{R_{0.01}+1}{r+1}\right)^{b1} * e^{u1(R_{0.01}+1)-\log_e(10^4)} \tag{4.6}$$

where r (mm/h) represents the rain rate exceeded during the fraction of the time P. Governed by the behaviour of the shape of rainfall rate cumulative distribution, the parameter b_1 is well approximated by the following analytical expression [31]:

$$b_1 = \left(\frac{r - R_{0.01}}{R_{0.01}}\right).\log\left(\frac{1+r}{R_{0.01}}\right) \tag{4.7}$$

The parameter "u_1" governs the slope of the rain cumulative distribution, according to the climate and the local geographical features. Due to the non uniformity of rain structure between the tropical and the temperate areas, "u_1" cannot be expressed analytically by the same relationship whatever the climate. Analysis by ITU-R Study Group 3 of available rain rate cumulative distribution data with 1 minute integration time leads to the two following relationships which characterize parameter "u_1", according to the climate:

(a) For the tropical localities :

$$u_1 = \frac{\log_e(10^4)}{R_{0.01}} . \exp\left[-\lambda \left(\frac{r}{R_{0.01}} \right)^Y \right] \tag{4.8}$$

with λ and Y positive constants such as that λ =1.066 and Y=0.214.

(b) For the temperate zones:

$$u_1 = \frac{\log_e(10^4)}{R_{0.01}} \times \frac{1}{(1+\eta(\frac{r}{R_{0.01}})^\beta)} \tag{4.9}$$

where η and β are positive constants such that η =4.56 and β =1.03.

Analysing the behaviours of parameters b and u, it appears that whatever the hydrometeorogical zone, we have:

$$\lim_{r \to 0} b(r) = 0$$

and

$$\lim_{r \to 0} u(r) = \frac{\log_e(10^4)}{R_{0.01}}$$

We can then deduce that :

$$\lim P(R \geq r) = e^{[\{\log_e(10^4)/R_{0.01}\} \times R_{0.01}] - \log_e(10^4)} = 1 \tag{4.10}$$

Moreover, using equations 4.7 and 4.8, we find that:

$$\lim_{r \to +\infty} u(r) = 0$$

Then, because we have b > 0 whenever r > $R_{0.01}$, this implies that:

$$\lim_{r \to +\infty} P(R \geq r) = 0 \tag{4.11}$$

The relationships of equation 4.9 and 4.10 show that equations 4.5 and 4.6 have probability law behaviour. This approach is an improved ITU-R rain rate distribution model for any hydromeoteological zones.

4.2. Rain Rate Distribution Models In South Africa.

An empirical but theoretically derived from rainfall rate measurements obtained for 8 regions from South Africa Weather Bureau over a period of five years are processed for empirical model for rainfall rate distribution for South Africa. The results provide a good fit of rainfall rate distributions observed in various locations in South Africa. They are presented in this section of the thesis. This rainfall rate distribution models are compared with the ITU-R currently accepted model (Probability law approach) and other results from other regions of the world. The investigation carried out on rainfall rate measurements obtained during a period of five years in South Africa, show that it is possible to represent rainfall rate distribution by a single function for the whole range of relevant values leading to the expression in equation (4.2) where a, b, and u are constants for a defined location as shown in Table 4-2.

Table 4-2: Estimated values of a, b, and u for 8 regions in South Africa

Name	**a**	**b**	**u**	$R_{0.01}$	**Years of data collected**
Pietermaritzburg	0.014	0.77	0.021	152.92	2000-2004
East London	0.017	1.529	0.021	125.27	2000-2004
Bloemfontein	0.81	1.39	0.02018	126.13	2000-2004
Brandvlei	0.016	0.769	0.022	73.0	2000-2004
Cape Town	0.013	0.98	0.0276	80	2000-2004
Newcastle	0.85	0.77	0.017	130	2000-2004
Pretoria	0.0117	0.768	0.0246	114.9	2000-2004
Durban	0.0115	0.77	0.0247	137.99	2000-2004

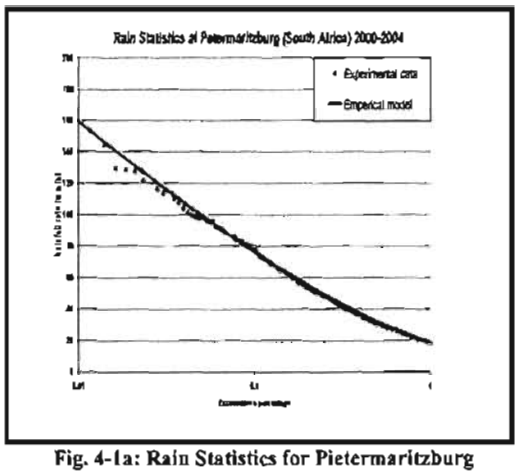

Fig. 4-1a: Rain Statistics for Pietermaritzburg

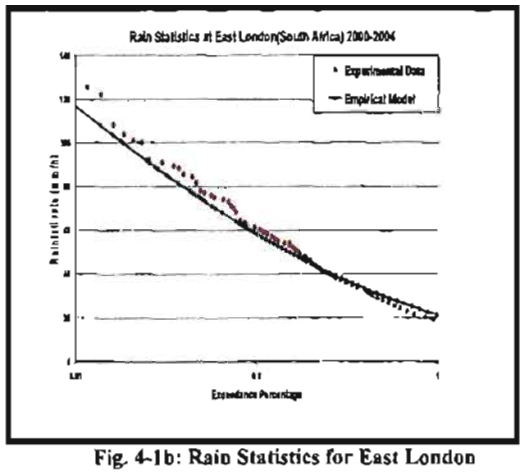

Fig. 4-1b: Rain Statistics for East London

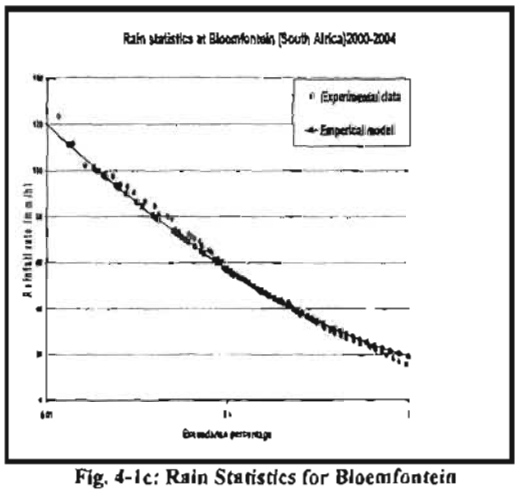

Fig. 4-1c: Rain Statistics for Bloemfontein

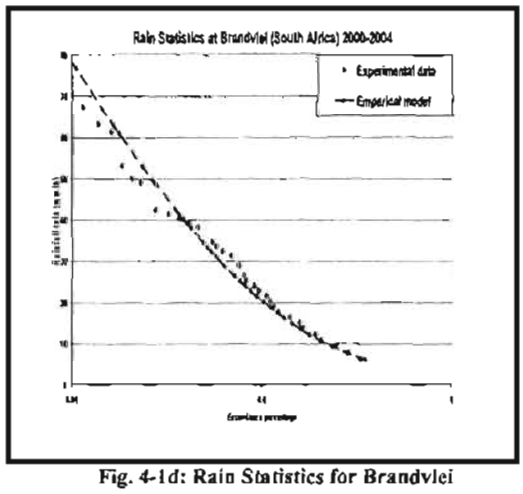

Fig. 4-1d: Rain Statistics for Brandvlei

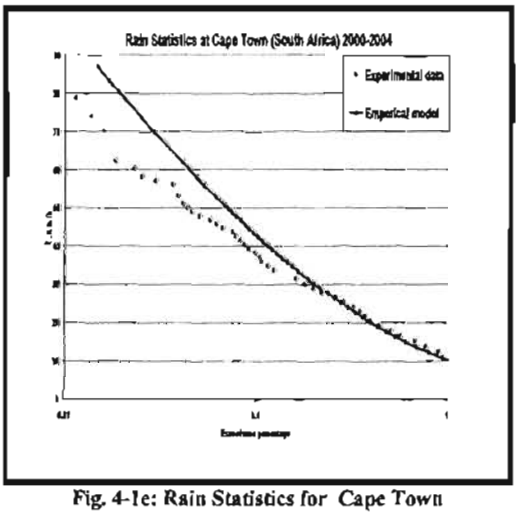

Fig. 4-1e: Rain Statistics for Cape Town

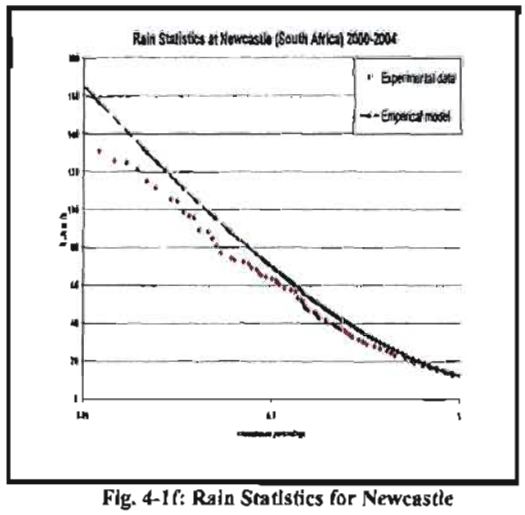

Fig. 4-1f: Rain Statistics for Newcastle

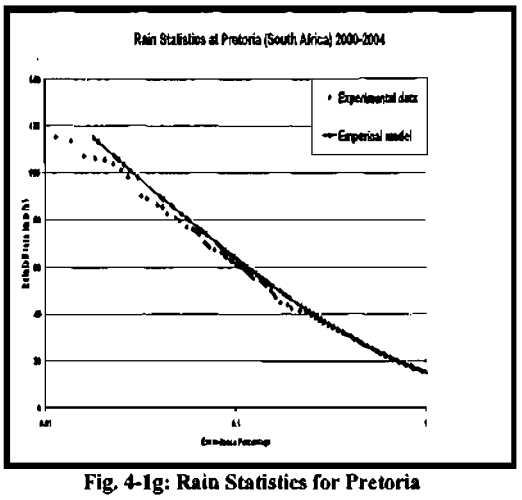

Fig. 4-1g: Rain Statistics for Pretoria

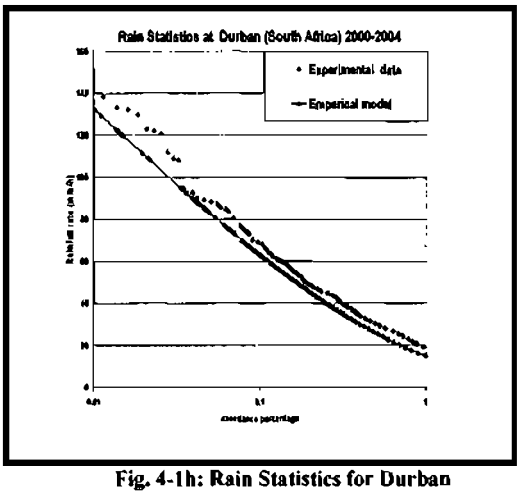

Fig. 4-1h: Rain Statistics for Durban

In figure 4-1, rainfall rate data from various regions in South Africa are fitted by the proposed distribution law. As can be seen, very good agreement is achieved both at higher and lower rates except in the case of Cape Town which is not fitted at higher rain rate.

Parameters a, b, and u in the empirical model of equation 4.1 must fulfill the following conditions:

$$\text{If} \quad F(r) = P(R \le r) \tag{4.12}$$

is the distribution function of the rainfall rate r, it follows that

$$F(r) = 1 - P(R \ge r) \tag{4.13}$$

$$F(r) = \begin{cases} 1 - a\dfrac{e^{-ur}}{r^b} & r > 0 \\ 0 & r \le 0 \end{cases} \tag{4.14}$$

$F(+\infty) = 1$, which implies u > 0 and b >0 (4.15)

Therefore the model of equation 4.2 has the following probability density function:

$$\frac{dF}{dr}(r) = f(r) = \begin{cases} a\dfrac{e^{-ur}}{r^{b}}\left(u + \dfrac{b}{r}\right) & r > 0 \\ 0 & r \le 0 \end{cases} \tag{4.16}$$

The $F(r)$ is always an increasing function, thus $f(r)$ is also positive and therefore $a > 0$, since u >0 and b>0.

Figure 4-2, shows rain statistics for selected regions in South Africa based on the developed models. The three-parameter approach is used to compute the distributions for the eight locations in South Africa.

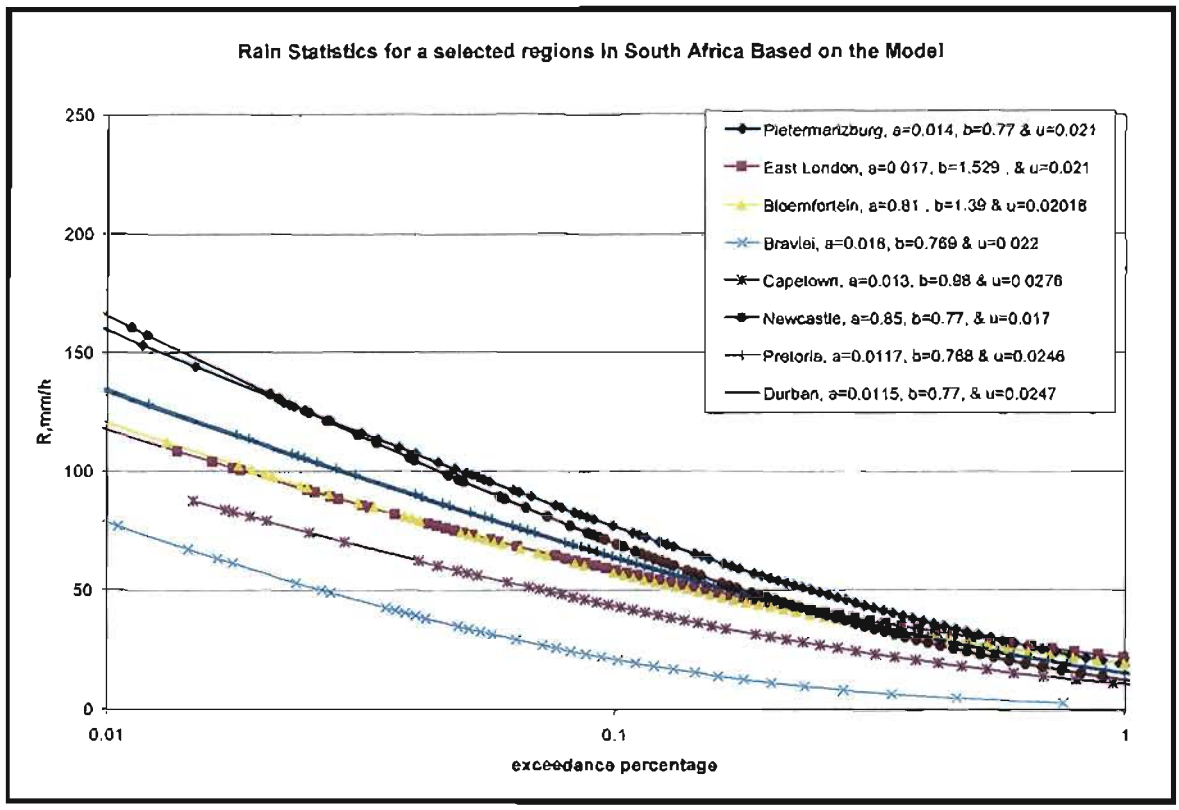

Fig. 4-2: Rain Statistics for selected regions in South Africa Based on the Model.

4.3 Evaluation Of The Model Parameters.

The CCIR (International Radio Consultative Committee) plenary assembly held in Geneva in 1982 gave contour maps of rainfall intensity $R_{0.01}$ (mm/h) exceeded for 0.01% of the time in different hydrometeorolgical regions of the world [42]. These values are highly interesting since they are used for radiowave attenuation prediction both Line-of –Sight and Earth-Space link [43]. The parameter b are plotted against the value of rainfall rate exceeded during 0.01% of time for each location, the corresponding points can be fitted by the relations for all the computed locations given in table 4-3. In figure 4-3, the values of parameter b, computed by extrapolating linear regression for various locations in the world at $R_{0.01}(mm/h)$ are obtained.

Table 4-3: Relationship between b and $R_{0.01}(mm/h)$ for 8 regions in South Africa.

Name	b	$R_{0.01}$	Years of data collected
Pietermaritzburg	$b = 5.2956 R_{0.01}^{-0.4637}$	152.92	2000-2004
East London	$b = 4.1113 R_{0.01}^{-0.3675}$	125.27	2000-2004
Bloemfontein	$b = 4.2935 R_{0.01}^{-0.4004}$	126.13	2000-2004
Brandvlei	$b = 6.9709 R_{0.01}^{-0.5422}$	73.0	2000-2004
Cape Town	$b = 6.3322 R_{0.01}^{-0.512}$	80	2000-2004
Newcastle	$b = 5.7062 R_{0.01}^{-0.4848}$	130	2000-2004
Pretoria	$b = 6.0236 R_{0.01}^{-0.4998}$	114.9	2000-2004
Durban	$b = 5.555 R_{0.01}^{-0.477}$	137.99	2000-2004

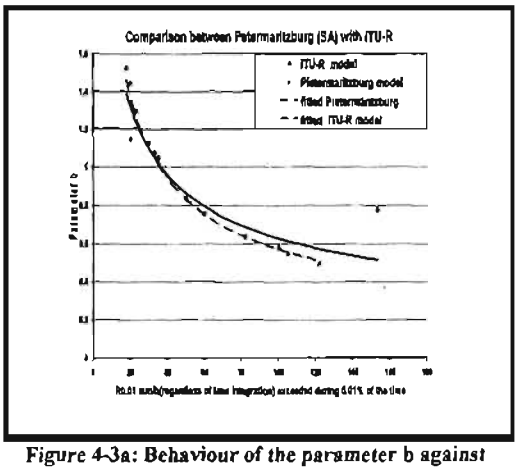

Figure 4-3a: Behaviour of the parameter b against $R_{0.01}$ (mm/h) for Pietermaritzburg

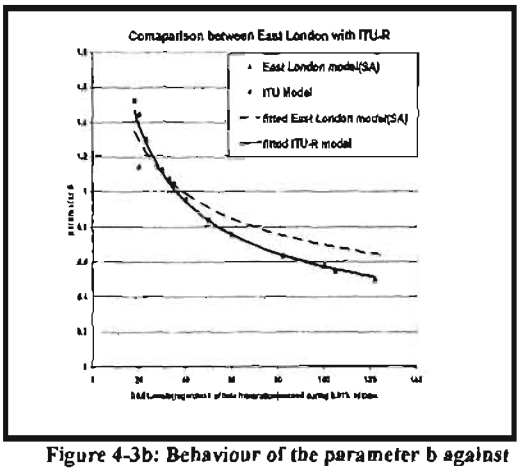

Figure 4-3b: Behaviour of the parameter b against $R_{0.01}$ (mm/h) for East London

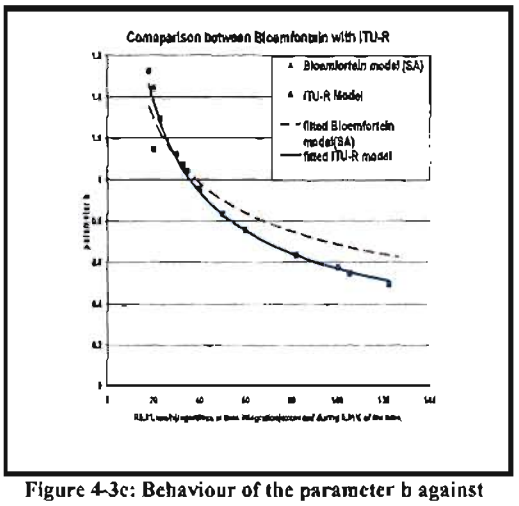

Figure 4-3c: Behaviour of the parameter b against $R_{0.01}$ (mm/h) for Bloemfontein

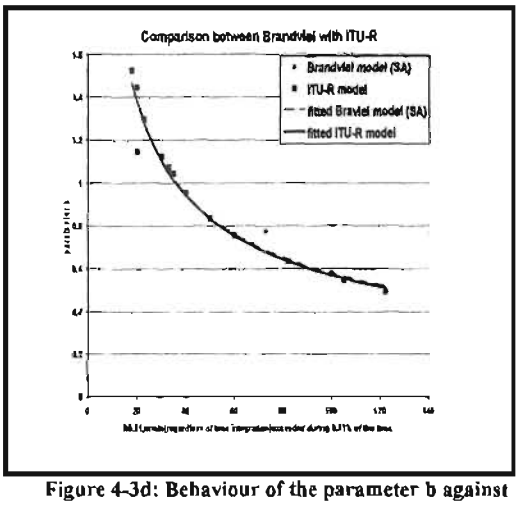

Figure 4-3d: Behaviour of the parameter b against $R_{0.01}$ (mm/h) for Brandvlei

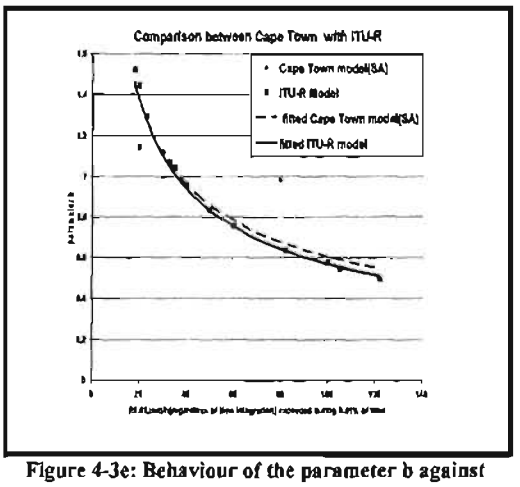

Figure 4-3e: Behaviour of the parameter b against $R_{0.01}$ (mm/h) for Cape Town

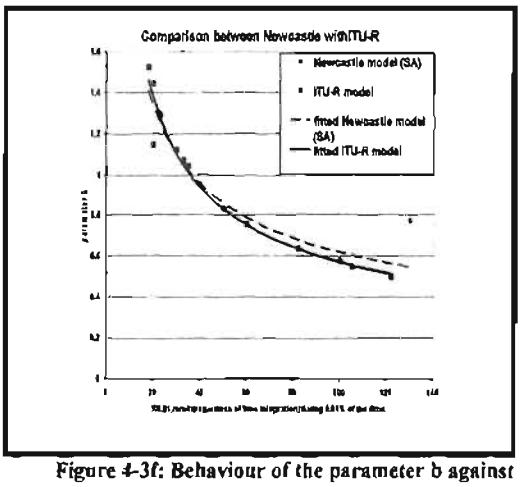

Figure 4-3f: Behaviour of the parameter b against $R_{0.01}$ (mm/h) for Newcastle

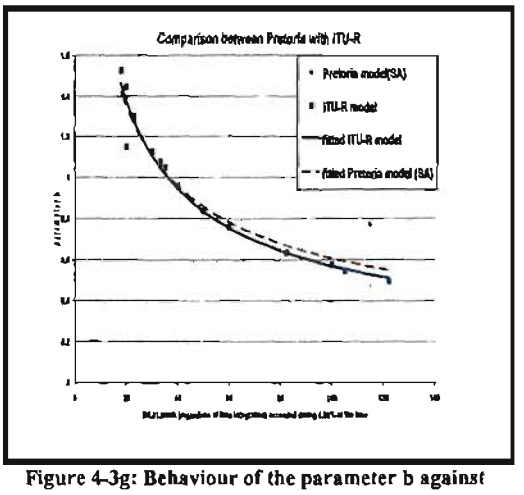

Figure 4-3g: Behaviour of the parameter b against $R_{0.01}$ (mm/h) for Pretoria

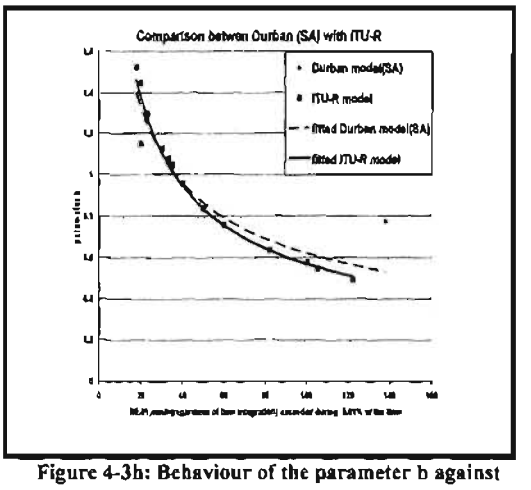

Figure 4-3h: Behaviour of the parameter b against $R_{0.01}$ (mm/h) for Durban

Figures 4-3(a) to (h) show a fairly good agreement with ITU-R (Moupfouma model) in some locations that have high rain intensities and very good agreement with location that have low rain intensities e.g. Brandvlei. It may be seen also that for higher rain rate (above 100mm/h) there is a rather sensible difference between predicted results and experimental values. This is not surprising since the accuracy of the model proposed here depends on that of the rain data, especially for the high intensities for which measurement inaccuracies may occur [44].

Once b is fixed, parameter a can be determined knowing any rain-rate value $R_{0.01}(mm/h)$ for any given time percentage .Then using $R_{0.01}(mm/h)$ and substituting into equation 4.1 one has

$$P(R \geq R_{0.01}) = a\frac{e^{-uR_{0.01}}}{R_{0.01}^{\ b}} = 0.01\% \tag{4.17}$$

thus

$$a = 10^{-4}\, R_{0.01}^{\ b}\, e^{uR_{0.01}} \tag{4.18}$$

4.4 Effect Of Integration Time On Rain Rate Distribution Model

The cumulative distributions for the two different integration times (1minute and 60 minutes) are shown in the figure 4-4. The 1-minute and 60-minutes interval cumulative distribution are distinguishable. Longer integration intervals remove the higher rate data and shift the distributions at low rates.

The large differences between the 1-minute and 60-minutes do not have effect on the models. At higher rain intensities of 60-minutes integration interval, the models are fairly deviated from the measured data. However, this may be accounted for as a result of insufficient rain event for that higher integration time. In addition, the deviation may also be a result of rain event durations that is longer than 60-minutes. In the case of 1-minute integration time the measured data agreed with the proposed empirical model.

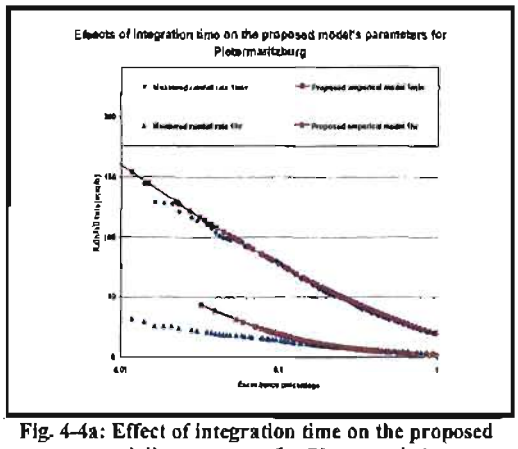

Fig. 4-4a: Effect of integration time on the proposed model's parameter for Pietermaritzburg

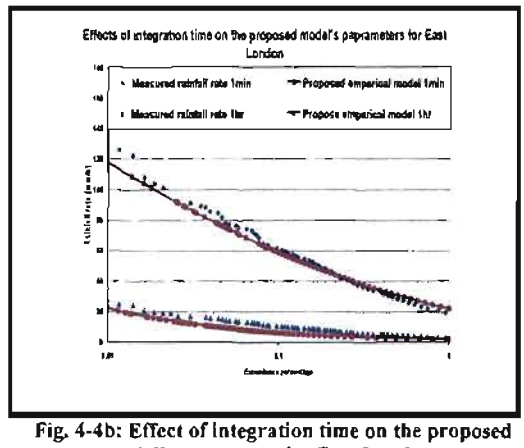

Fig. 4-4b: Effect of integration time on the proposed model's parameter for East London

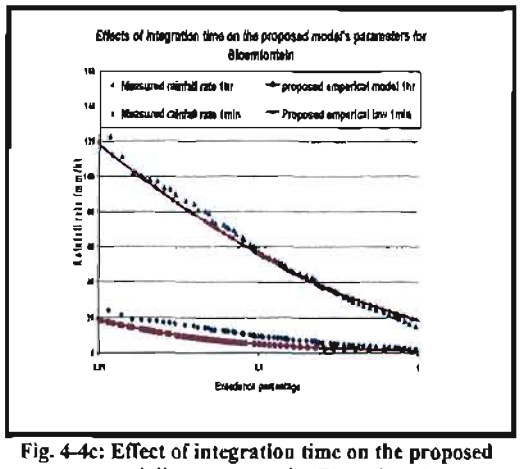

Fig. 4-4c: Effect of integration time on the proposed model's parameter for Bloemfontein

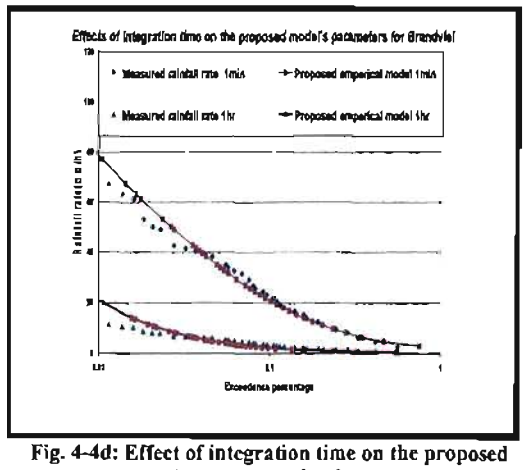

Fig. 4-4d: Effect of integration time on the proposed model's parameter for Brandvlei

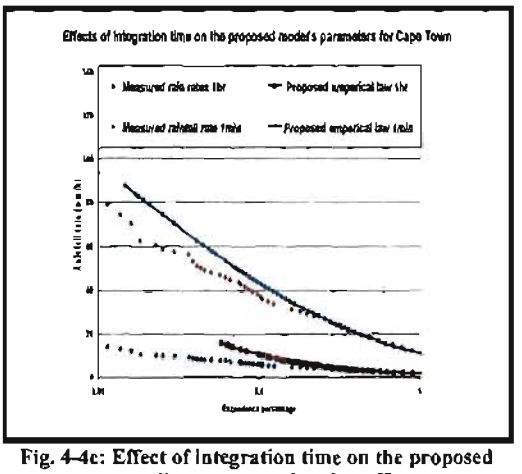

Fig. 4-4e: Effect of integration time on the proposed model's parameter for Cape Town

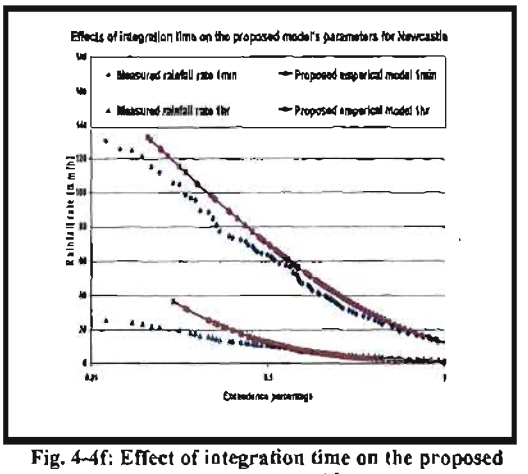

Fig. 4-4f: Effect of integration time on the proposed model's parameter for Newcastle

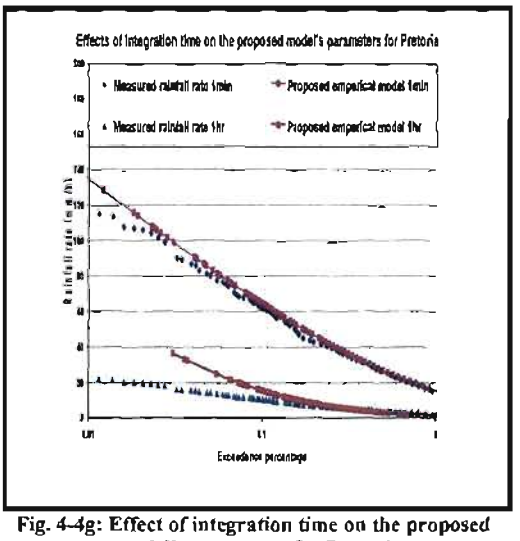

Fig. 4-4g: Effect of integration time on the proposed model's parameter for Pretoria

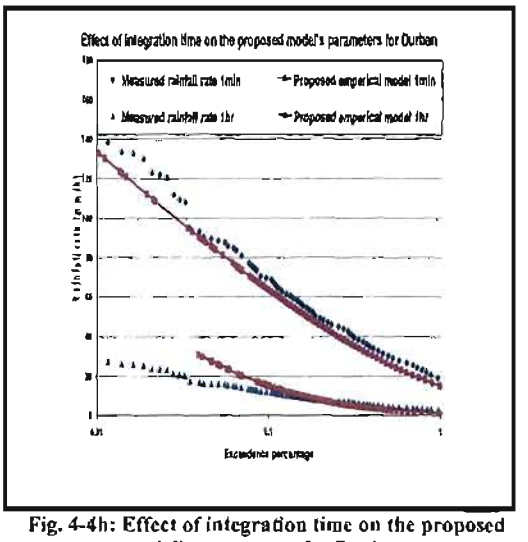

Fig. 4-4h: Effect of integration time on the proposed model's parameter for Durban

4.5 Comparison Of Rain Rate Models With ITU-R Model (Moupfouma Probability Law)

Figure 4-5a to 4-5h which deals with rain cumulative distributions concerning respective locations in South Africa, are compared with ITU-R (probability law) both for temperate and tropical zones. The statistical tools used for the comparisons are the root mean square (RMS) error, average probability ratio (APR), and the chi-square statistic (χ^2). Table 4-4 shows the comparison between the ITU-R, measured and proposed models for the 8 sites. We can see that a very good agreement exists between the proposed empirical model with the measured data and a fairly agreement with the ITU-R tropical zone model. This is so because most of South African locations are Sub-tropical.

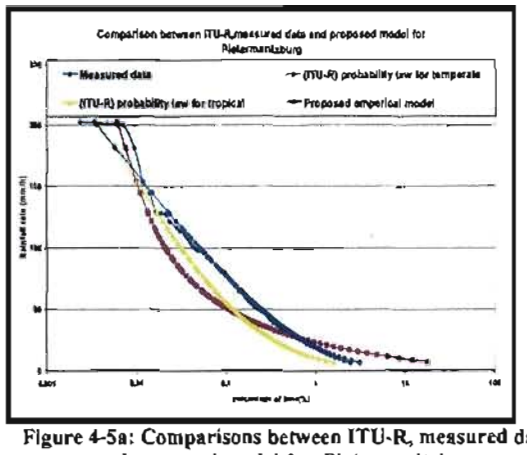

Figure 4-5a: Comparisons between ITU-R, measured data and proposed model for Pietermaritzburg

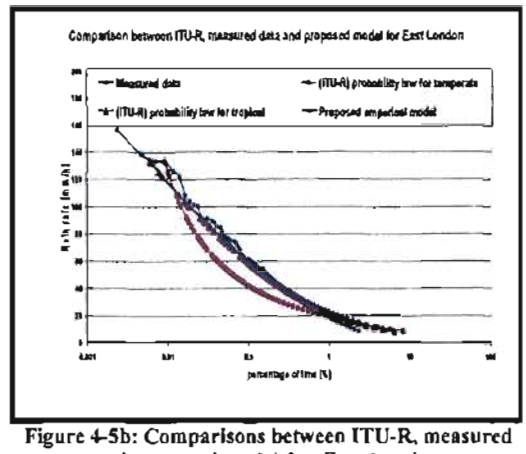

Figure 4-5b: Comparisons between ITU-R, measured and proposed model for East London

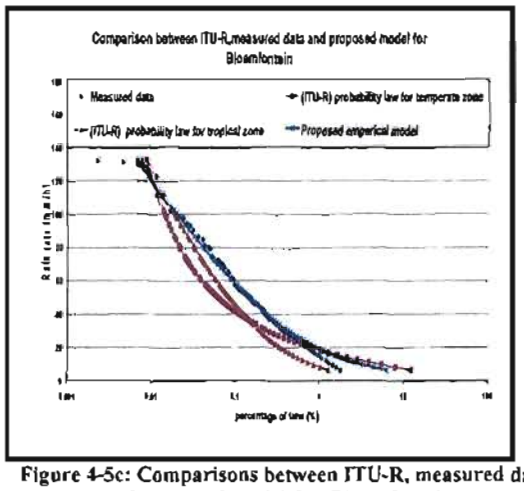

Figure 4-5c: Comparisons between ITU-R, measured data and proposed model for Bloemfontein

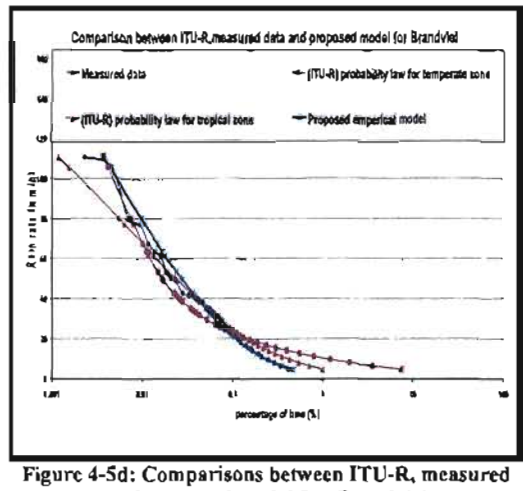

Figure 4-5d: Comparisons between ITU-R, measured and proposed model for Brandvlei

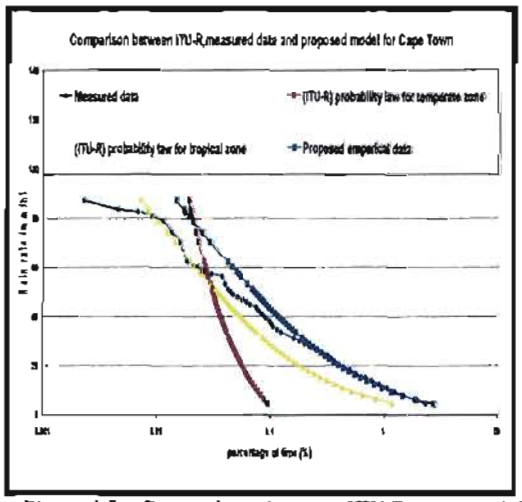

Figure 4-5e: Comparisons between ITU-R, measured data and proposed model for Cape Town

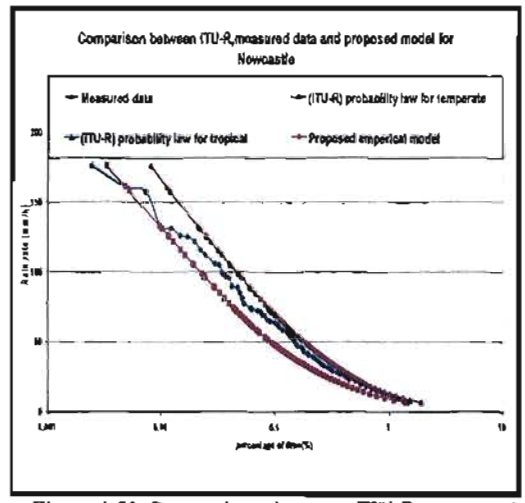

Figure 4-5f: Comparisons between ITU-R, measured and proposed model for Newcastle

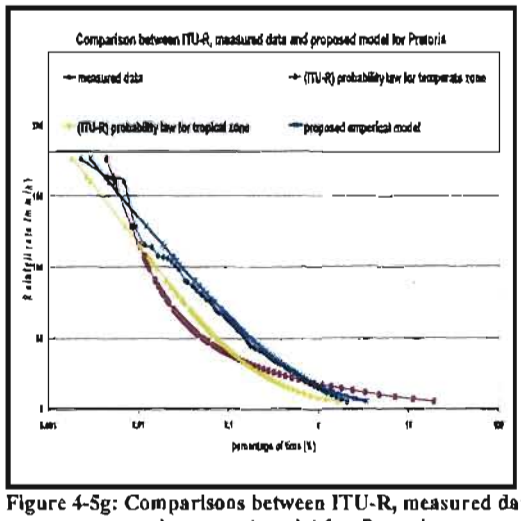

Figure 4-5g: Comparisons between ITU-R, measured data and proposed model for Pretoria

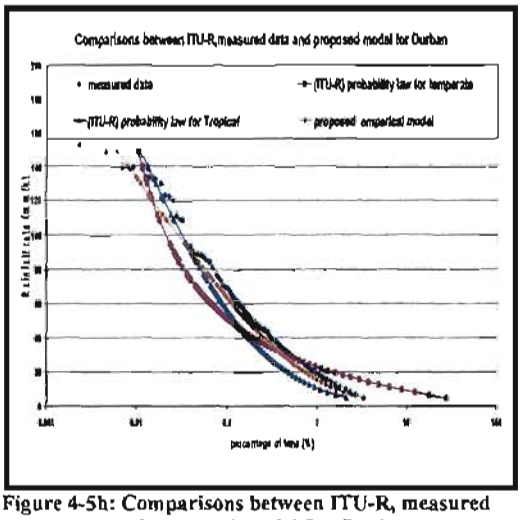

Figure 4-5h: Comparisons between ITU-R, measured and proposed model for Durban

4.6 Summary Of Chapter Four

Due to the interest raised by the precipitation effects, particularly those with high rainfall intensities for the design of terrestrial or satellite microwave radio links, it is necessary to have a simple and valuable mathematical model which can represent with good accuracy, the whole distribution for value ranging from 2 mm/h to 153 mm/h.

The empirical rainfall rate distributions model selected here give a good representation of rainfall rate cumulative distributions for eight hydrometeological locations in South Africa. It has a log-normal asymptotic behaviour for the low rain rates, and gamma asymptotical behaviour for the high rainfall rates.

The empirical model given by equation 4.2 with the parameter a, b, u which are displayed in the Table 4-2, appear to be suitable for the estimating rain intensity distributions for South Africa over the exiting global ITU-R rain rate distribution model.

The main improvement is observed from the comparison of the ITU-R, measured data and empirical model. The good agreement of the empirical model with the measured data confirmed the usefulness of the proposed empirical model for the proper and accurate rainfall rate distribution for radio system designer in South Africa.

Table 4-4: comparison between measured data with ITU-Rand Proposed models for 8 samples stations in SA (Note t_α is obtained with α =1%)

Site	Model	RMS error	APR	χ^2
Durban	ITU-R Temperate	0.51	0.85	16.46
	ITU-R Tropics	0.22	0.76	4.96
	Model	0.098	0.88	1.011
Bloemfontein	ITU-R Temperate	0.19	0.71	3.76
	ITU-R Tropics	0.17	0.70	3.45
	Model	0.14	1.09	1.36
East London	ITU-R Temperate	0.12	0.61	3.15
	ITU-R Tropics	0.21	0.62	5.11
	Model	0.14	0.99	1.50
Newcastle	ITU-R Temperate	0.29	0.80	8.71
	ITU-R Tropics	0.87	0.69	1.49
	Model	0.042	0.83	0.61
Pietermaritzburg	ITU-R Temperate	0.39	0.72	12.34
	ITU-R Tropics	0.19	0.60	4.98
	Model	0.024	1.062	0.090
Pretoria	ITU-R Temperate	0.21	0.59	5.44
	ITU-R Tropics	0.19	0.54	4.86
	Model	0.027	1.18	0.14
Cape Town	ITU-R Temperate	0.104	0.67	1.76
	ITU-R Tropics	0.16	0.73	2.35
	Model	0.031	1.01	0.52
Brandvlei	ITU-R Temperate	0.083	0.74	1.28
	ITU-R Tropics	0.030	1.079	0.186
	Model	0.007	1.078	0.025

CHAPTER FIVE

RAINDROP-SIZE DISTRIBUTION

5.1 Raindrop-size Distribution

As the communication services are demanding a access for higher frequencies at centimeter and millimeter wave band, a model to predict the propagation through rain is required in order to estimate the link budget and communication performance [44]. The rain drop size distribution (DSD) is the most important parameter in the attenuation prediction model. In this thesis, we established a drop diameter by using mean diameter relation developed by laws and Parsons [45]. They proposed empirically the median diameter D_m in relation to precipitation rate.

Many observations indicate that the specific rain attenuation is greatly dependent on the raindrop-size distribution, particularly in the wave bands range. Various raindrops size distribution models are in use in various regions of the world for estimating radio wave impairment on both terrestrial and earth-space paths. Models for the raindrop size distribution are required for the evaluation of microwave and millimeter wave propagation effects due to rainfall. Several models have been employed for rain scattering and propagation calculations [46].

Among the most widely used are the Laws and Parsons [45], Marshal and Palmer [47], the Joss et al., [21]. The over-estimation of the small diameter raindrops by Laws and Parsons and under-estimation by the Joss model when applied to the tropical path necessitated the study of Adimula and Ajayi [48] to obtain distinct drop size distribution models for drizzle, widespread, shower, and thunderstorm rain for the tropical region. The present work employs the Laws and Parsons and Marshall and Palmer approach in estimating raindrop size distribution models for Four locations in South Africa.

Theoretical calculations are usually based on the best available empirical data of the drop size distribution [46]. Most of the existing widely used raindrop size distributions are therefore described a follows:

5.1.1. Laws and Parson's Distribution Model.

The earliest paper on the size of raindrops was by Laws and Parsons [45]. They proposed empirically the median diameter D_m:

$$D_m = 1.238 R^{0.182} \tag{5.1}$$

where R is the precipitation rate in millimeter per hour. This is probably the best-known drop size distribution and is currently recommended by the ITU-R for the calculation of specific attenuation in the temperate region [49]. This distribution was obtained experimentally using quite rudimentary technique. It was concluded that the actual drop size distribution on the ground could be obtained from the volume distribution with a fall velocity, v (a) as :

$$n(a) = \frac{10^3 \, R \, \beta(m) \, da}{4.8 \pi a^3 v(a)} (m^{-3}) \tag{5.2}$$

where $\beta(m)da$ is the volume percentages, a is the radius in m, da represent the size interval from $a - da/2$ to $a + da/2$ and R is the rain rate in mm/h.

5.1.2. Marshall and Palmer Distribution Model

Distributions which describe N (D) directly, via an analytical expression, were initially proposed by Marshall and Palmer [47] and later by Joss et al., [21] for different types of rainfall. Both suggested a negative exponential model for the raindrops size distribution of the form [47]:

$$N(D) = N_O \exp(-\Delta D) \tag{5.3}$$

where N_O is a constant often obtained from:

$$N_O = \frac{4}{3\pi} \int N(D) D^3 V(D) dD \tag{5.4}$$

and Δ is a constant that tends to increase with rain rate. It is expressed as [47]:

$$\Delta = 4.1 R^{0.21} mm^{-1} \tag{5.5}$$

V (D) is raindrop terminal velocity expressed by Battan [47] for diameter range 1-4mm as:

$$V(D) = \sqrt{200.8a} \tag{5.6}$$

It describes the variation of raindrop sizes in terms of an analytical expression. The Marshall and Palmer distribution is particularly very close to the Laws and Parsons for $N_O = 8000 mm^{-1} m^{-1}$. Δ Satisfies the equation above so much that meteorologist regard it to be most applicable to widespread rain especially in the continental temperatures [50].

A disadvantage of the distribution is its tendency to overestimate the number of small drops below the diameter of about 1-5mm because of its exponential increase when D tends to zero. Therefore the use of the distribution will yield attenuation much higher than the actual attenuation at frequencies higher than about 30 GHz especially outside the continental temperate regions [51].

5.1.3. Modified Gamma Distribution Model

This distribution also presents N (D) directly, but in contrast to the negative exponential, it corrects the exponential increase of the raindrop number per unit volume when D tends to zero. It is expressed as:

$$N(D) = N_O D^m \exp(-\Delta D^\beta) \tag{5.7}$$

where N_O, m, Δ, and β are constant which are positive and real. The greatest difficulty in the use of this distribution is in obtaining experimentally the above four parameters. Another difficulty of using the distribution could be its tendency of cutting off both the large and small ends of the raindrop size spectrum for values of m in the range 3-5[52].

5.1.4. Joss et al., distribution model.

The use of electronic devices has been employed in the measurement of rain drop size distribution. Example is the electromechanical sensor called the distrometer that transforms the momentum of falling raindrops on a diaphragm into electrical pulses. Other types include electrostatic sensors that can measure the size dependent electric charges on the drops, and optical detectors that are made up of two parallel light beams capable of measuring both size and fall velocity of raindrops as they pass through the beam. Joss et al [21] measured raindrop size distribution with a distrometer at Lurcarno, Switzerland and found the distribution to vary considerably for different types of rain.

The parameters of average exponential distributions have been obtained for different types of rain. The "drizzle" distribution is associated with very light widespread rain composed mostly of small drops, while the "thunderstorm" distribution characterizes the drop-size distribution for convective rain with relatively high concentration of large drops [53]. Their work represents the first attempt to model raindrop size distribution with respect to the variation of drop size within each storm [54]. Equation 5.3 was concluded with the constants values as shown in the table 5-1 for different types of rain.

Table 5-1: The values for N_0 and Λ for different type of rain.

Type of rain	N_0	Λ
Drizzle(J-D)	30000	$5.7\,R^{-0.21}$
Widespread(J-W)	7000	$4.1\,R^{-0.21}$
Thunderstorm(J-T)	1400	$3.0\,R^{-0.21}$

5.1.5. Lognormal distribution model.

Due to the inadequacies of the negative exponential model as well as the modified gamma distribution in describing the small diameter drop range, a number of investigators have studied the lognormal distribution, which is expressed in the form:

$$N(D) = \frac{N_T}{\sigma D\sqrt{2\pi}} \exp\left[-\frac{1}{2}\left\{\frac{\ln(D)-\mu}{\sigma}\right\}^2\right] \tag{5.8}$$

where $N(D)$ is the number of drops per unit volume per diameter interval, μ is the mean of $\ln(D)$, σ is the standard deviation and N_T depends on climate, geographical location of measurement and rainfall type. Ajayi and Olsen [46] employed the lognormal distribution with a method of moment regression to produce a good theoretical fit to the measured data at Ile-Ife Nigeria. This was developed mainly for the tropical rainfall. The model is also expressed as equation (5.8) with the three parameters related to rain rates as

$$N_T = a_0 R^{b_0} \tag{5.9}$$

$$\mu = A_\mu + B_\mu \ln R \tag{5.10}$$

$$\sigma^2 = A_\sigma + B_\sigma \ln R \tag{5.11}$$

where $a_o, b_o, A_\mu, B_\mu, A_\sigma$, and B_σ are coefficients of moment regression [46]. Adimula and Ajayi [48] extended the results further by making measurements for a period of three years at two more locations in Nigeria. The distributions obtained confirmed the four classifications of raindrop size. The authors combined their results to obtain the propagation parameters; σ^2, μ, and N_T for the four rain types, which are useful for investigating rain induced microwave signal losses in tropical environments.

5.1.6. Wiebull Distribution Model

Wickerts measured one-minute drop-size distribution of drizzle, widespread rain, and rain showers using a distrometer in 1977 and 1978 15 km south of Stockholm [55]. Especially, he observed drizzle for a long period in which small drops less than D=1mm play an important role for rain attenuation at high frequencies. By analyzing the Laws and Parsons, Sander, and Wickerts data proposed Weibull distribution .The Weibull raindrop-size distribution was firstly proposed by Sekine and Lind [56] in 1982 as:

$$N(D) = N_0 \frac{\eta}{\sigma}\left(\frac{D}{\sigma}\right)^{\eta-1} \exp\left\{-\left(\frac{D}{\sigma}\right)^{\eta}\right\}, \tag{5.12}$$

where D is the diameter in millimeters and η and σ are functions of the precipitation rate R in millimeters per hour. The constants $N_0 = 1000 m^{-3}$, $\eta = 0.95 R^{0.14}$ and $\sigma = 0.26 R^{0.42} mm$ [53]. This distribution is retained for microwave applications for drizzle, widespread rain, and shower rain cases [58].

5.1.7. Other models for different regions in the world.

Considering the dependence of the relationship on the raindrop size distribution and the possible variability of the drop size distribution with climate, comparison is done with other regions of the world and the expressions are shown in table 5-2.

5.2 Drop Diameter, Rainfall Rate And Specific Attenuation

Rain as a major offender behaves like dissipative dielectric particles which absorbed and scattered radiowaves at frequencies above 10GHz. The relative contribution of these two effects in terms of wave attenuation depends on the relation between the drop size and the wavelength of the transmitted energy. The attenuation experienced by a wave crossing a rainy medium is given by the sum of the individual contributions of the drops that constitute the medium. Considering

the various raindrops of different dimensions, the specific attenuation is calculated by integrating each raindrop contribution.

The specific attenuation γ in dB/km due to precipitation can be evaluated on the basis of the classical Mie scattering theory. The evaluation depends on the knowledge of the complex refractive index of water at the raindrop temperature as well as the terminal velocity and the size distribution of the raindrops. This attenuation is expressed as [54]:

$$\gamma = 4.343 \int_0^\infty Q_t(D) N(D) dD \quad [dB/km] \tag{5.13}$$

Table 5-2: The raindrop size distribution models for different regions.

Region	**Model Type**	**Rain Drop size distribution model**
Japan [59]	Exponential distribution	$N(D) = 17300R^{-0.16}\exp(-5.11R^{-0.253}D)$
Europe [47]	Marshall and Palmer (exponential model)	$N(D) = N_0\exp(-\Lambda D)$ $\Lambda = 4.1R^{-0.21}$ $N = 8000$
Singapore [60]	Gamma distribution	$N(D) = N_0 D^m \exp(-\Lambda D)$ $m = 3,$ $N_0 = 31444.3R^{0.244},$ $\Lambda = 5.753R^{0.032}$
Europe [57]	Gamma distribution (Atlas and Ulbrich).	$N(D) = N_0 D^2 \exp(-\Lambda D)$ $N_0 = 64500R^{-0.5}$ $\Lambda = 7.09R^{-0.27}$

where $Q_t(D)$ is the extinction cross-section and $N(D)dD$ is the number density raindrops with equivalent diameter D in the interval dD. $Q_t(D)$ is determined theoretically, from the classical scattering theory developed by Mie for frequencies above 3 GHz or the Reyleigh approximation for frequencies between 1 and 3 GHz:

$$Q_T(D) = Q_s(D) + Q_A(D) \tag{5.14}$$

where Q_s and Q_A are scattering and absorption cross, respectively. $Q_t(D)$ is a function of drop size diameter, wavelength and complex refractive index m of the water drops. The rain rate is related to the drop size distribution by [31]:

$$R = 6\pi \times 10^{-4} \int_0^{\infty} D^3 N(D) V(D) dD \qquad [mm/h] \tag{5.15}$$

where $V(D)$ is the terminal velocity of drops in $mm^{-1}m^{-3}$. Equation 5.15 can alternatively be expressed as follows [31]:

$$R \approx 6\pi \times 10^{-4} \sum D^3 N(D) V(D) \Delta D \tag{5.16}$$

5.3. Estimation of Rain Drop-size Distribution Models

The method embarked upon in estimating the empirical model involves collection of rain rate data, collating the data and finding the diameter distribution of the data and finally proposing an analytical model to express the distribution of the data earlier collected. The data used for the study were gathered from South Africa Weather Services (SWAS), for a period of five years (2000-2004).

Due to lack of physical measurement of drop size distribution of rain, an estimation approach is used. This approach is achieved by using the available rain rate for period of 5-years for the estimation. We use empirical median drop diameter of Laws and Parson in equation 5.1 to calculate the median diameter of drop at different rain rates (D_m).

5.4. Data Sorting

The available data consists of rain rate at 1-hour which is the integration time at which the raw data is collected and converted to 1-minute integration and the calculated diameter at one minute integration time are done for Durban, Pretoria, Cape Town and Richards Bay. The calculations of rain drop diameter are processed and the distributions for the raindrop size are developed for each selected station.

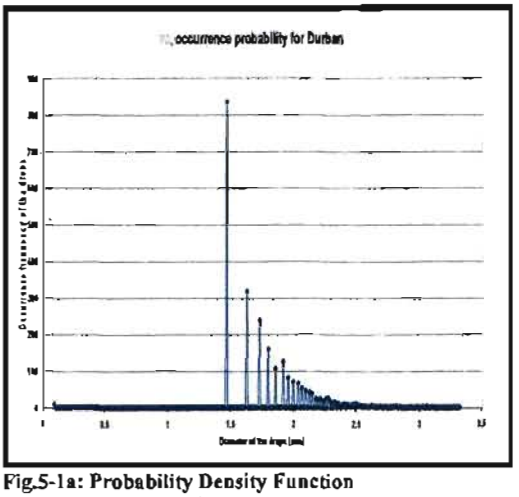

Fig.5-1a: Probability Density Function for Durban (2000-2004)

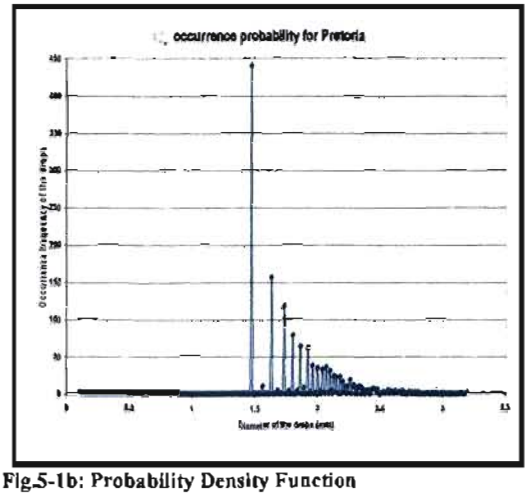

Fig.5-1b: Probability Density Function for Pretoria (2000-2004)

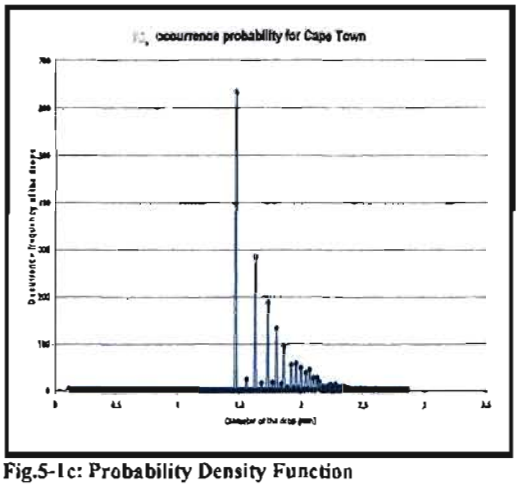

Fig.5-1c: Probability Density Function for Cape Town (2000-2004)

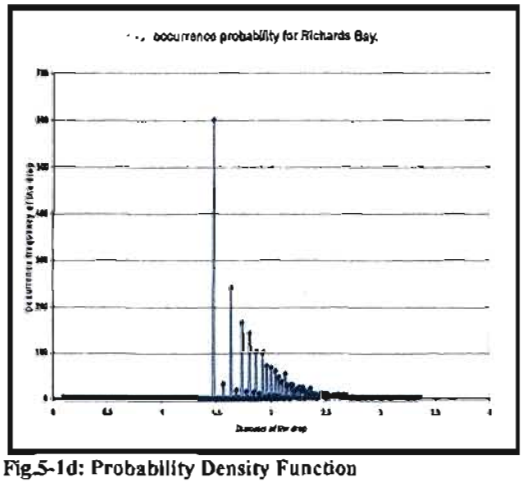

Fig.5-1d: Probability Density Function for Richards Bay (2000-2004)

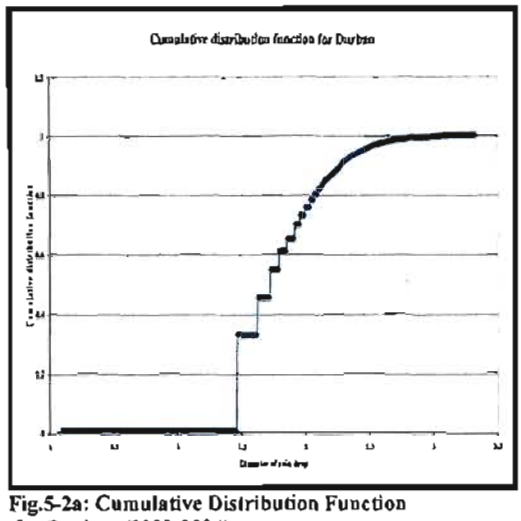

Fig.5-2a: Cumulative Distribution Function for Durban (2000-2004)

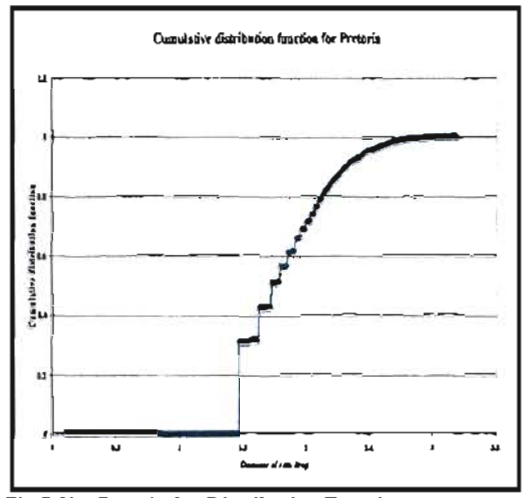

Fig.5-2b: Cumulative Distribution Function for Pretoria (2000-2004)

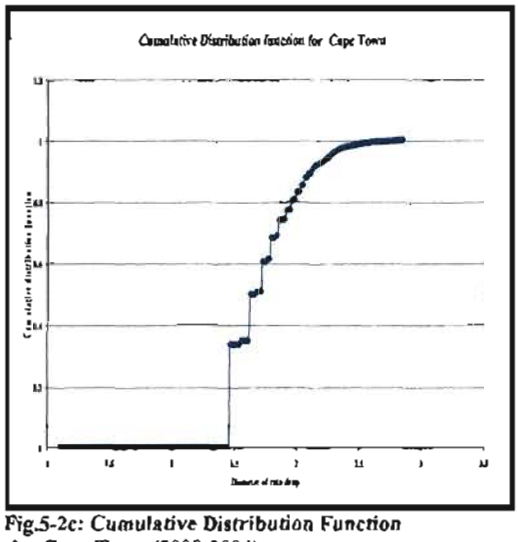

Fig.5-2c: Cumulative Distribution Function for Cape Town (2000-2004)

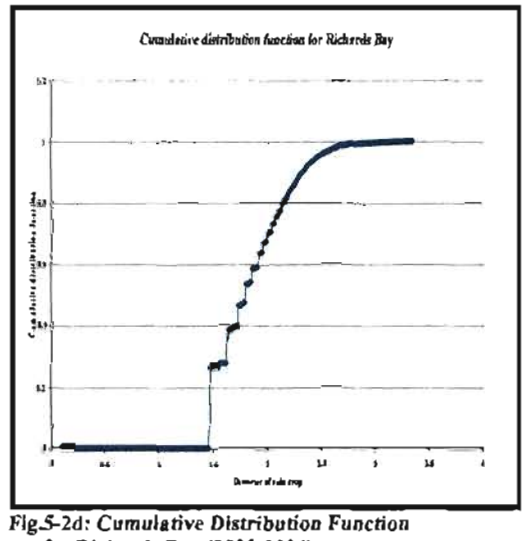

Fig.5-2d: Cumulative Distribution Function for Richards Bay (2000-2004)

The Probability density function (pdf) were then calculated and plotted. These are shown in figure 5-1a, 5-1b, 5-1c, and 5-1d, for Durban, Pretoria, Cape Town, and Richards Bay respectively. The probability density function has exponential pattern for the four selected sites. Fig. 5-2 a ,b ,c , and d represent cumulative distribution functions for Durban, Pretoria, Cape Town and Richards Bay for period of 2000-2004 respectively.

5.5. Drop Size Distribution Modeling Technique For Four Sites.

The calculated drop size distribution can be approximated by three parameters Δ, N_0 and median diameter of the drops. Both Δ, N_0 depend on rain rate. The shape of the pdf shows that the model takes the shape form of negative-exponential function of the drop diameter D. These three-parameters are related to the exponential functions parameter to set the conditions for the model. Since we concluded distribution N (D) as exponential and therefore propose the following pdf, $f(D_m)$:

$$f(D_m) = \lambda e^{-\lambda D_m} \tag{5.17}$$

The parameter λ is a real, positive constant. The task is therefore to determine λ, the conditions have to be satisfied:

$$\begin{pmatrix} f(D_m) = \lambda e^{-\lambda D_m}, & D_m \geq O \\ f(D_m) = 0 \quad , & otherwise \end{pmatrix} \tag{5.18}$$

$$\begin{pmatrix} F(D_m) = \int_0^{\infty} f(D_m) dD_m = \int_0^{\infty} \lambda e^{-\lambda D_m} = 1 - e^{-\lambda D_m}, & D_m \geq 0 \\ F(D_m) = 0 \quad , & D_m < 0 \end{pmatrix} \tag{5.19}$$

$$E(D_m) = \int_0^{\infty} D_m \lambda e^{-\lambda D_m} dD_m = \frac{1}{\lambda} \tag{5.20}$$

It is easy to show that if $f(D_m)$ defined in (5.17) is a true pdf, then once it satisfies (5.18), then (5.19) and (5.20) are automatically satisfied. In order to ascertain the estimated models of rain drops size distribution for the four sites, a test of hypotheses is done. The test of hypotheses we choose is the chi square χ^2 . Chi-square test is used to determine if a certain assumed distribution differs from some predetermined theoretical distribution. Another use of chi-square is in testing

null hypotheses of significant differences between or among the responses of individuals in two or more groups [61]. The chi-square statistics, χ^2 is obtained as follows:

$$\chi^2 = \sum_{K=1}^{N} [f(D_m) - f^*(D_m)]^2 / f^*(D_m) \tag{5.21}$$

$$F = (N-1) \tag{5.22}$$

where $f(D_m)$, $f^*(D_m)$, F , and N are measured value, predicted value, degree of freedom and number of the data respectively. The table 5-3a shows the threshold values for the chi-square test for the four sites. The values of χ^2 for Durban, Pretoria, Cape Town and Richards Bay are 6.556, 88.471, 82.537, and 3.210 at 70, 90, 60 and 40 degree of freedom. These values are compared with the threshold values for the chi-square test and found that the results for Durban, Pretoria Cape Town, and Richards Bay are below the threshold values .Thus we accept the null hypothesis at 1 percent level for the four cities.

Fig.5-3 a, b, c, and d show the fitted rain drop distributions for Durban, Pretoria, Cape Town and Richards Bay. Assuming $N(D_m)$ as pdf, therefore N_0 and Δ as the function of rainfall rate. By using Laws and Parsons median diameter method, a new empirical relation is obtained for raindrop-size distribution in the selected four sites which obeys an exponential distribution as shown in table 5-3b. The parameters for N_0 for the four sites are the same and the only parameter that changes is Δ as shown in the table 5-3b. The estimated models are valid for raindrop diameter greater or equal 1.5 mm, where D_m the median diameter in millimeters and R is is the precipitation rate in millimeters per hour.

Table 5-3a: The raindrop size distribution models for four selected sites

Site	Calculated threshold at $\alpha = 1\%$	Expected threshold at $\alpha = 1\%$	Degree of freedom
Durban	6.556	100.4252	70
Pretoria	88.471	124.1163	90
Cape Town	82.537	88.3794	60
Richards Bay	3.210196045	63.6907	40

Table 5-3b: The raindrop size distribution models for four selected sites.

Region	Model Type	Rain Drop size distribution model
Durban	Exponential distribution	$N(D_m) = N_0 \exp(-\Delta D_m^{1.41})$ $N_0 = 1500R^{0.26}$ $\Delta = 4.11R^{-0.153}$
Pretoria	Exponential distribution	$N(D_m) = N_0 \exp(-\Delta D_m^{1.41})$ $N_0 = 1500R^{0.26}$ $\Delta = 4.08R^{-0.149}$
Cape Town	Exponential distribution	$N(D_m) = N_0 \exp(-\Delta D_m^{1.41})$ $N_0 = 1500R^{0.26}$ $\Delta = 3.98R^{-0.146}$
Richards Bay	Exponential distribution	$N(D_m) = N_0 \exp(-\Delta D_m^{1.41})$ $N_0 = 1500R^{0.26}$ $\Delta = 4.01R^{-0.135}$

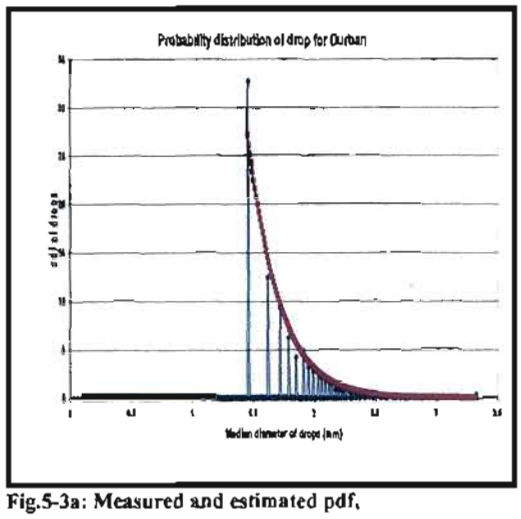

Fig.5-3a: Measured and estimated pdf, $f(D_m)$ and $f^*(D_m)$ for Durban.

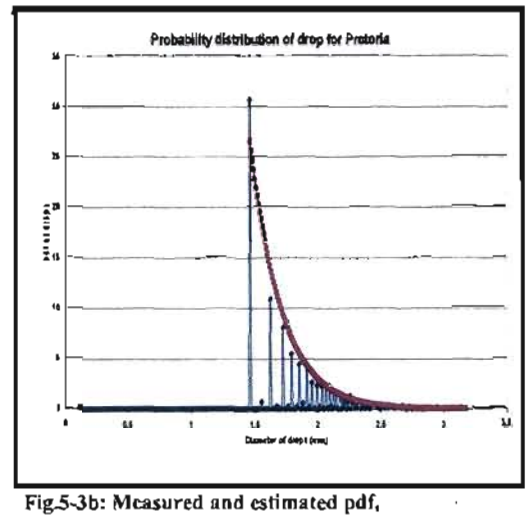

Fig.5-3b: Measured and estimated pdf, $f(D_m)$ and $f^*(D_m)$ for Pretoria

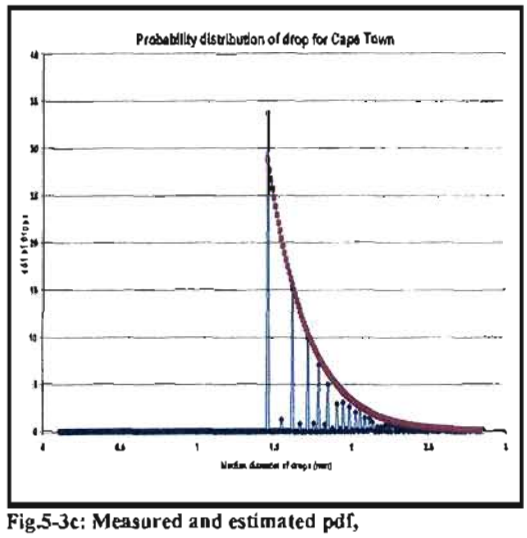

Fig.5-3c: Measured and estimated pdf, $f(D_m)$ and $f^*(D_m)$ for Cape Town

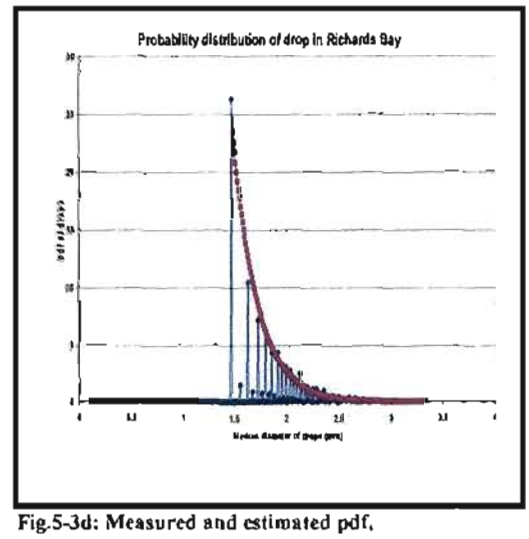

Fig.5-3d: Measured and estimated pdf, $f(D_m)$ and $f^*(D_m)$ for Richards Bay

5.6. Comparison Of The Empirical Model With Other Developed Models

As reported by many authors [42, 28, 44, 53, and 55] the plots for $N(D)$ versus rain drop diameter at different rainfall rates are used in application of their proposed model. Similarly, the same approach is used for the four selected cities in South Africa. These are shown from figures 5-4 to figure 5-7.

The empirical models for four selected sites are compared with other models from different regions in the world. The comparisons are done at rainfall rate of 20, 50, 100 and 150mm/h.The proposed models are compared with other models such as Japan model, Singapore, and finally, by Joss, Thams and Waldvogel model at Drizzle, widespread and Thunderstorm. The details of the relationship used in comparisons are found in table 5-1 and 5-2 of section 5.14 and 5.17 of the thesis respectively.

From 20 mm/h, the Singapore model is closest to the distribution obtained for Durban, Pretoria, Cape Town, and Richards Bay.

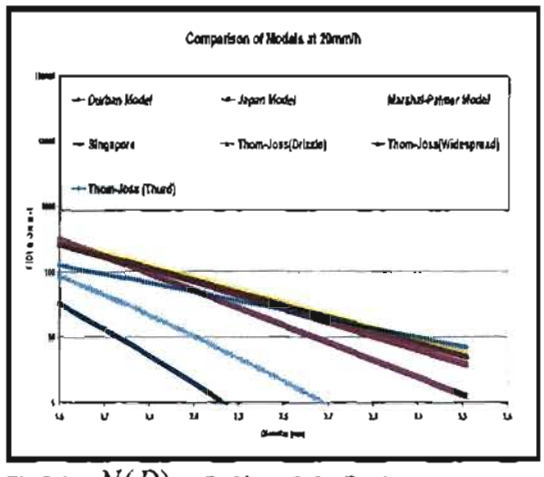

Fig.5-4a: $N(D)$ at R=20mm/h for Durban

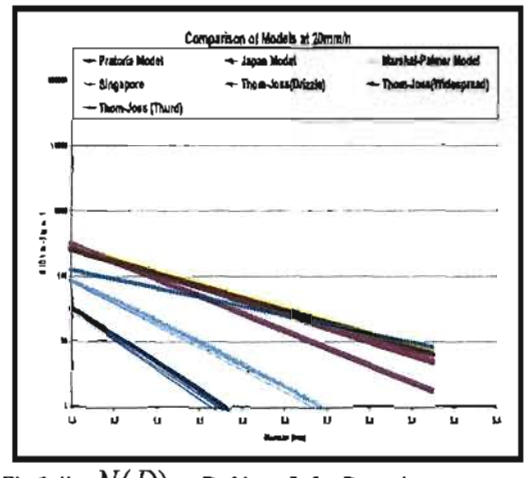

Fig.5-4b: $N(D)$ at R=20mm/h for Pretoria

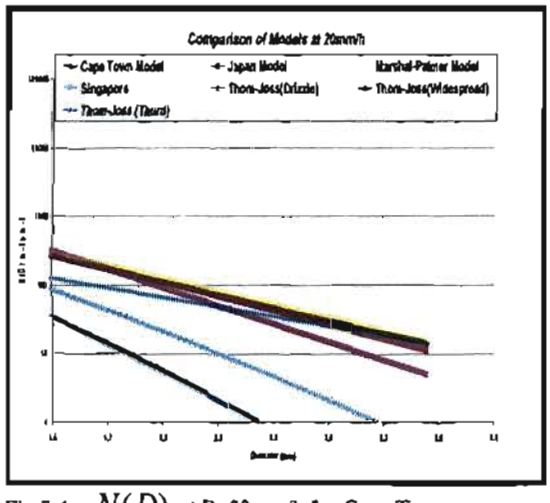

Fig.5-4c: $N(D)$ at R=20mm/h for Cape Town

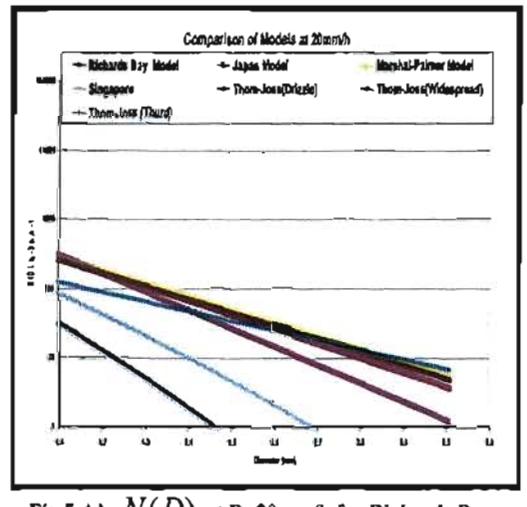

Fig.5-4d: $N(D)$ at R=20mm/h for Richards Bay

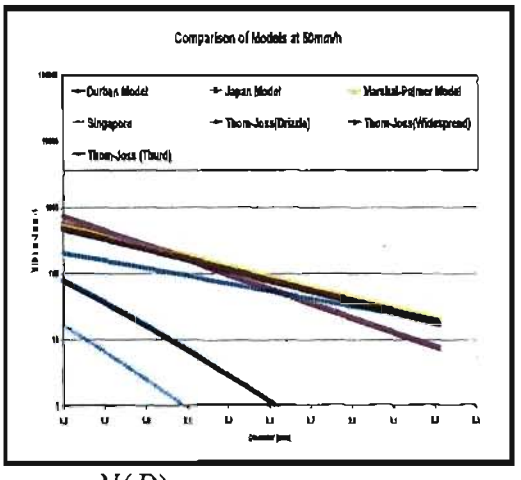

Fig.5-5a: $N(D)$ at R=50mm/h for Durban

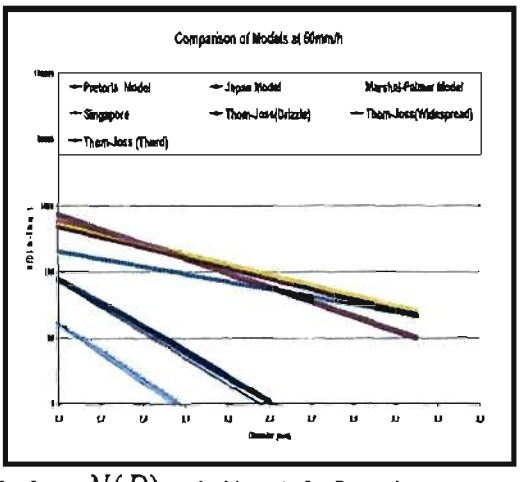

Fig.5-5b: $N(D)$ at R=50mm/h for Pretoria

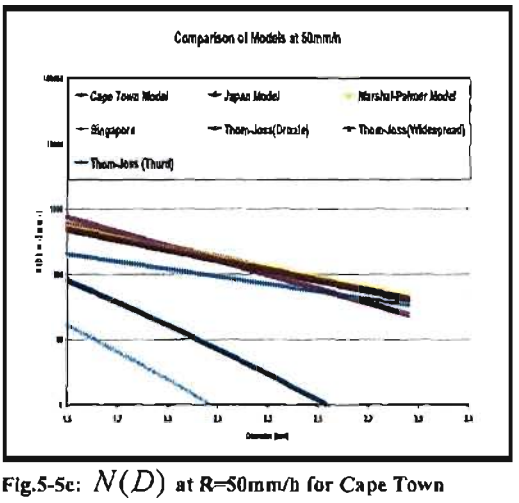

Fig.5-5c: $N(D)$ at R=50mm/h for Cape Town

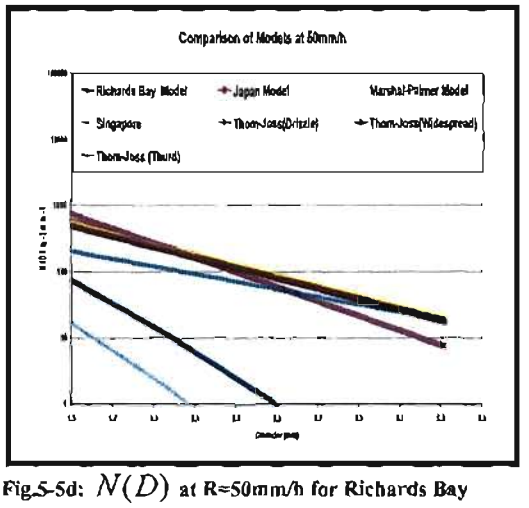

Fig.5-5d: $N(D)$ at R=50mm/h for Richards Bay

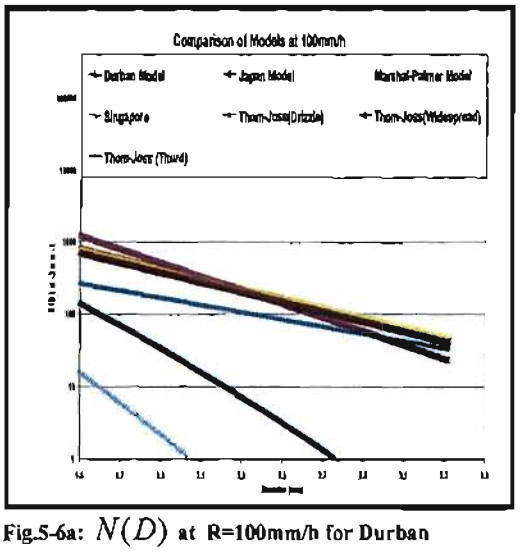

Fig.5-6a: $N(D)$ at R=100mm/h for Durban

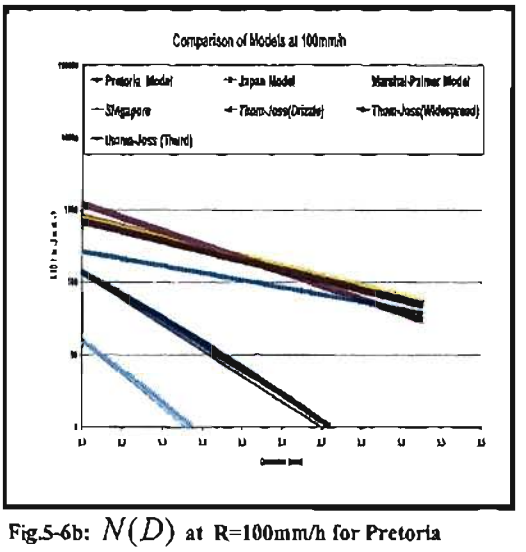

Fig.5-6b: $N(D)$ at R=100mm/h for Pretoria

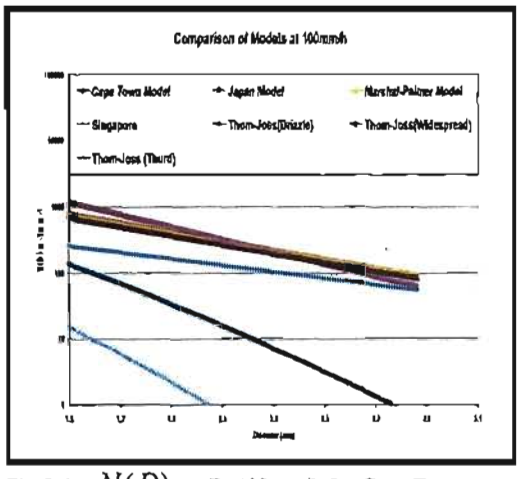

Fig.5-6c: $N(D)$ at R=100mm/h for Cape Town

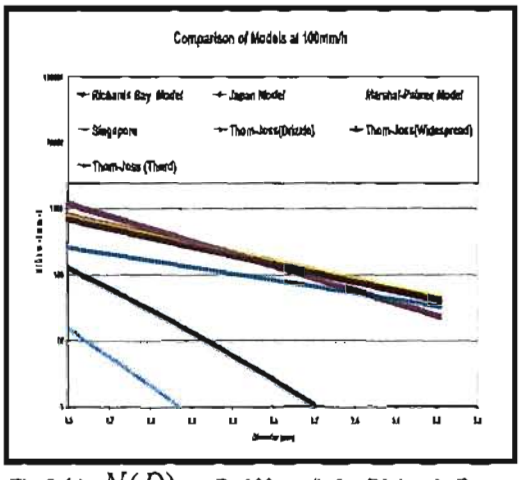

Fig.5-6d: $N(D)$ at R=100mm/h for Richards Bay

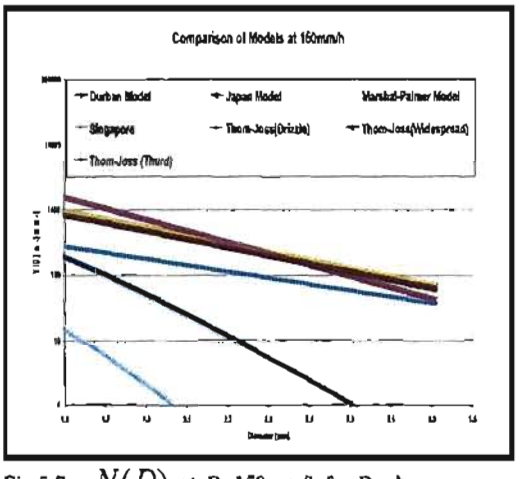

Fig.5-7a: $N(D)$ at R=150mm/h for Durban

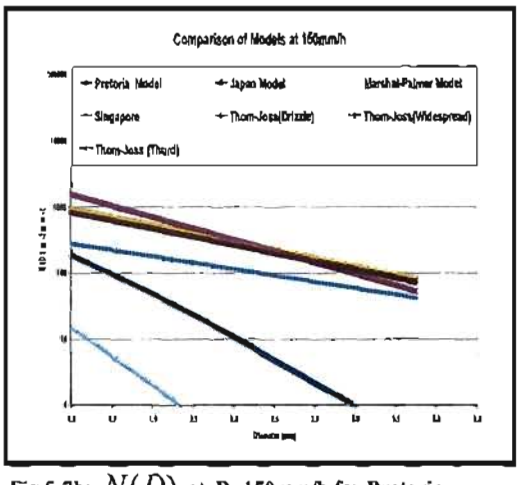

Fig.5-7b: $N(D)$ at R=150mm/h for Pretoria

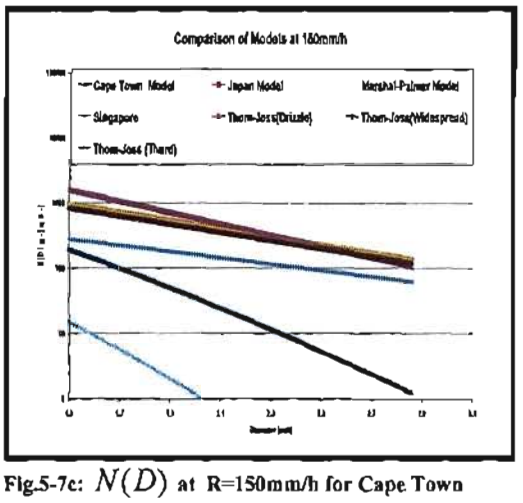

Fig.5-7c: $N(D)$ at R=150mm/h for Cape Town

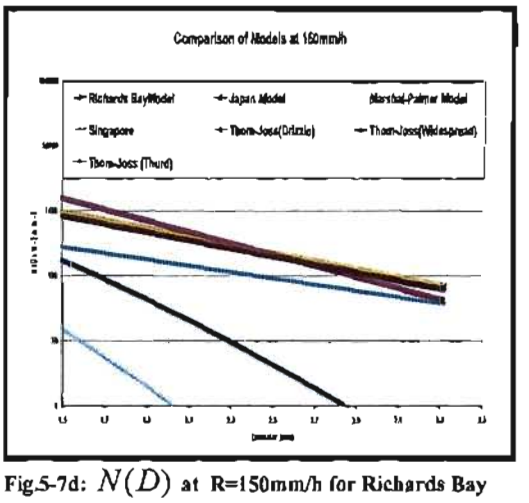

Fig.5-7d: $N(D)$ at R=150mm/h for Richards Bay

For higher rainfall rate of 100 mm/h and above, the South African models fall between Singapore and Thom-Joss (Thunderstorm). The Singapore model would then underestimate the distribution, while the other models overestimate the South Africa distributions.

5.7. Summary of chapter five

There are various existing rain drop size distribution models such as Laws and Parsons, Marshal and Palmer, Joss et. al, Lognormal and Gamma distribution. The over-estimation of the Laws and Parsons, Marshall and Palmer and under-estimation of Joss et al model actually raise a need for the estimation of rain drop size distribution for South Africa.

Employing a median diameter relation of Laws and Parsons, an equivalent diameter was derived for various rainfall rates of available data. The estimated empirical models were obtained for four sites which obey exponential distribution.

The Probability density function (pdf) are plotted as shown in Fig. 5-1a, 5-1b, 5-1c, and 5-1d, for Durban, Pretoria, Cape Tow, and Richards Bay respectively. The shape of the pdf shows that the model takes the shape form of negative-exponential function of the drop diameter D. The N_0 are constant for the four sites while Δ vary from site to site .

The empirical models for four selected sites are compared with other models from different regions in the world. The comparisons are done at rainfall rate of 20, 50, 100 and 150mm/h.The results show that at 20 mm/h, the Singapore model is closed to South African models and at higher rainfall rate such as 100 mm/h , the South Africa models lie between Singapore and Thom- Joss (Thunderstorm).At higher rainfall rate, Singapore model underestimate the distribution, while the other models overestimate the South Africa distribution.

CHAPTER SIX

CONCLUSION

6.1. CONCLUSION

Attenuation due to rainfall plays a significant role in the design of radio link at millimetric band. Rain attenuation measurement can be obtained directly or predicted from knowledge of rainfall rate and drop-size distribution. This work presents characteristics of rainfall rate, rainfall rate distribution model and rain drop size distribution models for South Africa.

The 5-year rainfall data collected from South Africa Weather Services for 12 location is converted from 60-minute to 1-minute integration time using the conversion factor .The coefficient of conversion factors is compared with those obtained in Ile-Ife, Nigeria and it is found to be close. The results also confirm the power law relationship.

Richards Bay has the highest rainfall rate of 182.66 mm/h and Brandvlei with lowest rainfall rate of 67.02mm/h. It is observed that Western Cape gets most of its rainfall in winter, while the rest of the country is generally a summer rainfall region.

The cumulative distribution of 1-minute rain rate is obtained for all the 12-location at different percentages of time .Based on the comparisons between the ITU-R climatic zones and the result from the cumulative distribution, three more rain zones are proposed for South Africa. Also, cumulative distribution of average 1-minute rainfall rate for the average year (AY) and the average worst month (AWM) are obtained. Relationship between percentage of exceedence for AY and AWM for each location shows that probability of occurrence is greater in the AWM than the AY. The percentage of exceedence of AY is underestimated by ITU-R while the percentage of exceedence of AWM is overestimated by ITU-R when both are compared with the measured.

The empirical rain rate distributions model proposed here give a good representation of intensity cumulative distributions for eight hydrometeological locations in South Africa. The results of the rainfall rate distribution model are compared with ITU-R (probability of law) and measured data. The observation showed that South Africa models show better agreement with measured data compared to ITU-R.

Estimated drop size distributions (DSDs) from four different sites (Durban, Cape Town, Pretoria and Richards Bay) have been calculated and analysed. The method embarked upon in estimating the empirical model involves collection of rain rate data, collating the data and converting rainfall rate to an equivalent diameter using median diameter D_m.The Probability density function (pdf) are plotted as shown in Fig. 5-3a, 5-3b, 5-3c, and 5-3d, for Durban, Pretoria, Cape Tow, and Richards Bay respectively. The shape of the pdf shows that the model takes the shape of a negative-exponential function of the drop diameter D. The N_0 are constant for the four sites while Δ vary from site to site .

The empirical models for four selected sites are compared with other models from different regions in the world. The comparisons are done at rainfall rate of 20, 50, 100 and 150mm/h. At 20 mm/h, the Singapore model is closest to the distribution obtained for the four cities while at higher rain rate (100 mm/h and 150 mm/h) the South Africa models fall between Singapore and Thom-Joss (Thunderstorms).At 20 mm/h, Singapore model overestimate the South Africa distribution while at higher rain rate (50 mm/h, 100 mm/h and 150 mm/h), it underestimate the distributions. The other compared models overestimate the South Africa distribution both at lower and higher rain rates (20 mm/h, 50 mm/h, 100 mm/h and 150 mm/h)

6.2. FUTURE WORK AND RECOMMENDATIONS

Though reasonable amount of work was done on this topic, there still remains a lot of room for improvement. There is a dearth need of data at different integration times,

namely 1-minute, 5-minute, 10-minute and 30-minute to really examine the effect of integration time on the cumulative distribution of rainfall rate and also to confirm rainfall event of duration. This should be pursued for the region.

There is also a need for physical measurement of raindrop size distribution at different locations and frequencies (greater than 10 GHz) in South Africa for at least one year for proper prediction of a drop size distribution model that is appropriate South Africa.

Further more, the available expertise in West and North Africa can be utilized in the Southern Africa region to measure and analysis propagation parameters relevant to terrestrial and Earth- space communication in the country.

REFERENCES

[1] M. Marcus and B. Pattan, "Millimeter Wave Propagation-Spectrum Management Implications," *IEEE Microwave Magazine*, Vol. 6, No2, June 2005, pp. 54- 61.

[2]. P. Kiddle, "Millimetric Wave Systems - the Attractive Access Radio Solution", *Radio Relay Systems,* 11-14 October 1993.

[3] C. J. Gibbins, "Radiowave Propagation in the Millimetric Bands," Rutherford *Appleton Laboratories, "Business Opportunities in the Millimetric Wavebands"*, London, Vol. 27, June 1990.

[4] C.J. Gibbins, "Studies of Millimetre-Wave Propagation and Related Meteorology over a 500 m path," *Proc. URSI Comm. F Open Symposium on wave Propagation and Remote Sensing*, Ravensercar, UK, 27 June 1990, pp.10.6.1-10.6.8.

[5]. http://www.ero.dk/documentation/docs/doc98/official/pdf/REP033.PDF

[6].ITU-R Report 719-3, "Attenuation by Atmospheric Gases," *Recommendations and Reports of the CCIR,* Vol. V, Geneva, 1986, pp.167-177.

[7] ITU-R Report 721-2, "Attenuation by Hydrometeors, in Particular Precipitation, and Other Atmospheric Particles," *Recommendations and Reports of the CCIR,* Vol.V, 1986, Geneva, pp.199-214.

[9] K. Robert Crane: *Electromagnetic Wave Propagation through Rain*, John Wiley, New York, 1996, Chapter 2-3.

[10] L. Roger Freeman: *Radio System Design for Telecommunications*, 2nd Edition, John Wiley, 1997, pp. 468-471.

[10] A. Tokay, A. Kruger and A.J Filho, "Measurements of drop size distribution in the southwestern Amazon basin," *J. of Geophysical Research*, Vol. 107, no. D20, 8052, doi: 10.1029/2001JD00355, 2002, pp 19-1-15

[12] B. Segal, "The Influence of Raingage Integration Time on Measured Rainfall-Intensity Distribution Functions," *J. of Atmospheric and Oceanic Tech*, Vol. 3, 1986, pp.662-671.

[13] G. O Ajayi and E.B.C. Ofoche, "Some Tropical rainfall rate characteristics at Ile-Ife for Microwave and millimeter Wave Application," *J. of Climate and Applied. Meteor.*, Vol. 23, 1983, pp 562-567.

[14] Recommendation ITU-R 837-1,2,3,4, "Characteristics of Precipitation for Propagation Modeling," Vol.1992-2003, P Series, *International Telecommunication Union*, Geneva, Switzerland, 2003.

[15] Recommendation ITU-R P.581-2, "The concept of Worst month", ITU-R Recommendations, P Series, *International Telecommunication Union*, Geneva, September 2001.

[16] http://www.newton.dep.anl.gov/askasci/wea00.htm

[17] R.Gunn, and G.D.Kinzer, 1949 "The terminal velocity of fall for water droplets in stagnant air," *Journal of Meteorology*, Vol .6, 1949, pp. 243-248.

[18] C. Mätzler, "Drop-size distributions and Mie computations for rain," *Institut für Angewandte physic Research report* No.2002-16, November 2002.

[19] D. Atlas, R.C Srivastava, and R.S. Sekho, "Doppler radar characteristics of precipitation at vertical incidence," *Rev. Geophys.* Vol. 11, 1973, pp. 1-35.

[20] http://www.islandnet.com/~see/weather/history/rdbentley.htm

[21] J. Joss, J.C Thams and A. Waldvogel. "The variation of raindrop size distribution at Lorano, Switzerland,"*Proc. Int. Conf. On cloud Physics*, Toronto, Canada.1968, pp.369-3

[22] South Africa Climate and Weather, in http://www.sa-venues.com/no/weather.htm.

[23] Republic of South Africa 1989-1990: *Official Year Book of the Republic of South Africa*, 15th Edition, Bureau for information pp1-22

[24] P. Bhartia, I.J. Bahl: *Millimeter Wave Engineering and Applications*, John Wiley & Sons, New York, 1984, Chapter 3 & 4.

[25] M.I. Skolnik, "Millimetre and sub millimetre wave applications," *Proceedings of the symposium on Submillimeter waves, Polytechnic Press of Poly. Institute of Brooklyn*, New York, 1970, pp9-25.

[26] V.W. Richard: "Millimetre wave Applications to Weapons Systems," *U.S. Army Ballistic Research Labs*, June 1976, Report No.2631.

[27]www.fcc.gov/Bureaus/Engineering_Technology/Documents/bullentins/oet70/oet70a.pdf.

[28] R.E. Collin: *Antennas and Radiowave Propagation*, McGraw-Hill International, 1985, pp. 401-410.

[29] ITU-R Recommendation 676-1, "Attenuation by atmospheric gases in the frequency range 1-350 GHz", 1992

[30] P.A. Owolawi, M.O. Fashuyi and T.J. Afullo, "Rainfall rate modeling for LOS radio systems in South Africa", *Accepted for publication in SAIEE Transactions*, March 2006.

[31] G.O Ajayi, S.Feng, S.M. Radicella, B.M Reddy (Ed): *Handbook on Radiopropagation Related to Satellite communications in Tropical and Subtropical Countries.* ICTP, Trieste, Italy, 1996, pp.7-14.

[32] P.A. Watson, Sathiaseelan and B. Potter: *Development of a Climatic Map of Rainfall Attenuation for Europe*, Post Graduate School of Electrical and Electronic Engineering, University of Bradford, U.K, Rep. No.300, 1981, pp. 134.

[33] R.K., Flavin, "Rain Attenuation Considerations for Satellite Paths", *Telecom Australia Research Laboratories*, Report No 7505, 1981.

[34] P.D Tyson, R.A Preston-Whyte, R.E. Schulze, "The Climate of the Drakensberg", *Natal Town and Regional Planning Commission*, 1976, pp50-60.

[35] Les Barclay: *Propagation of Radiowavws*, 2nd Edition, IEEE, London, UK, 2003, Chapter 4.

[36] F. Moupfouma, "More about rainfall rates and their prediction for radio system engineering", *IEE Proc.*, Vol.134, 1987, Pt. H, N.6,pp. 527-537.

[37] P.L. Rice, N.R. Holmberg, "Cumulative time statistics of surface-point rainfall rates", *IEEE Trans.Comm.*, COM-21, 1973, pp.1131-1136.

[38] E.J. Dutton, H.T Dougherty, R.F. Martin, "Prediction of European rainfall and link performance coefficients at 8 to 30 GHz", *NTIS U.S. Department of Commerce*, Rep. AD/A-000804, 1974.

[39] Poiares-Baptista., Salonen E., "Review of rainfall rate modeling and mapping", *Climpara'98*, Ottawa, Canada, 1998.

[40] F. Moupfouma, *'Etude des precipitations et de leurs effects sur les liaisons hertziennes en visibilite et par satellite dans les regions tropicales,* ' These de Doctorat d'Etat es-sciences physiques, CMET Universite Paris Nord, 1987.

[41] F. Moupfouma, and L. Martin, "Point Rainfall Rate Cumulative Distribution function valid at various Locations in the World", *Electronics Letters*, Vol. 29, No. 7, 1993, pp. 1503-1504.

[42] CCIR XVth Plen.Ass., Geneva, 1982, V, report 563-2.

[43] CCIR XVth Plen.Ass., Geneva, 1982, V, report 338-4 and 564-2.

[44] Chi-Huei Tseng, Kun-Shan Chen, Chih-Yuan Chu, "Variability Analysis of Ka Band Rain Attenuation in Taiwan". *Progress in Electromagnetics Symposium 2005*, Hangzhou, August 23-26, 2005, pp.1-2.

[45] J.O. Laws, and D.A. Parsons, "The relation of raindrop-size to intensity", *Transactions of America Geophysics Union*, Vol. 24, 1943, pp.452- 460.

[46] G.O. Ajayi and R.L Olsen, "Modeling of a raindrop size distribution for microwave and millimetre wave applications," *Radio Science*, Vol. 20, No. 2, pp. 193-202.

[47] J.S. Marshall and W.M.K. Palmer, "The distribution of raindrops with size," Journal of Meteorology, Vol. 5, pp 165-166.

[48] I. A. Adimula and G.O. Ajayi, "Variation in Raindrop Size Distribution and Specific Attenuation due to Rain in Nigeria," *Ann. Telecom*, Vol.51, No. 1-2, pp.87-93.

[49] ITU-Recommendation (1982): "Draft handbook on radio meteorology". *Int. Telecommunication union study groups* Doc.3/11-E.

[50] M.P.M. Hall and L.W. Barclay, L.W, "*Radio wave propagation*". Peter Peregrinus Ltd, London, pp1-279.

[51] M. Ajewole, L.B Kolawole and G.O Ajayi., "Cross polarization on Line-of –sight Links in a Tropical location: Effect of the variation in canting Angle and Rain drop size distribution" *IEE transaction on antenna and propagation.* Vol 47, No 8.pp 1254-1259.

[52] ITU-Recommendation (1982), "Draft handbook on radio meteorology," *International Telecommunication Union Study Group* Doc.3/11-D.

[53] T. Oguchi, "Electromagnetic wave propagation and scattering in rain and other Hydrometeors," *Proceedings of the IEEE*, Vol. 71, No. 9, September, 1983. pp. 1029-1049.

[54] M.O. Ajewole, *Scattering and attenuation of centimetre and millimetre radio signals by tropical rainfall,* Ph.D thesis, Federal University of Technology, Akure Nigeria

[55] S.Wickerts, "Drop Size Distribution in Rain," *FOA (Nat. Defence Res. Inst.) Rep.* C20438-EI (E2), Sweden, 1982

[56] M. Sekine and G. Lind :'Rain attenuation of centimetre, millimetre and sub-millimetre radio waves.' *Proceedings of the 12th European Microwave conference*, 1992.Helsinki, Finland, pp.584-589.

[57] H. Jiang, M. Sano and M. Sekine, "Weibull raindrop-size distribution and its application to rain attenuation." *IEE Proc. Microwave Antennas Propag.*, Vol.144, No.3, June 1997, pp. 197-200.

[58] M.Sekine and C.D. Chen, "Rain attenuation in terrestrial and satellite communications links," *in Proc. 15th European Microwave Conf., Paris, France*, Sept. 1985, pp.985-990.

[59] T. Nonabe, T Ihara, J. Awaka and Y.Furuham, "The relationship of raindrop-size Distribution to Attenuations Experienced at 50, 80, 140, and 240 GHz". *IEEE Transactions on Antenna and Propagation,* Vol. AP-35, No.11, Nov.1987.

[60] K. Isaiah Timothy, Jin Teong Ong, and Emily B.L. Choo, "Raindrop Size Distribution Using Method of moments for Terrestrial and Satellite Communication Applications in Singapore" *in IEEE Transactions on Antennas and Propagation*, Vol. 50, No. 10, Oct. 2002.

[61] N.M. Downie, R.W. Heath: *Basic statistical methods, second edition*, Harper and Row, New York, pp. 160-175.

APPENDIX A

RECOMMENDATION ITU-R P.837-4

Characteristics of precipitation for propagation modeling

(Question ITU-R 201/3)

(1992-1994-1999-2001-2003)

The ITU Radiocommunication Assembly,

considering

a) that information on the statistics of precipitation intensity is needed for the prediction of attenuation and scattering caused by precipitation;

b) that the information is needed for all locations on the globe and a wide range of probabilities,

recommends

1 that the model in Annex 1 be used to obtain the rainfall rate, R_p, exceeded for any given percentage of the average year, p, and for any location (with an integration time of 1 min). This model is to be applied to the data supplied in the digital files ESARAINxxx.TXT; (the data files may be obtained from that part of the ITU-R website dealing with Radiocommunication Study Group 3);

2 that, for easy reference, Figs. 1 to 6 in Annex 2 be used to select the rainfall rate exceeded for 0.01% of the average year. These Figures were also derived from the model and data described in Annex 1.

Annex 1

Model to derive the rainfall rate exceeded for a given probability of the average year and a given location

The data files ESARAINPR6.TXT, ESARAIN_MC.TXT and ESARAIN_MS.TXT contain respectively the numerical values for the variables P_{r6}, M_c and M_s while data files ESARAINLAT.TXT and ESARAINLON.TXT contain the latitude and longitude of each of the data entries in all other files. These data files were derived from 15 years of data of the European Centre of Medium-range Weather Forecast (ECMWF).

Step 1: Extract the variables P_{r6}, M_c and M_s for the four points closest in latitude (Lat) and longitude (Lon) to the geographical coordinates of the desired location. The latitude grid is from +90° N to –90° S in 1.5° steps; the longitude grid is from 0° to 360° in 1.5° steps.

Step 2: From the values of P_{r6}, M_c and M_s at the four grid points obtain the values $P_{r6}(Lat,Lon)$, $M_c(Lat,Lon)$ and $M_s(Lat,Lon)$ at the desired location by performing a bi-linear interpolation, as described in Recommendation ITU-R P.1144.

Step 3: Derive the percentage probability of rain in an average year, P_0, from:

$$P_0(Lat,Lon) = P_{r6}(Lat,Lon)\left(1 - e^{-0.0117(M_s(Lat,Lon)/P_{r6}(Lat,Lon)}\right) \quad (1$$

If P_{r6} is equal to zero, the percentage probability of rain in an average year and the rainfall rate exceeded for any percentage of an average year are equal to zero. In this case, the following steps are unnecessary.

Step 4: Derive the rainfall rate, R_p, exceeded for p % of the average year, where $p \leq P_0$, from:

$$R_p(Lat,Lon) = \frac{-B + \sqrt{B^2 - 4AC}}{2A} \quad \text{mm/h} \quad (1$$

where:

$$A = a\,b \quad (2a)$$

$$B = a + c\,\ln(p / P_0(Lat,Lon)) \quad (2$$

$$C = \ln(p / P_0(Lat,Lon)) \quad (2c)$$

and

$$a = 1.11 \quad (2d)$$

$$b = \frac{(M_c(Lat,Lon) + M_s(Lat,Lon))}{22932 P_0} \quad (2e)$$

$$c = 31.5b \quad (2f)$$

NOTE 1 – An implementation of this model and the associated data in MATLAB is also available from the ITU-R website dealing with Radiocommunication Study Group 3.

FIGURE 1

Rain rate (mm/h) exceeded for 0.01% of the average year

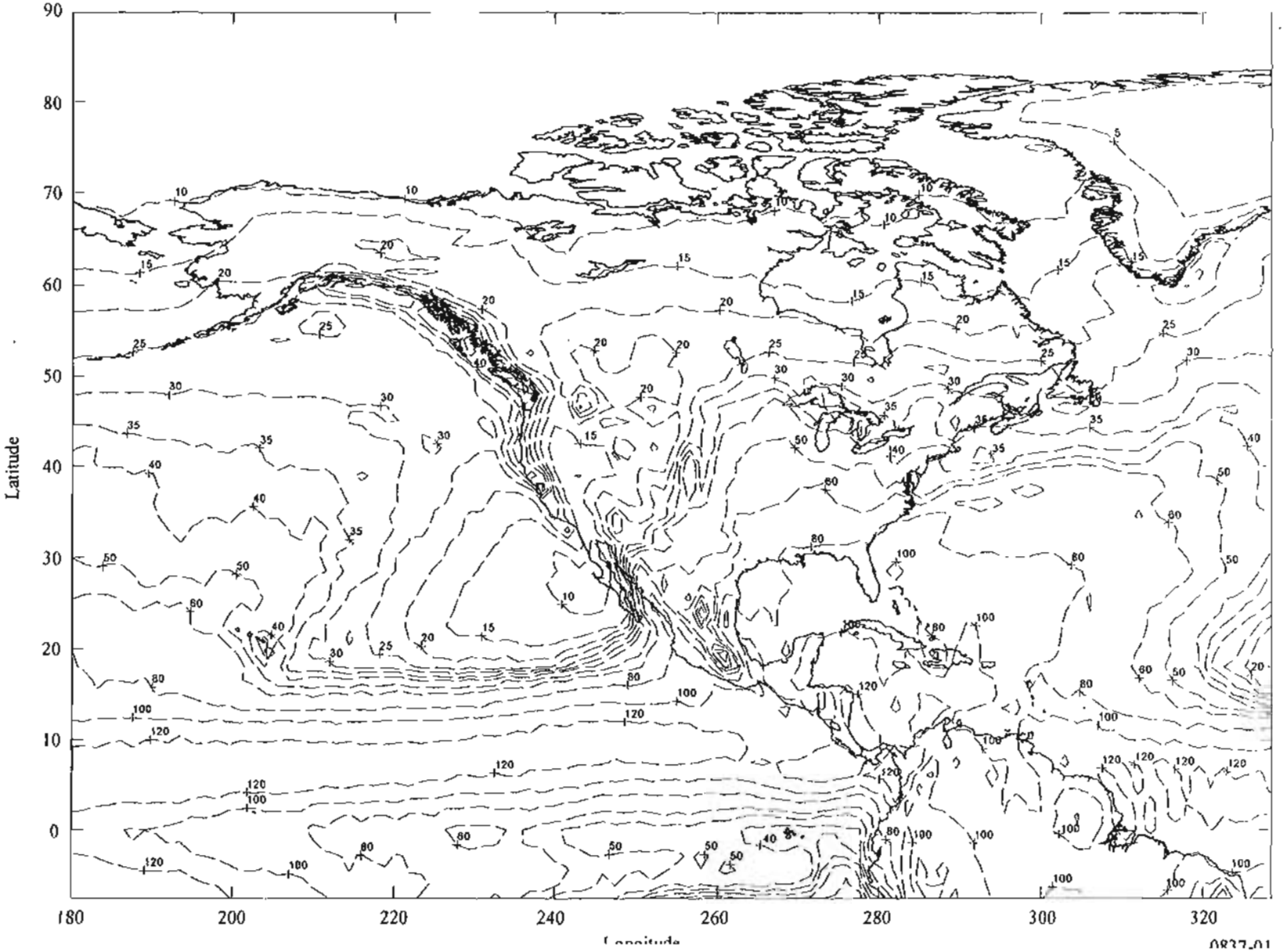

FIGURE 2

Rain rate (mm/h) exceeded for 0.01% of the average year

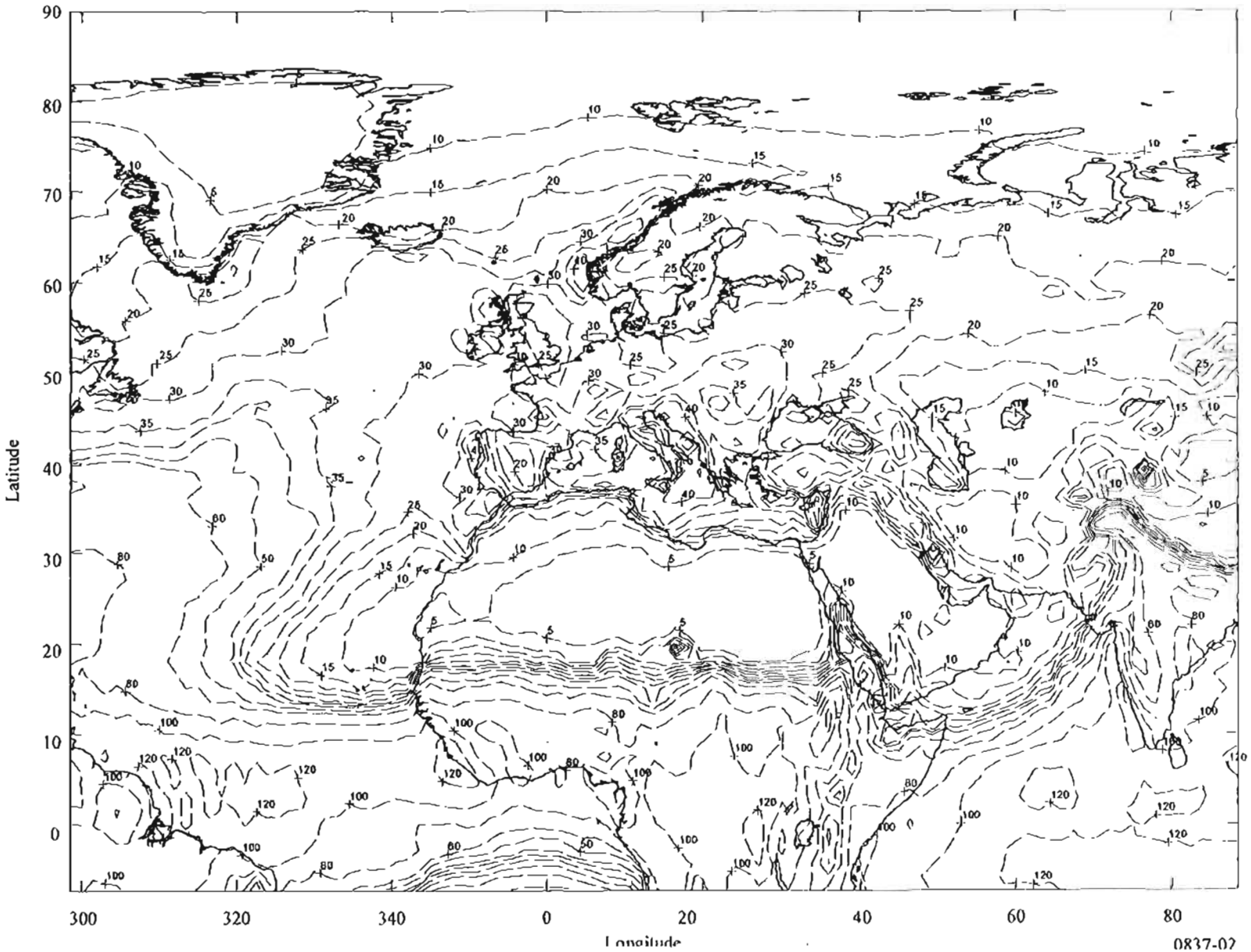

FIGURE 3

Rain rate (mm/h) exceeded for 0.01% of the average year

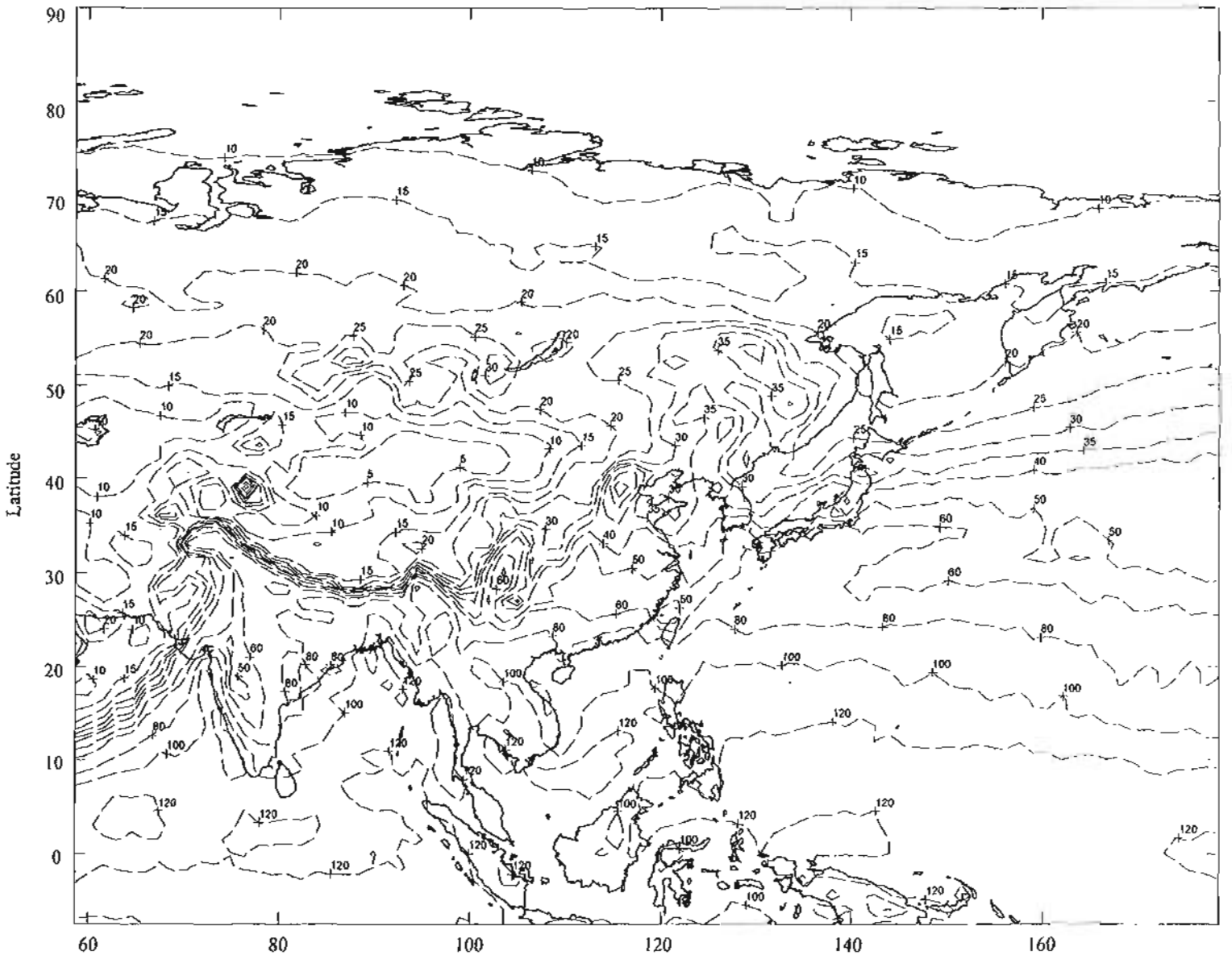

FIGURE 4

Rain rate (mm/h) exceeded for 0.01% of the average year

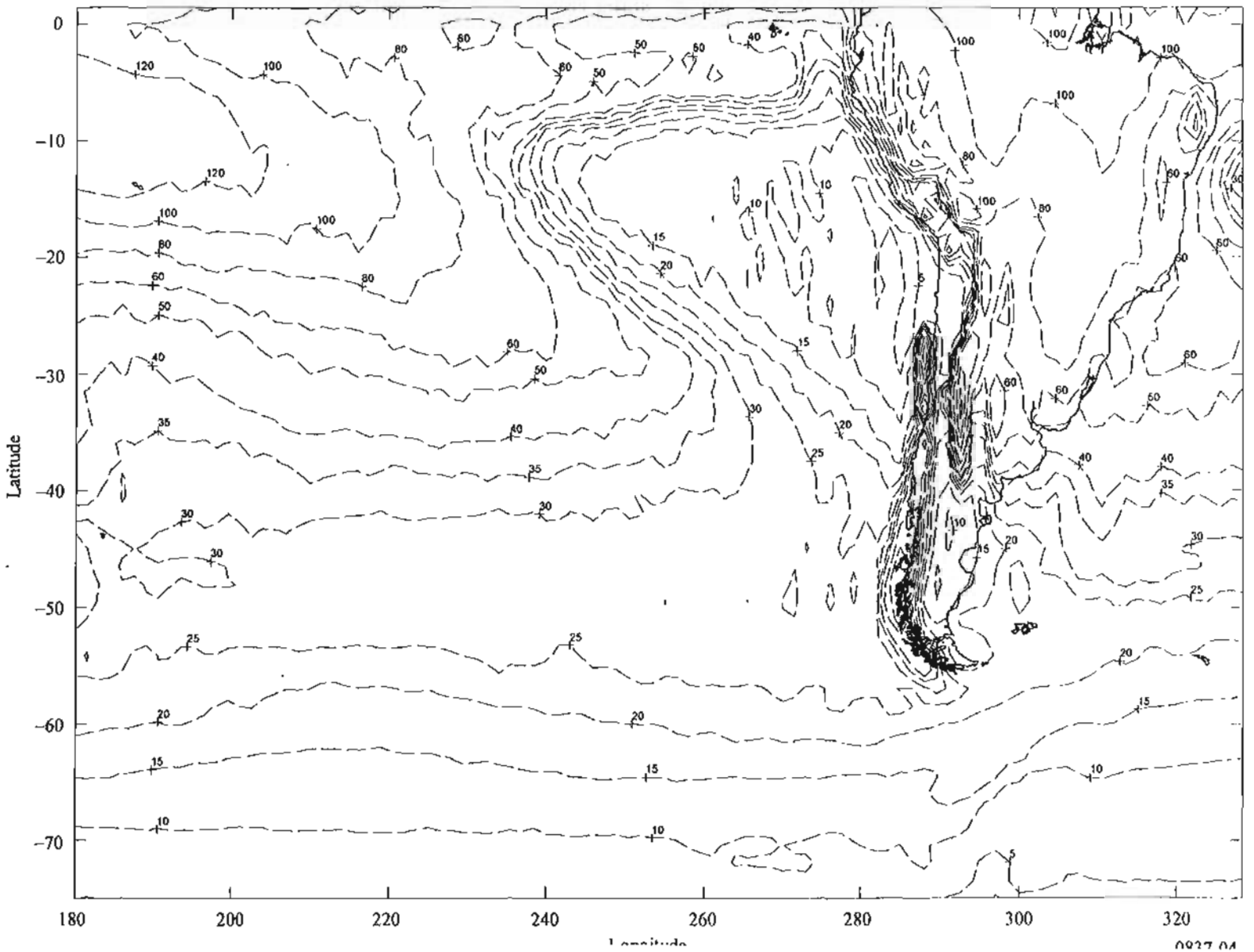

FIGURE 5

Rain rate mm/h) exceeded for 0.01% of the average year

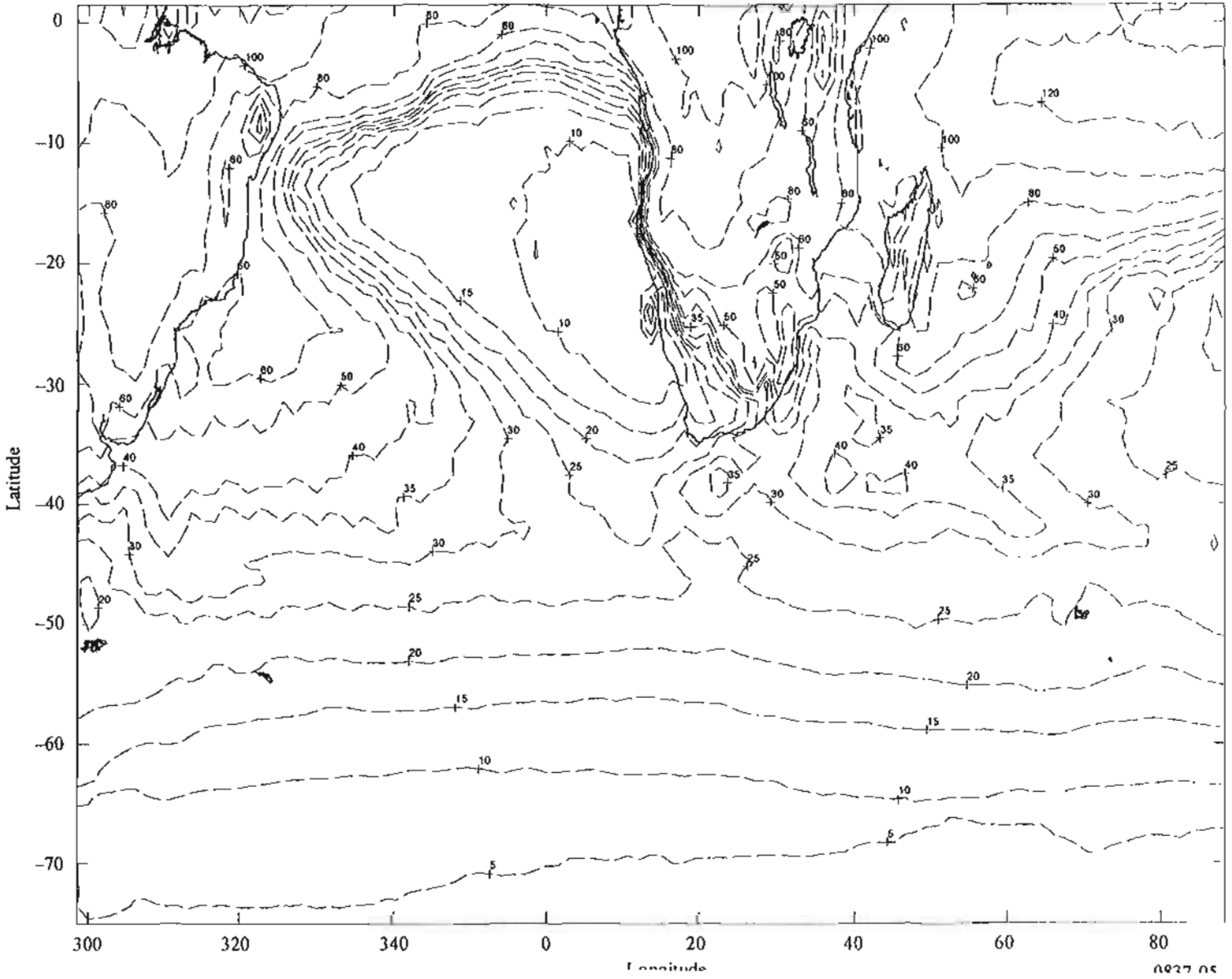

FIGURE 6

Rain rate (mm/h) exceeded for 0.01% of the average year

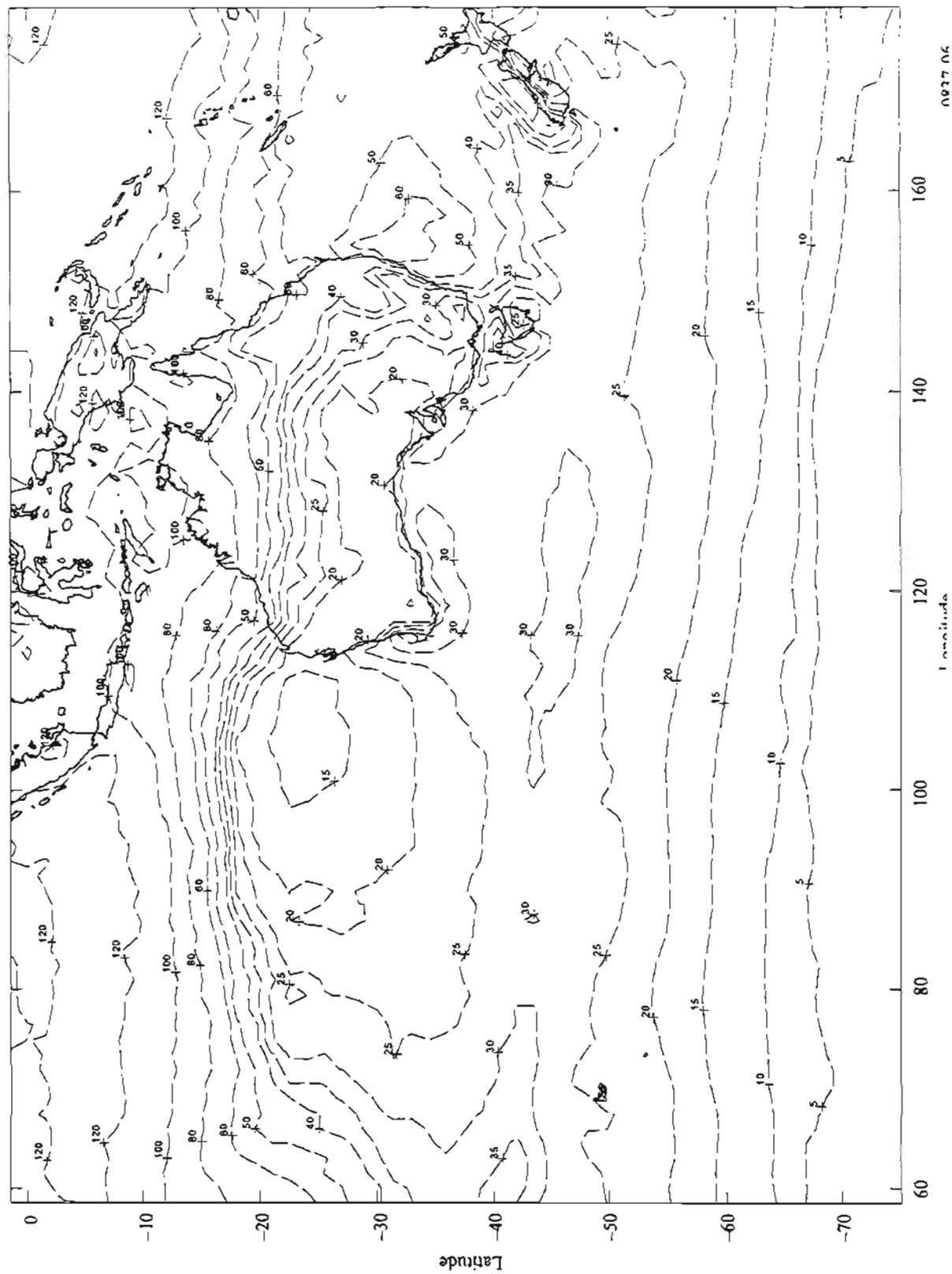

RECOMMENDATION ITU- R P.581-2*

THE CONCEPT OF "WORST MONTH"

(1982-1986-1990)

The ITU Radiocommunication Assembly,

considering

a) that performance criteria for radiocommunication systems often refer to "any month" as the period of reference;

b) that for the design of such systems it is necessary to have statistics of propagation effects that are relevant to the

period of reference of the performance criteria;

c) that consequently there is a need for an unambiguous definition for the period of reference,

recommends

1. that the fraction of time during which a preselected threshold is exceeded in the worst month of a year is referred to as "the annual worst-month time fraction of excess";

2. that the statistic relevant for the performance criteria referring to "any month" is the long-term average of the

annual worst-month time fraction of excess;

3. that the worst month of a year for a preselected threshold for any performance degrading mechanism, be that

month in a period of twelve consecutive calendar months, during which the threshold is exceeded for the longest time.

The worst month is not necessarily the same month for all threshold levels.

Note – Recommendation ITU-R P.841 presents a model for the conversion of the average annual time fraction of excess

to the average annual worst-month time fraction of excess. Global values of the parameters of this model are given, as

well as more detailed values for several regions of the world.

---

* Radiocommunication Study Group 3 made editorial amendments to this Recommendation in 2000 in accordance with Resolution

ITU-R 44.

RECOMMENDATION ITU-R P.841-3

Conversion of annual statistics to worst-month statistics

(Question ITU-R 201/3)

(1992-1999-2001-2003)

The ITU Radiocommunication Assembly,

considering

a) that for design of radiocommunication systems the required statistics of propagation effects pertain to the worst-month period of reference;

b) that the reference statistics for many radiometeorological data and propagation prediction methods is "the long-term average annual" distribution;

c) that consequently there is a need for a model that provides for the conversion of the "annual" to the "worst-month" statistics,

recommends

1 that the model given in Annex 1 be used for the conversion of the average annual time percentage of excess to the average annual worst-month time percentage of excess.

Annex 1

1 The average annual worst-month time percentage of excess, p_w, is calculated from the average annual time percentage of excess p by use of the conversion factor Q:

$$p_w = Q\,p \qquad (3)$$

where $1 < Q < 12$, and both p and p_w refer to the same threshold levels.

2 Q is a two parameter (Q_1, β) function of p (%):

$$Q_{(p)} = \begin{cases} 12 & \text{for} \quad p < \left(\frac{Q_1}{12}\right)^{\frac{1}{\beta}} \% \\ Q_1\, p^{-\beta} & \text{for} \quad \left(\frac{Q_1}{12}\right)^{\frac{1}{\beta}} < p < 3\% \\ Q_1\, 3^{-\beta} & \text{for} \quad 3\% < p < 30\% \\ Q_1\, 3^{-\beta} \left(\frac{p}{30}\right)^{\frac{\log\left(Q_1\, 3^{-\beta}\right)}{\log(0.3)}} & \text{for} \quad 30\% < p \end{cases} \qquad (4$$

3 The calculation of the average annual time percentage of excess from the given value of the average annual worst-month time percentage of excess is done through the inverse relationship:

$$p = p_w / Q \qquad (5)$$

and the dependence of Q on p_w can be easily derived from the above given dependence of Q on p. The resulting relationship for $12\, p_0 < p_w(\%) < Q_1\, 3^{(1-\beta)}$ is ($p_0 = (Q_1/12)^{1/\beta}$):

$$Q = Q_1^{1/(1-\beta)}\, p_w^{-\beta/(1-\beta)} \qquad (6)$$

4 For global planning purposes the following values for the parameters Q_1 and β should be used:

$Q_1 = 2.85, \quad \beta = 0.13$

(see Fig. 7). This leads to the following relationship between p and p_w:

$$p(\%) = 0.30\; p_w(\%)^{1.15} \qquad (7)$$

for $1.9 \times 10^{-4} < p_w(\%) < 7.8$.

FIGURE 7

Example of the dependence of Q on p (solid line) with parameter values $Q_1 = 2.85$ and $\beta = 0.13$

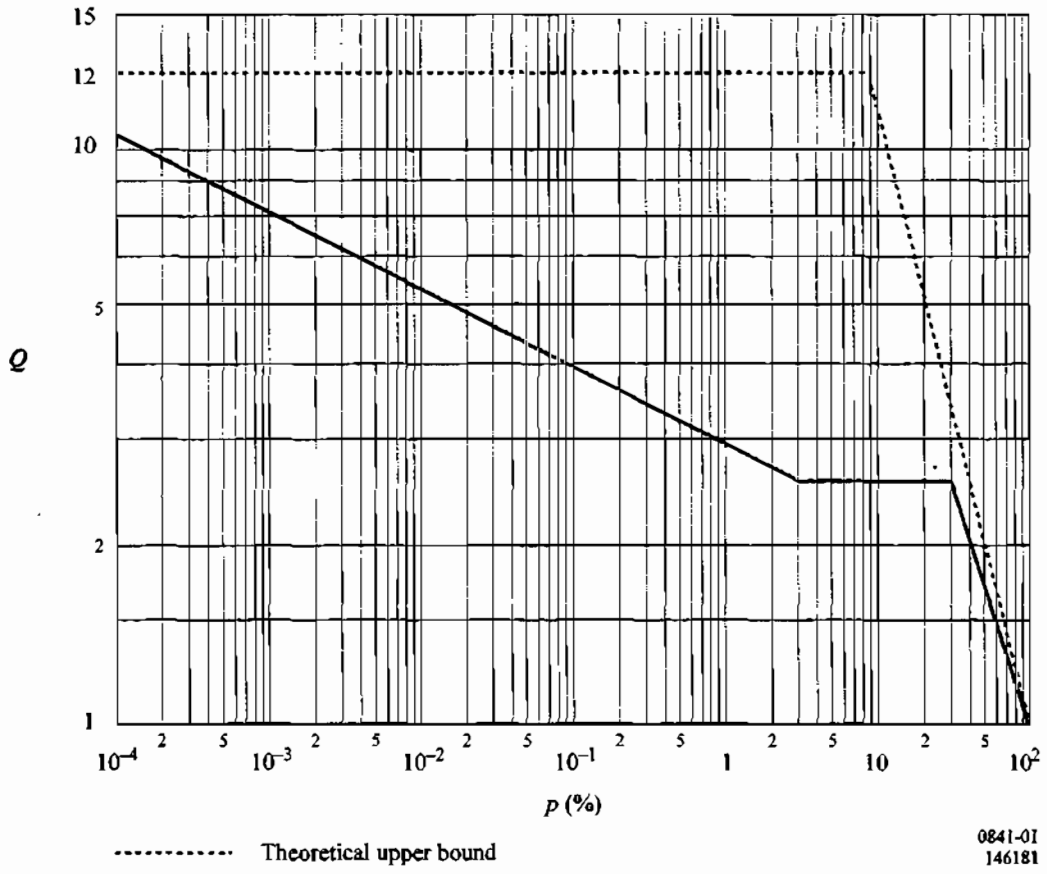

5 For more precision the values of Q_1 and β for the different climatic regions and various propagation effects given in Table 1 should be used where appropriate.

6 For trans-horizon mixed paths, the β and Q_1 values are calculated from those values for sea and land given in Table 1, through linear interpolation using the fractions of the link traversing sea and land respectively as weights.

7 Entries under rain rate for Australia are based on 6-min time interval measurements taken from 20 sites over periods lasting from 25 to 101 years. Examples of site locations for each climatic region in Australia are given in the first column of Table 1. Entries under rain rate for Brazil have been derived for measurements of rainfall rates at nine sites over a 46-year period using fast response rain gauges.

TABLE 1

β and Q_1 values for various propagation effects and locations

	Rain effect terrestrial attenuation	**Rain effect slant path attenuation**	**Rain rate**	**Multipath**	**Trans-horizon land**	**Trans-horizon sea**
Global	0.13, 2.85	0.13, 2.85	0.13, 2.85	0.13, 2.85	0.13, 2.85	0.13, 2.85
Europe North West	0.13, 3.0	0.16, 3.1		0.13, 4.0	0.18, 3.3	
Europe North West 1.3 GHz						0.11, 4.9
Europe North West 11 GHz						0.19, 3.7
Europe Mediterranean	0.14, 2.6	0.16, 3.1				
Europe Nordic	0.15, 3.0	0.16, 3.8		0.12, 5.0		
Europe alpine	0.15, 3.0	0.16, 3.8				
Europe Poland	0.18, 2.6					
Europe Russia	0.14, 3.6					
Europe UK 40 and 50 GHz		0.13, 2.54				
Congo	0.25, 1.5					
Canada Prairie and North	0.08, 4.3					
Canada Coast and Great Lake	0.10, 2.7					
Canada Central and Mountains	0.13, 3.0					

TABLE 1 (*continued*)

	Rain effect terrestrial attenuation	Rain effect slant path attenuation	Rain rate	Multipath	Trans-horizon land	Trans-horizon sea
United States of America Virginia		0.15, 2.7				
Russia North European region			0.10, 4.57			
Russia Central and West European region			0.16, 2.38			
Russia Middle Volga region and South Ural			0.10, 4.27			
Russia Central Steppe and South European region			0.15, 2.69			
Russia West Siberian region			0.14, 3.72			
Russia Middle Siberian Plateau and Jakutia			0.11, 5.04			
Russia South Far East			0.13, 3.53			
Australia Temperate/ coastal			0.17, 2.65			
Australia Subtropical/ coastal			0.15, 3.15			
Australia Tropical/arid			0.12, 4.35			
Brazil Equatorial			0.13, 2.85			
Brazil Tropical maritime			0.21, 2.25			
Brazil Tropical inland			0.13, 3.00			

TABLE 1 (*end*)

	Rain effect terrestrial attenuation	**Rain effect slant path attenuation**	**Rain rate**	**Multipath**	**Trans-horizon land**	**Trans-horizon sea**
Brazil Subtropical			0.13, 2.85			
Indonesia	0.22, 1.7					
Japan Tokyo	0.20, 3.0					
Japan Yamaguchi		0.15, 4.0				
Japan Kashima		0.15, 2.7				
South Korea			0.12, 4.6			